Pressure Compensator Design for a Variable Displacement Swash-Plate Type Axial Piston Pump

Thesis submitted by

Nitesh Mondal

DOCTOR OF PHILOSOPHY IN ENGINEERING

MECHANICAL ENGINEERING DEPARTMENT

FACULTY COUNCIL OF ENGINEERING AND TECHNOLOGY

JADAVPUR UNIVERSITY

KOLKATA-700 032

INDIA

2019

JADAVPUR UNIVERSITY
FACULTY COUNCIL OF ENGINEERING AND TECHNOLOGY
KOLKATA – 700 032, INDIA

1. **Title of Thesis**:

   Pressure Compensator Design for a Variable Displacement Swash-Plate Type Axial Piston Pump

2. **Name, Designation & Institution of the Supervisor:**

   Prof. Rana Saha

   Professor, Mechanical Engineering Department,

   Jadavpur University,

   Kolkata-700032

3. **List of Publications (Referred Journals):**

   1. Mondal, N., Saha, R., Mookherjee, S. and Sanyal, D., 2019. "A novel method to design pressure compensator for variable displacement axial piston pump," Proceedings of the Institution of Mechanical Engineers, Part E: Journal of Process Mechanical Engineering, 233(2), pp.314-334. DOI: 10.1177/ 0954408918783409.

   2. Mondal, N., Saha, R. and Sanyal, D. 2019. "An experimental exploration on pressure compensated swash plate type variable displacement axial piston pump," Journal of The Institution of Engineers (India): Series C. (Under Review)

   3. Mondal, N., Saha, R. and Sanyal, D. 2019. "Design and Dynamic Evaluation of a Single Stage Spool Valve for a Variable Displacement Swash Plate Type Axial Piston Pump," Proceedings of the Institution of Mechanical Engineers, Part E: Journal of Process Mechanical Engineering. (Communicated).

International Conference Publications:

1. Mondal, N., Saha, R. and Sanyal, D. "An Experimental Study on Variable Displacement Pressure Compensated Yoke Type Axial Piston Pump", 7th International and 45th National Conference on Fluid Mechanics and Fluid Power (FMFP), December 10-12, 2018, IIT Bombay, Mumbai, India, FMFP2018–PAPER NO. (469).

2. Mondal, N., Saha, R. and Sanyal, D. "An Experimental Investigation on Pressure Compensated Variable Displacement Swash Plate Type Axial Piston Pump", 1st International Conference on Mechanical Engineering, Jadavpur University, 2018. Paper ID-55.

3. Mondal, N., Mandal N.P., Saha, R., Mookherjee, S. and Sanyal, D. " Design Sensitivity of Pressure Compensator of a Variable Displacement Swash-Plate Type Axial, Piston Pump", 6th International and 43rd National Conference on Fluid Mechanics and Fluid Power. MNNITA, Allahabad, U.P. 2016. Paper ID-157.

National Conference Publications:

1. Mondal, N., Mandal N.P., Saha, R., Mookherjee, S. and Sanyal, D. "A Study on Pressure Compensated Variable Displacement Swash-Plate Type Axial Piston Pump", 44th National Conference on Fluid Mechanics and Fluid Power. Amrita University, Amritapuri Campus, Kollam, Kerala. 2017. Paper ID-105.

2. Mondal, N., Saha, R. and Sanyal, D. "Design of a Pressure Compensator of a Variable Displacement Swash-Plate Type Axial Piston Pump", The National Conference on Advance in Thermal Engineering. Jadavpur University, Kolkata. 2016. Paper No-ATE006.

3. Mondal, N., Mandal N.P., Saha, R., Mookherjee, S. and Sanyal, D. "Analysis of a Pressure Compensated Variable Displacement Swash Plate Type Axial Piston Pump with Rate Piston Pressure Feedback", 42nd National Conference on Fluid Mechanics and Fluid Power. NITK Surathkal, Karnataka. 2015. Paper ID-134.

4. **List of Patents:**   Nil

5.   List of Presentations in National/ International Conferences:

1. Mondal, N., Saha, R. and Sanyal, D. "An Experimental Study on Variable Displacement Pressure Compensated Yoke Type Axial Piston Pump", 7th International and 45th National Conference on Fluid Mechanics and Fluid Power (FMFP), December 10-12, 2018, IIT Bombay, Mumbai, India, FMFP2018–PAPER NO. (469).

2. Mondal, N., Saha, R. and Sanyal, D. "An Experimental Investigation on Pressure Compensated Variable Displacement Swash Plate Type Axial Piston Pump", 1st International Conference on Mechanical Engineering, Jadavpur University, 2018. Paper ID-55.

3. Mondal, N., Mandal N.P., Saha, R., Mookherjee, S. and Sanyal, D. "Design Sensitivity of Pressure Compensator of a Variable Displacement Swash-Plate Type Axial, Piston Pump", 6th International and 43rd National Conference on Fluid Mechanics and Fluid Power, MNNITA, Allahabad, U.P. 2016. Paper ID-157.

4. Mondal, N., Mandal N.P., Saha, R., Mookherjee, S. and Sanyal, D. "A Study on Pressure Compensated Variable Displacement Swash-Plate Type Axial Piston Pump", 44th National Conference on Fluid Mechanics and Fluid Power, Amrita University, Amritapuri Campus, Kollam, Kerala. 2017. Paper ID-105.

5. Mondal, N., Mandal N.P., Saha, R., Mookherjee, S. and Sanyal, D. "Analysis of a Pressure Compensated Variable Displacement Swash Plate Type Axial Piston Pump with Rate Piston Pressure Feedback", 42nd National Conference on Fluid Mechanics and Fluid Power. NITK Surathkal, Karnataka. 2015. Paper ID-134.

6. Mondal, N., Saha, R. and Sanyal, D. "Design of a Pressure Compensator of a Variable Displacement Swash-Plate Type Axial Piston Pump", The National Conference on Advance in Thermal Engineering, Jadavpur University, Kolkata. 2016. Paper No-ATE006.

6.   Poster Presentation: Nil

Department of Mechanical Engineering

JADAVPUR UNIVERSITY

KOLKATA-700032, INDIA

CERTIFICATE FROM THE SUPERVISOR

*This is to certify that the thesis entitled "**Pressure Compensator Design for a Variable Displacement Swash-Plate Type Axial Piston Pump**" submitted by **Sri Nitesh Mondal** who got his name registered on **27.08.2014** for the award of Ph.D. (Engineering) degree of Jadavpur University, is absolutely based upon his own work under the supervision of **Prof. Rana Saha** and that neither his thesis nor any part of the thesis has been submitted for any degree/diploma or any other academic award anywhere before.*

Prof. Rana Saha
Department of Mechanical Engineering
Jadavpur University
Kolkata-700032
India

JADAVPUR UNIVERSITY

KOLKATA-700032

Index No.:- 22/14/E

BIBLIOGRAPHY OF DOCTORAL DISSERTATION

Faculty	: Faculty of Engineering & Technology
Department	: Mechanical Engineering
Name of the Degree	: Doctor of Philosophy in Engineering
Name of the Candidate	: Sri Nitesh Mondal
Fellow	: Senior Research Fellow (RGNF)
Title of the Thesis	: Pressure Compensator Design for a Variable Displacement Swash-Plate Type Axial Piston Pump
Date of Registration	: 27th August, 2014
Date of submission of thesis	:
Name of Supervisor	: Prof. Rana Saha
Nationality	: Indian
Signature of the candidate	:

To

Dima and Dadu

Acknowledgements

First and foremost, I would like to thank my thesis advisor, Prof. Rana Saha, for his valuable guidance, advice, encouragement and warm support at every step of my doctoral programme. He continually and realistically conveys a spirit of adventure about research, scholarship and an excitement regarding teaching. This has been a precious opportunity for me not only to gain knowledge and skills, but also to learn much more about approaches, attitudes towards work and interpersonal relations.

I would like to express my sincere gratitude to Prof. Dipankar Sanyal and Dr. Saikat Mookherjee for their insightful guidance during all phases of this research and I owe them lots of thanks for his help on numerous questions. I would like to express my heartfelt thankfulness to my senior lab mate Dr. Nimai Pada Mandal for his significant guidance and continuous support toward the work. I would also like to convey my special thanks all the faculty in Neptune lab of Mechanical Engineering Department to Prof. Kamalesh Mazumder, Prof. Sankar Dhar, Prof. Swarnendu Sen, Prof. Achintya Mukhopadhyay, Dr. Kaushik Gosh and Dr. Nirmal Kumar Manna for their continuous support, encouragement and useful suggestion during all phases of this research and give me a homely place at Neptune at every moment. I would like to extend my sincere thanks to Prof. Goutam Majumder, Head, Department of Mechanical Engineering, Jadavpur University.

I am also very grateful to my friends - a long time with a great accompany Susil Kumar Mondal, Tapan Sarkar, Barun Mondal, Md. Anwar Kabir, Manas Chowdhury, Sanchita Biswas, my lab-mate - Pranibesh Mandal, Shouvik Choudhuri, Sibsankar Dasmahaptra, Debojit Saha, Arindam Mondal, Shrisendu Mandal, Aniruddha Sarkar, Aritra Mukherjee, Krisnendu Maji, Abu Bakkar Shiddiki Thakur, Pallab Sinha Mahapatra, Nripen Mondal, Arijit Banerjee, Nirmalendu Biswas, Priyankan Datta, Aranyak Chakravarty, Ritobrata Saha, Amlan Garai, Sourav Sarkar and JU short hand cricket team who made this long and arduous Ph.D. process, an enjoyable and memorable time.

I would like to address my gratitude to all members of Mechanical Engineering Department and Hydraulics Laboratory for making the everyday work enjoyable and inspiring. I gratefully acknowledges to UGC RGNF Fellowship, ARDB for providing

i

Nomenclature

A_L : area of load orifice (m^2)

c_d, c_v : discharge and velocity coefficient respectively

c_{rc}, c_{sc}, c_{bc} : radial clearances between rate piston and cylinder, stroking piston and cylinder and barrel piston and cylinder respectively (μm)

d_d d_{rp}, d_{sp} : diameters of the capillary hole through the piston, rate piston and stroking piston respectively (m)

d_p : diameter of barrel piston (m)

d_s, d_{sr} : diameters of spool land and modified spool land at the return side respectively (m)

d_{or} : diameter of the orifice of spool at right end side (m)

I_s : mass moment of inertia of cradle and its lever (kg-m^2)

k_r, k_s : stiffness of rate cylinder spring and spool bore spring respectively (N/m)

l_b : length of the orifice inside the each barrel piston (m)

l_{rt}, l_{st} : respective distances from barrel axis to rate piston axis and stroking piston axis (m)

m_r, m_s : masses of rate piston and stroking piston respectively (kg)

m_p, m_{sv} : masses of barrel piston and spool respectively (kg)

n : number of barrel pistons

n_p : number of ports at control spool

P_l : pressure at the right side of spool chamber (Pa)

P_{rc}, P_{sc} : pressures inside the rate piston and Pressure at stroking piston respectively (Pa)

P_d, P_r, P_s : delivery port, reservoir and suction port pressures respectively (Pa)

P_{dci}, P_{dco} : cut-in and cut-off pressures of pressure compensator respectively (Pa)

P_{pi} : pressure inside i^{th} piston chamber (Pa)

Q_L : flow rate through discharge orifice (m^3/s)

Q_{sc} : flow rate from the spool valve to stroking piston (m^3/s)

Q_{rc} : flow rate through the feedback orifice to the rate cylinder (m^3/s)

Q_{lrc} : leakage flow rate through the annulus due to the radial clearance between the rate piston and cylinder (m^3/s)

Q_{lsc} : leakage flow rate through the annulus due to the radial clearance between the stroking piston and cylinder (m^3/s)

Q_{lki} : leakage flow rate through the annulus due to the radial clearance between the barrel piston and cylinder (m^3/s)

Q_{lci} : leakage flow rate through the clearance between slipper and swash plate (m^3/s)

R_p : pitch circle radius of piston on barrel (m)

r_p : radius of the port cut on control spool

T_s, T_{rp}, T_{sp} : swivelling torque due to the barrel pistons, Torque offered by the stroking piston and rate piston respectively

V_{pd}, V_{ps} : volumes between delivery port and needle valve and between reservoir and suction port respectively (m^3)

x_r, x_s : displacements of bias piston and control piston respectively (m)

x_{pi} : displacement of ith piston from TDC (m)

$\delta_0, \delta_0, \delta_{s0}$: precompressions of bias spring and spool spring respectively (m)

β, μ, ρ : bulk modulus (Pa), viscosity (Pa-s) and density (kg/m^3) of oil respectively

λ : swash angle (rad)

ω : angular speed of barrel (rad/s)

Abstract

Variable displacement axial piston pump mostly used in energy efficient electrohydraulic circuits in applications like agricultural, forestry, construction, mining, automotive, aerospace industries etc. Such pump has the capability of adjusting the discharge as per the requirements in the loading circuit by deploying a pressure compensator arrangement. In this work, an experiment analysis and a methodology have been developed to design a pressure compensator for a swash plate type axial piston pump. Based on this methodology a parametric study has been carried out through simulink to identify some critical dimensions. Towards the end a proposition of an alternate simple control spool valve has been made as a replacement for a rather two stage control valve of the compensator.

In the first step of the work, an experimental study of pressure and flow dynamics for a commercial variable displacement axial piston pump has been carried out on different demand and different operating conditions. The effects of precompression of the top and bottom spool springs of the control spool valve on the pump dynamics have been investigated. The coupled effect of the deadband of the load valve and the pump has been identified to become critical towards maximum loading to the pump. The experimental study has also revealed that the pressure setting of the PRV should be kept substantially away (at least twice) from the cut-off setting of the pump to avoid overshoot in the pressure dynamics of the pump. It has been observed that the flow and pressure of the pump effectively depends on the rotation speed of the motor at no load condition but at full load the pressure and flow dynamics is controlled by the reference cut-off pressure setting. It is also observed that the load dynamics has a role in the performance of the pump.

In the next step, a mathematical model followed by a static design methodology has been reported for the pressure compensator with two stage spool valve of the pump at a fixed cut-in and cut-off setting. The design principle is based on the torque balance condition for a chosen cut-in and cut-off setting with an objective to check the working of the pump at various other settings. Using the developed dynamic simulation tool, some critical design parameters have been tuned, which have important role in the pump performance.

Finally, a simplified spool valve instead of a two stage spool valve has been theoretically incorporated in the pressure compensator of a variable displacement axial piston pump in order to perform a comparative study with the commercial pump. The design sensitivity of the spool valve has been carried out through simulation to identify the critical size of the parameters, which affects the pump performance. The designed compensator system has been compared first with the one having two stage spool valve through simulation and then both have been compared with the experimental result obtained from the commercial pump. The simulated results are in reasonable agreement with the experimental ones.

Table of Contents

List of Figures

List of Tables

CHAPTER-1

INTRODUCTION AND SCOPE OF WORK

1.1 Introduction to axial piston pump

Hydraulic pump is the combination unit of the pumping system and driving motor. Generally, hydraulic pump takes working fluid, mostly hydraulic oil, from the reservoir and delivers it to the rest part of the hydraulic circuit. So pump acts as a heart of a hydraulic circuit. Hydraulic pumps are classified in two categories; dynamic pressure pump and positive displacement pump. Centrifugal pump, Propeller pumps are the example of dynamic pressure pump or rotodynamic pump. This type of pump generally used in the field of agriculture, domestic services, chemical and sugar industries etc.

Positive displacement pumps are further classified in two categories one is reciprocating pump and another is rotary pump. Piston pump, Plunger pumps are the example of reciprocating pump. Gear pump, Lobe pump, Vane pump and Screw pump are rotary pump. The positive displacement pump is most commonly used in industrial hydraulic systems. A positive displacement pump delivers to the system, a specific amount of fluid per stroke, revolution, or cycle. This type of pump is classified as fixed or variable displacement.

The piston pumps are basically of three types (a) Axial piston pump (b) Radial Piston pump and (c) In-line piston pump. Axial piston pump has two groups, one is the Bent axis pump and another is the Axial piston pump with swash plate, both pumps can be made fixed and variable displacement. In case of axial piston pump the rotational axis and the pistons associated with the pump are parallel. Figure 1.1 represents the schematic of bent axis pump and Fig. 1.2 represents a CAD model of swash plate type axial piston pump with some important components. Radial piston pump also can be made variable type or fixed displacement type. In this case the pistons are connected radially with the rotating shaft. In case of In-line piston pump the positional geometry of the rotating shaft and the pistons are perpendicular.

The axial piston pump consists of a rotating group setting involving a number of axial pistons housed in the bores of a barrel that in turn is splined to the pump shaft (not shown in the figure). The number of pistons is usually kept odd (Manring 2000). Generally in hydraulic control, fixed displacement type pump and motor is used because the simple construction and control over variable type hydraulic machine. Some additional parts are required to make a pump variable from fixed displacement pump.
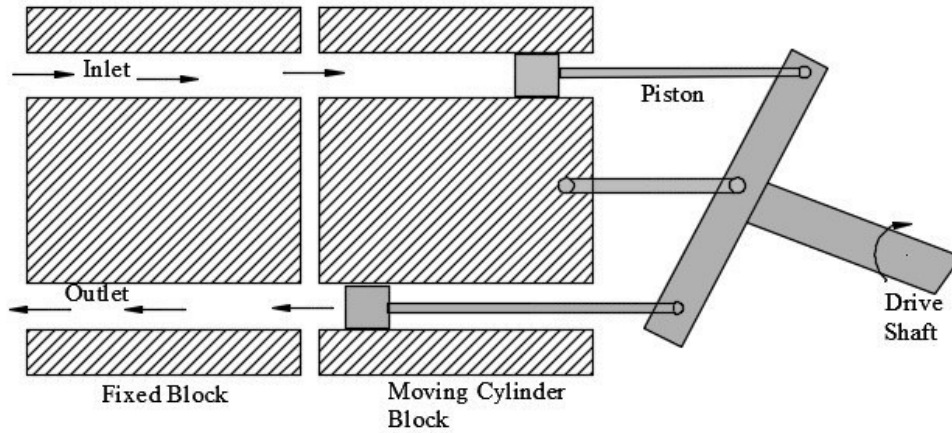
Figure 1.1: Schematic of the bent axis pump

A: Stroking Cylinder

B: Rate Cylinder

C: Swash Plate

D: Driving Shaft

E: Valve Plate

F: Retainer Plate

G: Piston Shoe

H: Barrel Piston
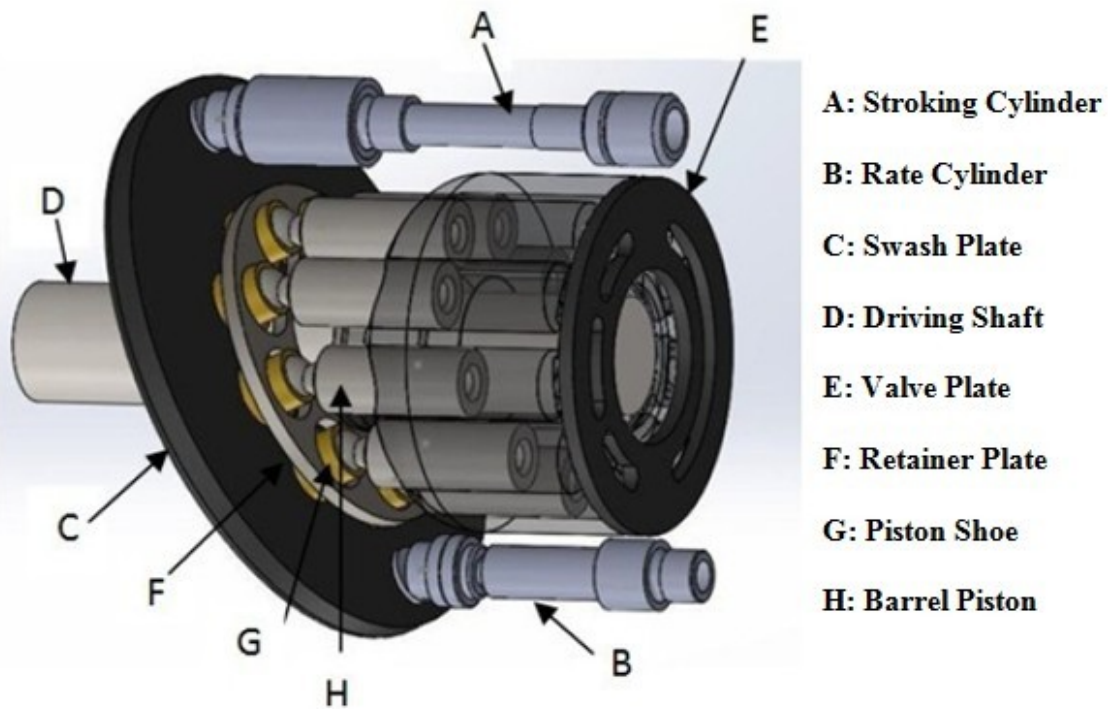
Figure 1.2: CAD model of the swash plate pump without casing

The flow control arrangement in a variable displacement pump is called the pressure compensator, in which a small fraction of the main flow is passed through a passive valve for adjusting the orientation of a component controlling the stroking volume of the pump. A swash plate is a component that is used to adjust the stroking volume of the barrel pistons. Using the delivery pressure through a spool valve to a stroking or control cylinder and directly to a rate or bias cylinder, a control torque is

produced to achieve a swivelling motion of the swash plate. Only beyond a set delivery pressure, the precompression setting of a spring in the spool valve allows the swivelling torque to develop. This is called the cut-in pressure. As the available torque becomes higher for higher delivery pressure above the cut-in limit, the steady inclination of the swash plate with respect to the plane normal to the axis of pump rotation attains a lower equilibrium value. With the reduction of the steady angle, the stroking volume of each piston becomes smaller leading to reduced delivery flow. Beyond a pressure limit known as cut-off pressure, the steady swash plate inclination approaches zero and the effective delivery flow overcoming the internal leakages becomes negligible. Such an arrangement of flow control at the pump provides large power saving over conventional valve-controlled systems. This additional arrangement provides discharge as per the requirement of the hydraulic circuit. This pressure compensator maintains the system pressure within a prescribed limit without any pressure relief valve (PRV). Consequently, the power loss through the PRV is minimized. Pressure compensated axial piston pump has the ability to provide full pump flow at pressures below the compensator pressure setting.

The demand of the pressure compensated pump has increased day by day due to its power saving performance. The typical application areas of this pump are CNC machine, agricultural, forestry, construction, mining, automotive, aerospace, excavators, loaders and transport equipment (Daher and Ivantysynova 2014, Kemmetmüller et al. 2010, Norhirni et al. 2011, Mandal et al. 2014) Such pump is also used in the regenerative braking system discussed by Norhirni et al. (2011). Achten et al. (2005) discussed about the two types of conventional pressure compensated pump such as swash plate type and bent-axis type. A pump controlled system (Daher and Ivantysynova 2014) has greater energy-saving potential than a valve controlled system and uses either a variable displacement pump driven by constant speed motor or a fixed displacement pump driven by variable speed motor. Contrasting the nearly constant delivery flow rate irrespective of the pressure rise across a fixed displacement pump, the delivery flow is adjusted in a variable displacement pump. In response to pressure rise beyond a certain limit, a valve-controlled mechanical device within the pump reduces the displacement or stroking volume in each revolution of the pump shaft. The flow rate can alternatively be

adjusted by controlling the rotational speed of the prime mover driving a variable speed fixed displacement pump. Such a pump is expected to have higher efficiency (Cho and Burton 2011), but at the cost of slower control response. Since fast control response is prerequisite in most applications, the use of the variable displacement pump remains more prevalent. Following section illustrate some significant work in the area of axial piston pump.

1.2 Review of previous work

Documented research in the area of variable displacement axial piston pump dates back more than thirty five years. Baz (1983) developed a mathematical model to describe the flow and dynamic behavior of the pump as well as the mechanism of flow control. Later this model was used as a source for devising optimal control design procedures with a target of reducing the control error as well as the response time. The frequency response analysis of the pump had been done at various conditions. Zeiger and Akers (1985) identified that the swash plate motion was controlled by the imposed torque on the swash plate due to the pumping stroke of actions of the barrel piston. This torque was found to depend on the geometrical features of the pump like radius of the rotating barrel, maximum swash angle etc. Basically linearized mathematical model had been used to get linear parameters for the equation of motion of the swash plate. Zeiger and Akers (1986) developed a mathematical model of an axial piston pump along with a swash plate control actuator with the help of a second-order differential equation of the swash-plate motion along with two first-order equations to describe the flow continuity into the pump discharge chamber and into the swash-plate control actuator. In the mathematical modelling the motion equation of the swash-plate angle contained torque components due to operating states of the pump. To determine the average torque on the swash plate an optimal method was developed considering the geometry of the pump and operating conditions. A coefficient of the equation had been evaluated through the calculation of average torque acting on the plate, which was finally validated experimentally. In a companion work, Akers and Lin (1988) applied an optimal control theory to the design a regulator for pressure control of an axial piston pump with a combination of single-stage electrohydraulic valve. In this work two spring loaded actuators had been arranged in the

two opposite ends of the swash plate to guide the dynamics of the swash plate. The motion of the spool valve was controlled by the torque motor. Two ports of the spool valve were connected with two actuators. Depending on the direction of the motion of the spool valve one of the actuators became pressurized and controlled the swash plate dynamics.

Schoenau et al. (1990) developed a simulation based model of variable displacement pump when subjected to a pressure control signal. In their work a control piston and a return spring were held in a line against the swash plate to adjust the dynamics motion of the yoke or swash plate. A detailed study of different types of torques was focused on this work considering the geometry of all parts of the system. In the simulation model four types of torque were considered to estimate the net torque acting on the swash plate. The torques were swash plate torque, yoke damping torque, torque due to return spring and control piston torque. The linearity of the control spring had great influence on the dynamic behavior of the system. In the study it was found that even though the spring was considered to be linear from static condition, during real action, the spring was bent a bit as it was compressed, the time trace of the yoke could be appreciably altered. This might be the reason for the deviations in their predicted versus measured yoke angles at small angles. Their model indicated that spring constant had a great influence at the transient response. Goto et al. (1994) modelled a hydraulic control cylinder to control the swash plate toward a large inclination-angle position, an input shaft was used to drive the pump with the help of electrical energy and a torque limiter arranged between the input and drive shafts so as to be able to disconnect the drive shaft from the input shaft when an abnormal excessive load was applied to the drive shaft thereby pro testing internal elements and parts of the pump from damage and breakage. An early study by Kaliafetis and Costopoulos (1995) pertained to modelling and simulation of the dynamic characteristics of a variable displacement pump. Barrel pistons of the pump adjust the position of swash plate and those piston are called main pistons and another pistons which is spring loaded also has a great role to adjust the swash position. The swivelling motion of the plate has been controlled by the two pistons through a certain angle. An additional orifice has been modelled in between the spool valve and stroking piston to provide better damping in the dynamic characteristics. The

control and containment forces and moments performing on the swash plate of an axial-piston pump are evaluated by Marning (1999). Manring and Damtew (2001) presented a non traditional and innovative pump which utilized a piston bore spring in its design. The purpose of the spring was holding the cylinder block against the valve plate and for forcing the pistons in a particular direction. From a practical standpoint, swash plate control and containment devices might take on many different designs; however, they must all resist the same essential moments and forces that would enable angular displacement of the swash plate from its appropriate location. In a later work, Manring (2002) focused on the control and containment forces, which were acted on the cradle-mounted, axial-actuated swash plate. To control the swash plate two control devices were introduced, which were placed two ends of the swash plate. It was concluded that an appropriate design of the control device might be used to load the cradle bearings equally during high-pressure operation. From this work it was found that an axial-actuated swash-plate tends to maintain the swash-plate fine seated within the cradle during all operating conditions. Khalil et al. (2004) mathematically evaluated the moment acting on the swash plate comes from the cylinder block due to the barrel pistons. The total moment components acting on the swash plate can be found by superimposing components due to the whole piston group.

With the advent of powerful software and computational platforms, the interest to revisit into the modelling and analysis of variable displacement pump through simulation has been increased among the researchers. Seeniraj and Ivantysynova (2006) developed a well designed valve plate, which decrease both flow pulsations as well as oscillating forces on the swash plate and investigated the effect of valve plate design on flow ripple (fluid borne noise), oscillating forces (structure borne noise) on the swash plate through a computational tool, CASPAR. Bergada et al. (2008) analyzed the pressure distribution, leakage, force, and torque between the barrel and the port plate of an axial piston pump at different condition through a complete set of mathematical equation taking into account various important factors like tilt, clearance, speed of rotation etc. A detailed study on mean force and torque over the barrel had been done and compared the torque acting on the barrel with respect to two separate axes. Kemmetmuller et al. (2009) established a mathematical model of self supplied variable displacement axial piston

pump, which can control the pressure as well as flow rate as per the demand of fast changing undefined loads. In this work a variable axial piston pump was coded for the injection molding machines, where liquid plastics was injected into a die by a screw conveyor. Using the mathematical model an excellent change in the pressure and flow had been found according to the change of load and the performance of the control theory was verified with experiments.

Gilardino et al. (1999) presented an analysis of the simulated behavior of two displacement control systems of an axial piston pump using AMESim software package. The load sensing system operation subjected to varying load was discussed.Using the similar simulation environment, a hydraulic model of a high pressure variable displacement vane pump was validated experimentally in terms of steady-state flow-pressure characteristics and of displacement control dynamics (Rundo and Pavanetto 2018). Park et al. (2013) developed a pressure regulated variable displacement pump model coded with commercial software AMESimto simulate the performance of the pump at different condition. The robustness of the simulation based mathematical model of the constant power regulator system was demonstrated by comparing simulation results with real time results. To regulate the pressure and flow of the pump two cylinders are used, namely control cylinder and counter balance cylinder attached with the two ends of the swash plate. A spring loaded spool known as pressure regulator was also used to control the dynamics of the control cylinder and counter balance cylinder. Study was conducted, using simulation model, to find the source of the rough performance of the mechanical-type constant power regulator system, the effects of main components such as the spool, sleeve, and counterbalance piston. The shape modification of the counterbalance piston was proposed to improve the undesirable performance of the mechanical-type constant power regulator.

Ericson (2013) developed a simulation model for understanding the behavior of pump-motor assembly at variable displacement angles. Different forces on the swash plate due to the pressure ripple in the pump and the consequent oscillations of the swash-plate were modelled and investigated. It was found that the pulsating pressure in the control actuator had no major impact on the flow and force pulsations. The swash plate oscillations due to the internal piston forces, however, were significant and expected to

affect the outlet flow pulsations. In fact, in another work (Ericson, 2014), it had been shown that the oscillations on the swash plate had an effect on both efficiency and flow pulsation responsible for the noise level.

The reporting of design aspect of the variable displacement axial piston pump is scanty. Gao et al. (2013) designed a pulsation attenuator for a variable axial piston pump for aircraft application. In this work a pressure compensator had been used to control the flow and pressure. The delivery line of the pump was connected to the spring loaded control valve but it was not connected with the bias actuator. Instead of pressure feedback a high stiffness spring was used in the bias actuator. Pressure at the control actuator was governed by the spool valve. An attenuator was placed in the discharge line to reduce the flow ripples of the system. Mandal et al. (2014) carried out a simulation based optimal design of a pressure compensated variable displacement axial piston pump to minimize the transient oscillations of the swash plate and the compensator spool, proper pressure control inside the control and bias cylinder to avoid over pressurization and cavitation at any circumstances. The study revealed that the orifice diameters in the spring side and at the metering port of the spool valve and in the backside of the bias cylinder had critical role for the performance of the pump.

Till date most of the researchers have analyzed, through mathematical modelling, the various aspects of displacement pumps like swash plate characteristics (Achten 2013, Ericson, 2013, 2014), leakage and flow ripple characteristics (Bergada et al. 2012, Lin and Hu 2015), flow and pressure dynamics characteristics towards minimizing this fluid-borne noise for fixed cut-in and cut-off settings (Schoenau et al. 1990, Mandal et al. 2008, 2012, Zaki and Baz 1979, Baz 1983) as well as lubrication aspects in the slipper pad (Tang et al. 2017).

From the above review in the relevant area, it is found that the design of a pressure compensator is important for achieving low-noise flow control over wide range cut-in and cut-off pressure variations. Also, real time understanding of the dynamic characteristics of variable displacement axial piston pump under different operating condition remains another important aspect that needs to be explored.

1.3 Scope of work

The study is aimed at developing an experimental setup in which a commercially available pressure compensated variable displacement pump could be tested at different operating conditions. The principal of operation of such pump is elaborated in the next section. For this pump, the conditions could be setting of different cut-in and cut-off pressure, different loading to the pump as well as different speed of the driving motor. The main focus is to capture the flow and pressure dynamics of the pump under such conditions. Also an attempt will be made to understand whether there are any coupled effects of other components of the test setup on the performance, particularly on the dynamics of the flow and pressure. Since the pressure compensator consists of a two stage control valve, the effects of precompression of the top and bottom spool springs of the control spool on the pump dynamics have been aimed at.

A design methodology for pressure compensator with two stage spool valve of a variable displacement swash plate type axial piston pump has been aimed at based on some simple mechanistic principle. The methodology involves a static design step to find the appropriate sizes of the pressure compensator components for specified cut-in and cut-off pressure limits. In the design process, a comprehensive mathematical model of the pump compensator system will be developed, which could be used for the dynamic simulation to identify some critical parameters of the pressure compensator. The simulated performance of the designed model of the pump compensator system is aimed to be verified through the experimental result.

The design methodology, once qualified, could be used to design an alternate single stage control spool valve instead of two stage complicated spool valve. Lastly, performance comparison between proposed and existing spool valves of the pressure compensator will be carried out through simulation and experimental result.

1.4 Operating principle of pressure compensated axial piston pump under study

The variable displacement swash-plate type axial-piston pump studied here, is an adaptation from the commercially available A10VSO series pump from Rexroth (Rexroth Bosch Group, 2004) having multipurpose applications (DR, DFR or DRG) through single

unit. For the sake of study, the pump has not been used in the usual way it is meant for. As shown in Fig. 1.3. One of its main components is the pressure compensator and the other is the rotating group with nine pistons. The pistons, supported by a tilted stationary swash-plate, are able to reciprocate inside respective bores of a barrel set in rotation by a splined shaft. The angle between the swash-plate and the barrel face determines the amount of swept volume during one cycle of rotation of any piston. Facing a flat end of the cylindrical barrel, there is a valve plate having kidney-shaped suction and delivery manifolds separated by two bridges, all having a small radial spread about a common pitch circle. Each barrel bore, which is essentially cylindrical, is given a matching kidney shape of smaller angular extent towards the valve plate. As each piston discharges a specific volume of liquid, the discharge at the pump outlet is sum of all the discharges from the individual chambers. An in-line pressure compensator used for actuating the swash plate, which has a spool valve and two piston-cylinder pairs parallel to the rotating shaft located on its opposite sides.

A:Suction Port   B: Delivery Port   C: Valve Plate   D:Suction Kidney Port   E:Delivery Kidney Port   F: Barrel   G: Barrel Bore
H: Barrel Piston   I: Swash Plate   J: Bearing   K: Double Spool Valve   L: Stroking Piston   M: Rate Piston   N:Retainer   O: Bush
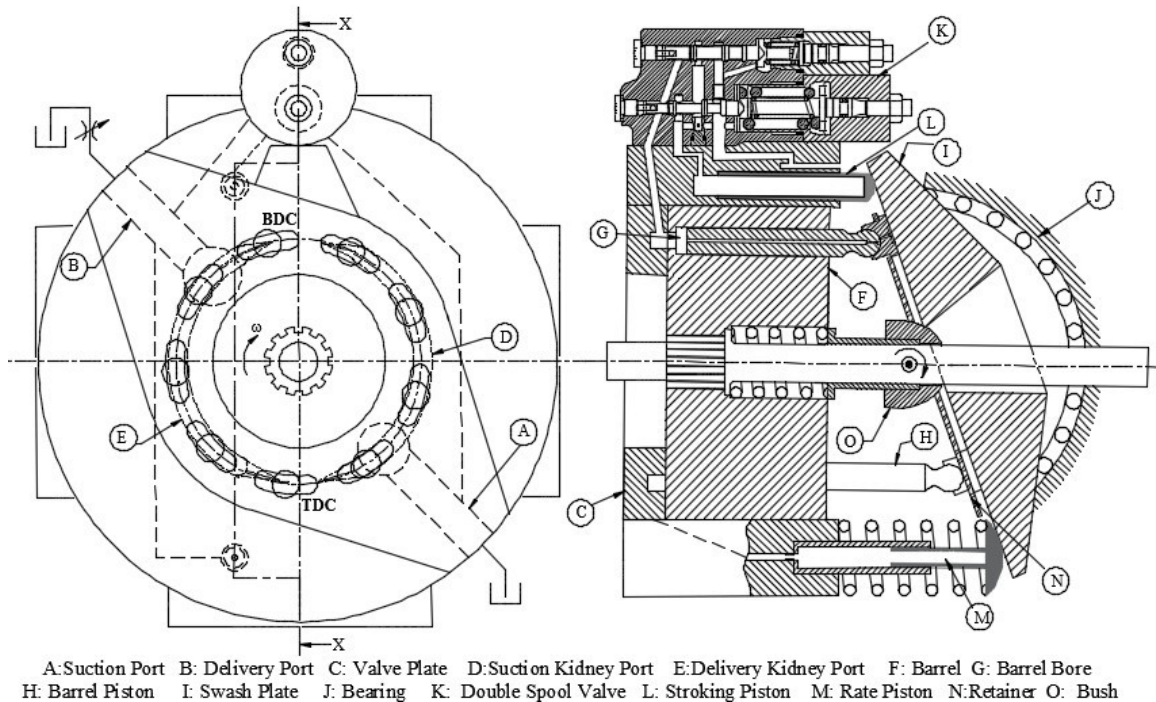
Figure 1.3: Schematic of a swash-plate axial piston pump with pressure compensator

As detailed in Fig. 1.4, the control spool valve has two stages, each with a spool. The top spool valve is considered as load sensing valve having a spring of stiffness lower than that on the bottom spool. Since the maximum pressure of the system is controlled by

11

the bottom spool, this is considered as a part of a pressure sensing valve. Two concentric springs are used to achieve high stiffness against the displacement of the bottom spool. The operating principle of both the spools is identical. Through a number of circumferential holes meeting a connecting axial hole cut within each spool, its flat face towards the plug side receives the delivery pressure. Oil enters the volume between the spool and the plug from the delivery side of the pump through inlet port **P** and the corresponding valve chamber. A set screw is provided for adjusting the spring precompression and the oil pressure tends to move the spool against the spring. As long as the spring force dominates, the spool remains stationary. Once the pressure force overcomes the spring force, the spool starts moving rightward causing the control port **A** to get connected with the inlet port **P**. One of the actuators, called the stroking piston is actuated by the flow connected with the control port **A** of the spool valve. The other piston, termed as the rate piston, is concurrently actuated by a pilot flow from the delivery line of the pump. The rate piston is also loaded by a spring to ensure the initial swash angle for obtaining the pumping action. The preset compression of the bias spring in the rate piston determines the swash angle corresponding to the rated discharge of the pump.
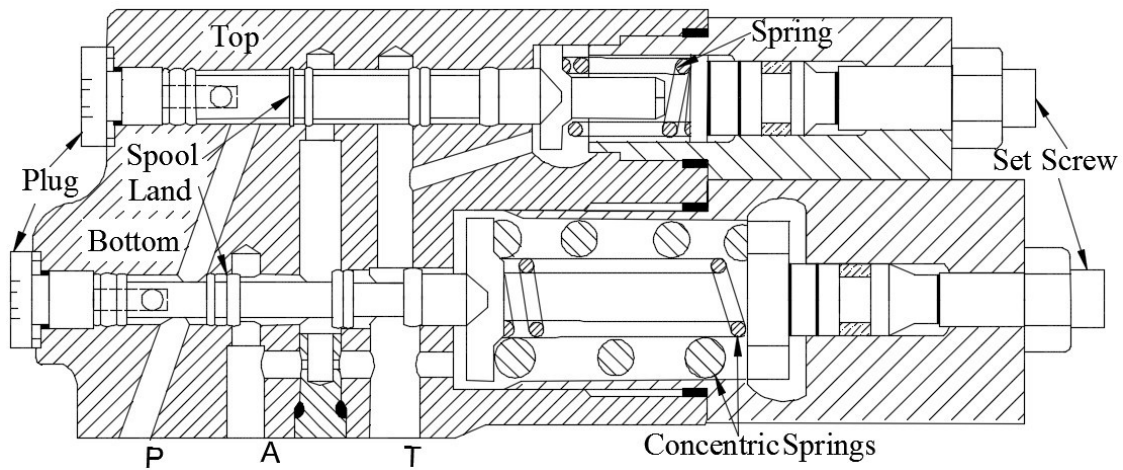
Figure 1.4: Schematic of the two-stage control spool valve

The pressure at which the spool starts moving towards right against the spring is denoted as cut-in pressure. Depending on the set precompressions, the top and bottom spool can have different cut-in pressures. Normally the top spool is set at a lower cut-in pressure than the bottom spool. For a delivery pressure range below the lower cut-in

value, the top spool of the control valve is held against a precompressed spring so as to keep the valve closed and thereby isolating the stroking piston from the pump delivery line. With pressurization above the lower cut-in value, the top spool is displaced, eventually connecting the stroking cylinder with pump delivery. A flow is thus initiated to the stroking cylinder that causes the stroking piston to extend, resulting in swash-plate rotation to reduce the swash angle. Correspondingly, the swept volumes of the rotating pistons are reduced and so also the pump discharge. The rotation of the swash-plate under the action of the stroking cylinder is in opposition to the torque exerted on the swash-plate by the spring-loaded rate piston. Thus, equilibrium is attained at a lower swash-angle. Due to the spring action, higher displacement of the top spool calls for higher delivery pressure. Increase in the delivery pressure beyond the upper cut-in limit leads to the displacement of the bottom spool. Due to the displacement of this spool, the stroking piston receives flow from the delivery side through the metered orifice of the bottom spool at a higher pressure. This causes the stroking piston to exert higher torque on the swash plate leading to lower swash angle. The minimum angle actually corresponds to the cut-off condition of the pump, in which the delivery flow becomes zero and the corresponding pressure is denoted as cut-off pressure.

1.5 Outline of the thesis

Other than Chapter 1, the main work of this thesis is organized in another five chapters followed by two appendixes. In Chapter 1, a general description of an axial piston pump is followed by literature review to identify the present scope of work. A detailed overview of the pump under study has been provided in this chapter. Chapter 2 details the experimental setup and the exhaustive testing done on the pump at different conditions. The design methodology including the mathematical modelling has been documented in Chapter 3. Simulation study to obtain the sizes of critical parameters followed by comparison with experimental results has been presented in Chapter 4. The proposition of an alternate spool valve keeping the other parts of the pump same has been reported in Chapter 5. Finally, the salient features of the overall work, conclusion of the overall study and future scope of work has been included in Chapter 6.

CHAPTER-2

EXPERIMENTAL STUDY OF A PRESSURE COMPENSATED AXIAL-PISTON PUMP

2.1 Overview

In order to study the characteristics of variable displacement axial piston pump with pressure compensator, an experimental setup has been developed. It consists of electrical, electronic and hydraulic components and instruments. In this chapter, a detailed description of the experimental setup has been presented. Since capturing of dynamic behavior is of prime concern, it is important to identify the role of other components in the setup that could affect mainly the dynamic performance of the pump. First, the role of precompression of the two separate springs of the spool valve of the pressure compensator has been established experimentally. From observation it is found that the presence of the load valve and the pressure relief valve in the circuit could affect the performance of the pump. Through experiment an attempt has been made to isolate the effects of those components in the dynamic performance of the pump. The experimental study has been extended to understand the behavior of the pump under different speed of the motor. It is also important to identify the response of the pump under different rate of change of loading.
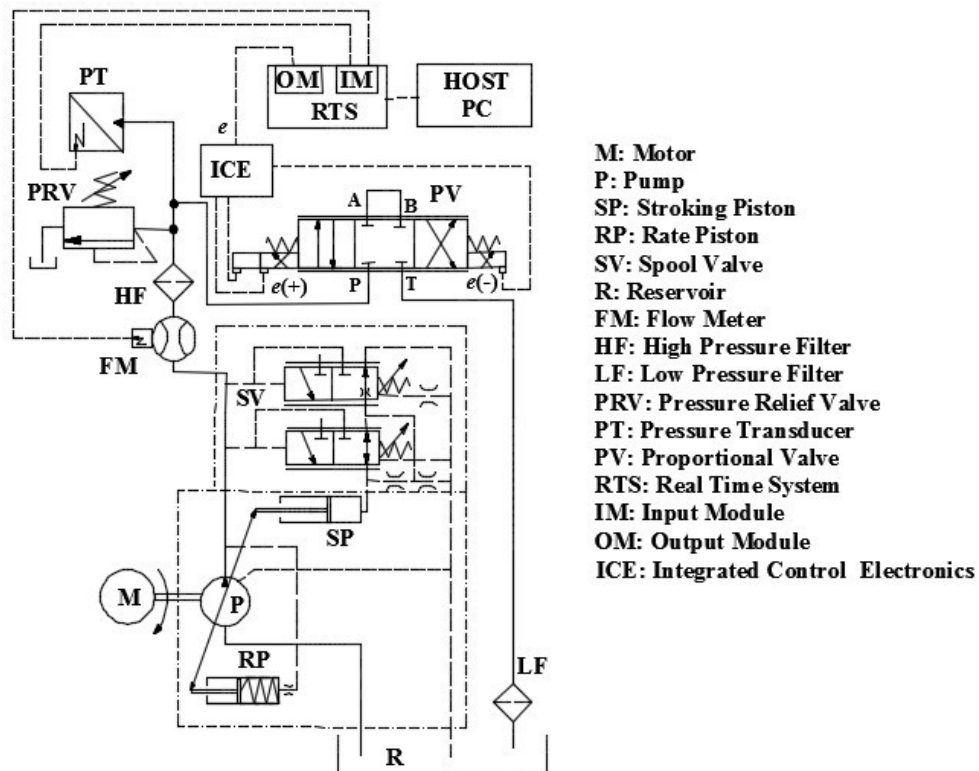
Figure 2.1: Circuit diagram of the system

15

2.2 Description of the hydraulic circuit and test setup

Figure 2.1 shows the symbolic representation of the hydraulic and electric components of the experimental setup that consists of a Rexroth A10VSO series, size 45 with DR pressure control variable displacement axial piston pump. The volumetric displacement of the pump is 45cc with maximum speed of 3100 rpm. The rated operating pressure at the suction side is 0.8bar whereas the nominal and maximum peak pressures at the delivery side are 280bar and 350bar respectively. Unless otherwise mentioned, the experiment is conducted at a speed of 1200rpm. A 3 phase, 2-pole induction motor from ABB is attached with the pump through the drive shaft. A variable frequency drive (VFD) is used to control the speed of the motor as per requirement. The working fluid of the system is typical petroleum based hydraulic oil (HLP68), which is pumped from the reservoir (R) and discharged back to the same reservoir of dimension 1mx 0.6m x 0.5m. Filtration of the hydraulic fluid is very important for the longer service life of the pump and all other hydraulic components of the setup (Rexroth Bosch Group 2004). A commercial high pressure filter (HF) is used for the filtration of the hydraulic oil in addition to the return line low pressure filter (LF). Although pressure relief valve is not mandatory in system employed with variable displacement pump, a two stage Pressure Relief Valve (PRV) is used in the present setup for safety. The maximum pressure is set at 200bar by the PRV. The symbolic diagram of the pump showed in the envelope of long chain lines consists of two parts. The pump body and the two single acting cylinders of the pressure compensator, namely rate and stroking cylinders, are arranged in a single casing known as pump casing, whereas the control spool valve is fitted on the pump casing. Symbolically, the arrow in the pump can be thought of as the swash plate, which is acted upon by the two cylinders at its end. The rate cylinder is connected with the pump delivery through a pilot line via an orifice, whereas the stroking cylinder gets oil from the delivery side of the pump through the control valve denoted as SV. This control valve has two spools as shown in the figure, which is set against individual springs the precompression of which are adjustable by set screws. From the pilot lines shown in the symbolic diagram, it is evident that the SV can be operated by any one of the spools or by combination of both the spools to connect the stroking cylinder with the delivery of the pump through a pilot line.

16

Loading to the pump in the experimental setup is achieved using a Rexroth 4WREE series proportional valve (PV), the control ports (A and B) of which are being short circuited. The main delivery line of the pump is connected with the P port of PV as shown in the figure. By regulating the command voltage *e* through the onboard Integrated Control Electronics (ICE), the flow passage of PV can be throttled, which result pressure would build up in the delivery side of the pump. Clearly, the PV acts as the load orifice for the pump. Zero area of opening of the orifice indicates the spool land completely covers up the valve port. This implies full closure of the path for the pump flow, which will lead to pressure build up in the hydraulic circuit till the cut-off pressure set by the set screws of the SV is reached. Full or 100% area opening indicates maximum opening area of the orifice, which would lead to maximum flow to the system at a nominal pressure. The first situation is analogous to full-load condition whereas the second one is analogous with no-load condition of the pump. A typical variation of PV voltage with time used in the experiment is shown in Fig.2.2.
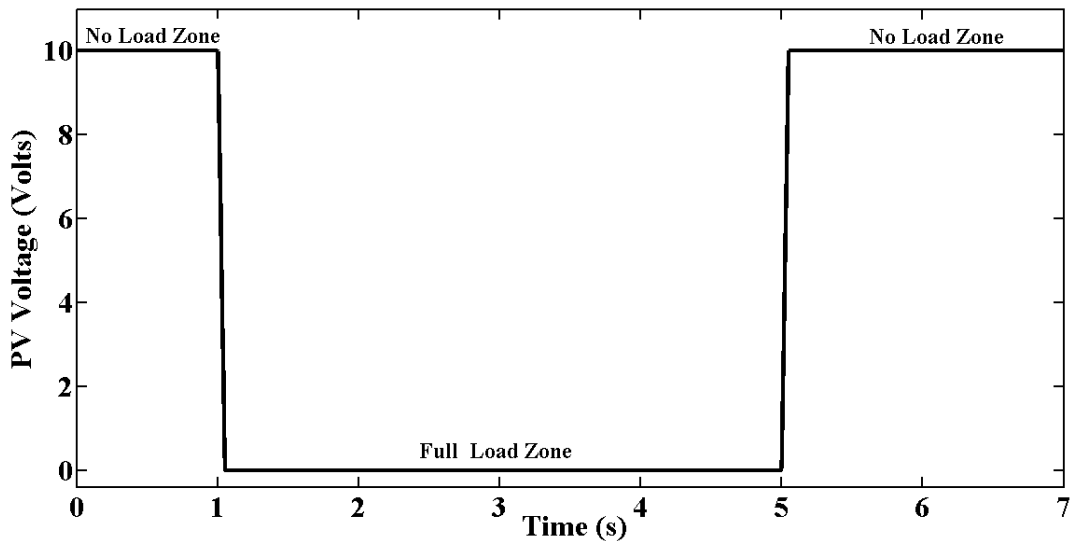
Figure 2.2: Loading pattern on the pump through PV voltage variation

The delivery pressure of the pump has been measured by a pressure transmitter (PT) from Kistler having range 0-200bar (abs) with accuracy of ±0.25% (Full scale) and about 3 to 4kHz -3dB bandwidth. A flow meter (FM) is installed very near to the pump casing on delivery line of the pump. The captured data have been processed through an

17

input module (IM) of the real time system (RTS) from NI. From the host PC, the load orifice opening profile has been processed through an output module (OM) and is sent to the PV through the ICE. The delivery pressure and the flow rate of the pump are measured corresponding to this voltage feed via the pressure transducer and the flow meter respectively. These analog signals from the flow meter and pressure transducer are relayed back to the HOST PC for purposes of storage and analysis via the input module (IM) of the real time system. This electrohydraulic system is controlled through a Graphical User Interface (GUI) developed in the LabVIEW software environment installed in the HOST PC. So the HOST PC is the controller of the system. The control law implemented in the hardware RTS generates analogue voltage, which is fed to the PV via the output module OM. The assembled view of the setup has been shown in Fig. 2.3. The details of the hydraulics and electrical components have been given in Table 2.1. The experiment has been conducted an open atmosphere keeping oil temperature around 40^0c. The readings have been recorded after 5 minutes of running the system at no load condition.
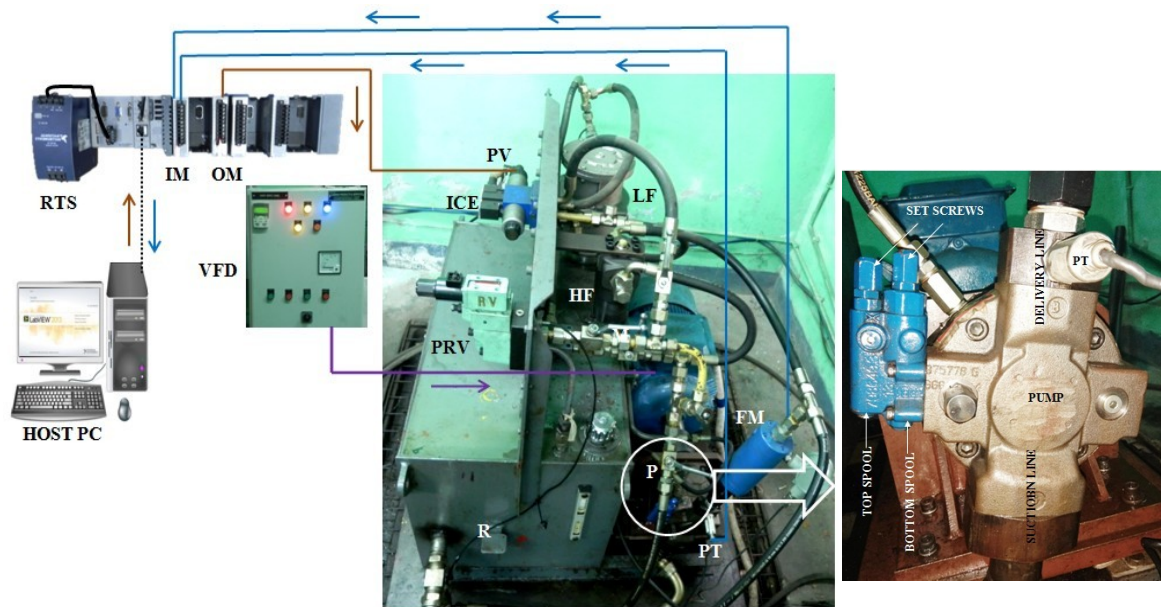
Figure 2.3: Photographic view of pump testing system

Table 2.1: Details of the set-up components

Component (make)	Specifications
Motor, **M** (ABB)	3-phase; 37 KW; 2945 rpm;
Varibale Frequency Drive, **VFD** (ABB)	30 kW
Pump,**P**(Rexroth)	A10VSO 45DR/31; 45cc nominal displacement
Pressure Transducer, **PT** (Kistler)	0-200 bar;Temp:-20 to 85°C; Linearity, Hysteresis and Repeatability ±0.25%
Flow meter, **FM** (Kralsupplied by Rockwin Industries)	Working Pr.0-250 bar; Flow 2-100 lpm; Maximum temp 120°C;Accuracy±0.1%
Filtter, **F** (Stauff)	Maximum working pressure 420 bar
Proportional valve, **PV** (Rexroth)	4WREE series;50 lpm at 10 bar pressure drop
Hose Pipe (Parker)	250 bar;16mm(5/8)
Pressure Relief valve,**PRV**(Yuken)	EBG-03-H-11; 205bar
Real-time system, **RTS**(NI systems)	1GHz, 32-bit NI-cRIO 9081
Input module, **IM** (NI systems)	±10VA/D NI-cRIO 9215
Output module, **OM** (NI systems)	±10V D/A NI-cRIO 9263

2.3 Experimental study

2.3.1 Study of precompression of the spool valve

Keeping the load dynamics as shown in Fig. 2.2, and top spool fully compresed, the effect of precompression of bottom spool spring has been studied at the rotation speed 1200 rpm of the pump shaft. Generally, at full load condition the flow rate of the pump is minimum and pressure is maximum. This is violated when the pressure goes beyond the relief valve setting. The meaning of percentages in the legend of the following figures needs some explanation, which is given below.

In case of bottom spool there are 11 possible turns to compress its spring maximum from its initial preset or minimum precompression. Therefore, each turn indicates 9.09% increment in the spring compression. As a consequence, 10 turns

indicate about 91% increase in the precompression. Similarly in case of top spool 3.5 turns is enough to reach the full compression state of the spring from its minimum precompression. Hence, in this case one tuns indicates 28.5% increment in the compression length of the spring. Thus 2.5 turns indicates 71.4% increase in the compression and 0.5 turns indicates 14.28% increase in the compression and so on. In this context, minimum precompression is defined as 0%.
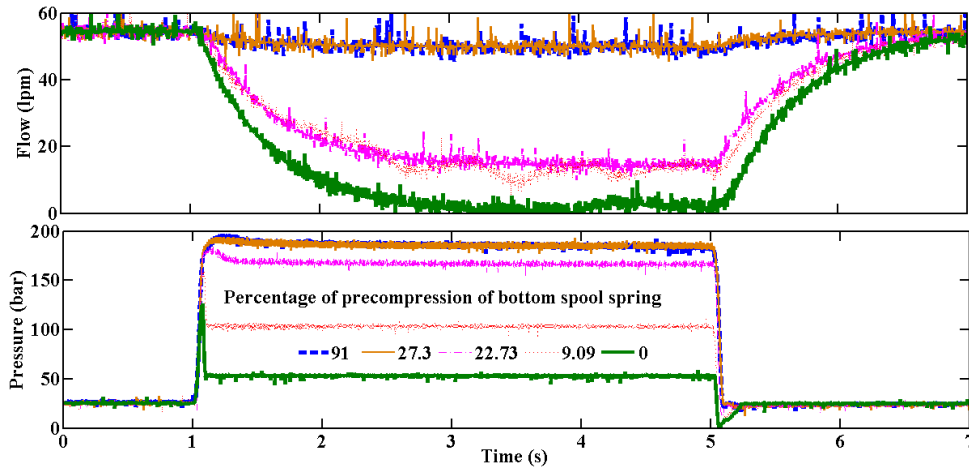
Figure 2.4: Effect of precompression of bottom spool spring of spool valve 1200 rpm
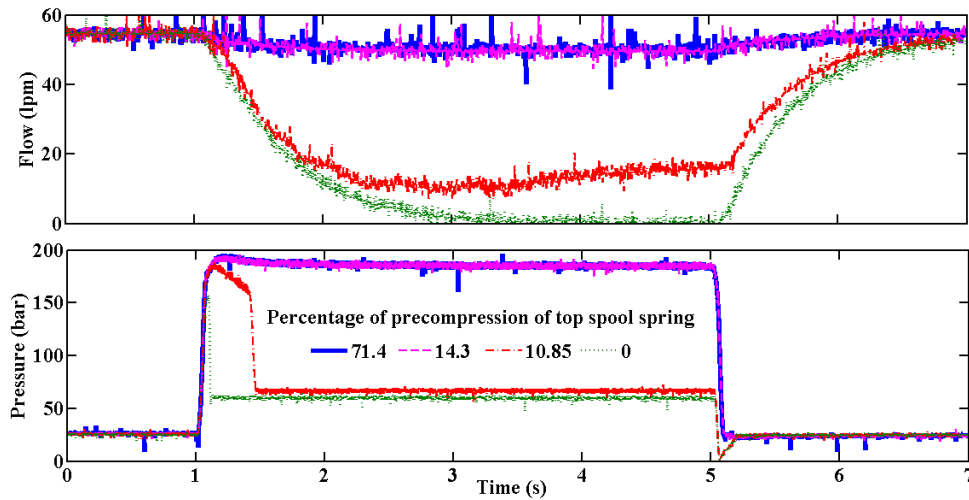
Figure 2.5: Effect of precompression of top spool spring of spool valve at 1200 rpm

Due to the high stiffness of the bottom spool spring the precompression can not be increased beyond 27.3% with the present setting of PRV. The pump beyond this precompression operates as a fixed displacement pump which is evident from the flow

20

and pressure saturation for 91% and 27% precompression. If is precompression below 27.3% the pump pressure attains value less than the PRV setting and the flow gets reduced indicating the variable displacement nature of the pump.

Similarly the effect of precompression of the top spool spring has been studied keeping the bottom spool precompressed at it maximum. This spring shows high sensitivity in the range of 10.85% to 0% precompression as evident from Fig.2.5. Upon reduction in precompression from 10.85% to 0%, a sharp fall in pressure can be witnessed from around 200 bar to 60 bar at full load.
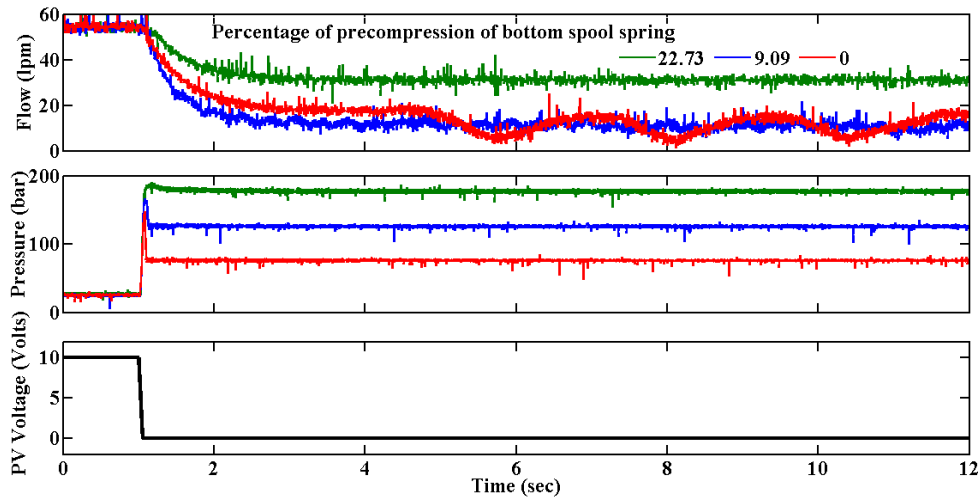
Figure 2.6: Effect of precompression of bottom spool spring on steady state at 1200 rpm
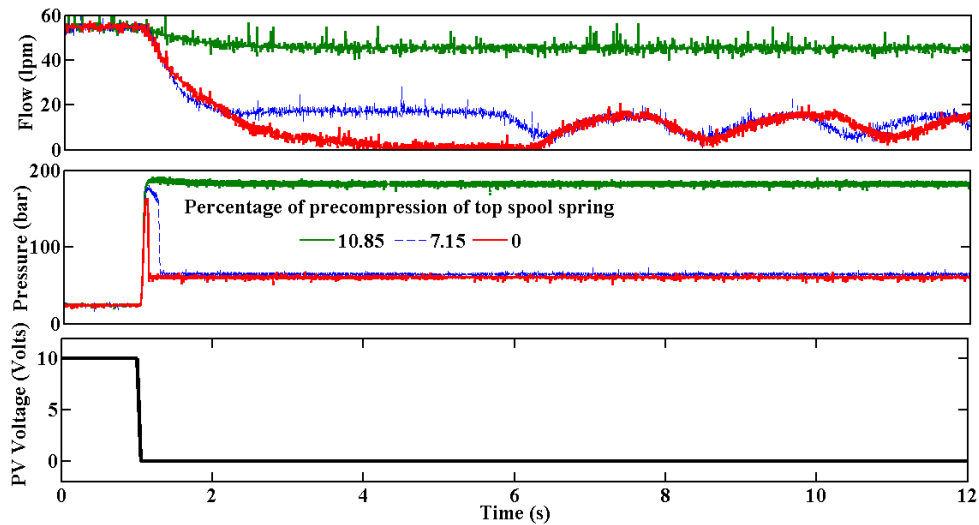
Figure 2.7: Effect of precompression of top spool spring on steady state at 1200 rpm

21

Observing increase in flow rate with time particularly for 10.85% precompression, experiments were conducted for extended time keeping PV closed. These have been done for both the cases, controlling bottom and top spool as done earlier.

As shown in Figs. 2.6 and 2.7 it was observed that there were low frequency flow oscillations although the pressure for all the cases attain steady state within fraction of second after closing the PV.

Based on such pump dynamics, it is evident that control of the spring precompression percentage becomes a critical issue within the lower compression zone, especially when the precompression is adjusted manually. It would be useful for the user, if a digital interface is provided in order to precisely view this percentage.

2.3.2 Separation of deadband of PV from pump dynamics

Theoretically, zero control voltage to the PV indicates full closure of the flow passage, which will result the delivery pressure to reach at the cut-off setting of the pump. However, experimentally an interesting feature has been found on the flow dynamics of the pump. As shown in Fig 2.8a, zero control voltage to the PV, the flow rate of the pump shows an oscillating of about 0.33 Hz and amplitude of about 7.5 lpm. This feature of the flow dynamics at high loading apparently hints towards unsteadiness of the swash plate of the pump. However, repetitive experiments have carried out to check the consistency of flow oscillation for zero command voltage on PV as shown in Fig. 2.8(a). While the delivery pressure dynamics remain unaffected, the flow rates have been observed to remain oscillatory. Instead of zero command voltage, a small non-zero voltage to the PV results a steady and consistent minimum flow rate of the pump maintaining the pressure at the cut-off. It is thus revealed that the inconsistencies in the flow characteristics in terms of phase the oscillations at zero command voltage are attributed to the deadband of PV (typically 20%) (Chaudhuri et al. 2017, Sarkar et al. 2013) Thus, the maximum loading can be considered as that corresponding to the minimum voltage at which a steady, minimum and consistent flow rate can be found from the pump. Incidentally, it has been found that the minimum flow rate of the pump under testing is not zero, indicating that the swash plate does not orient itself at zero degree swash angle during full load. Instead a minimum angle is maintained to provide a

22

nominal flow essential for internal leakages. As shown in Fig. 2.8(b), the minimum voltage of 1.8 volts to the PV, where the pump gives the minimum steady flow is considered as 0% opening area of load valve. The full flow and minimum pressure on the pump delivery line are achieved from the pump applying 10 volts to PV. This 10 volts indicates the full or 100% opening area of load valve.

Figure 2.8: (a) Effect of deadband in PV on the pump performance – same, repetitive PV voltage
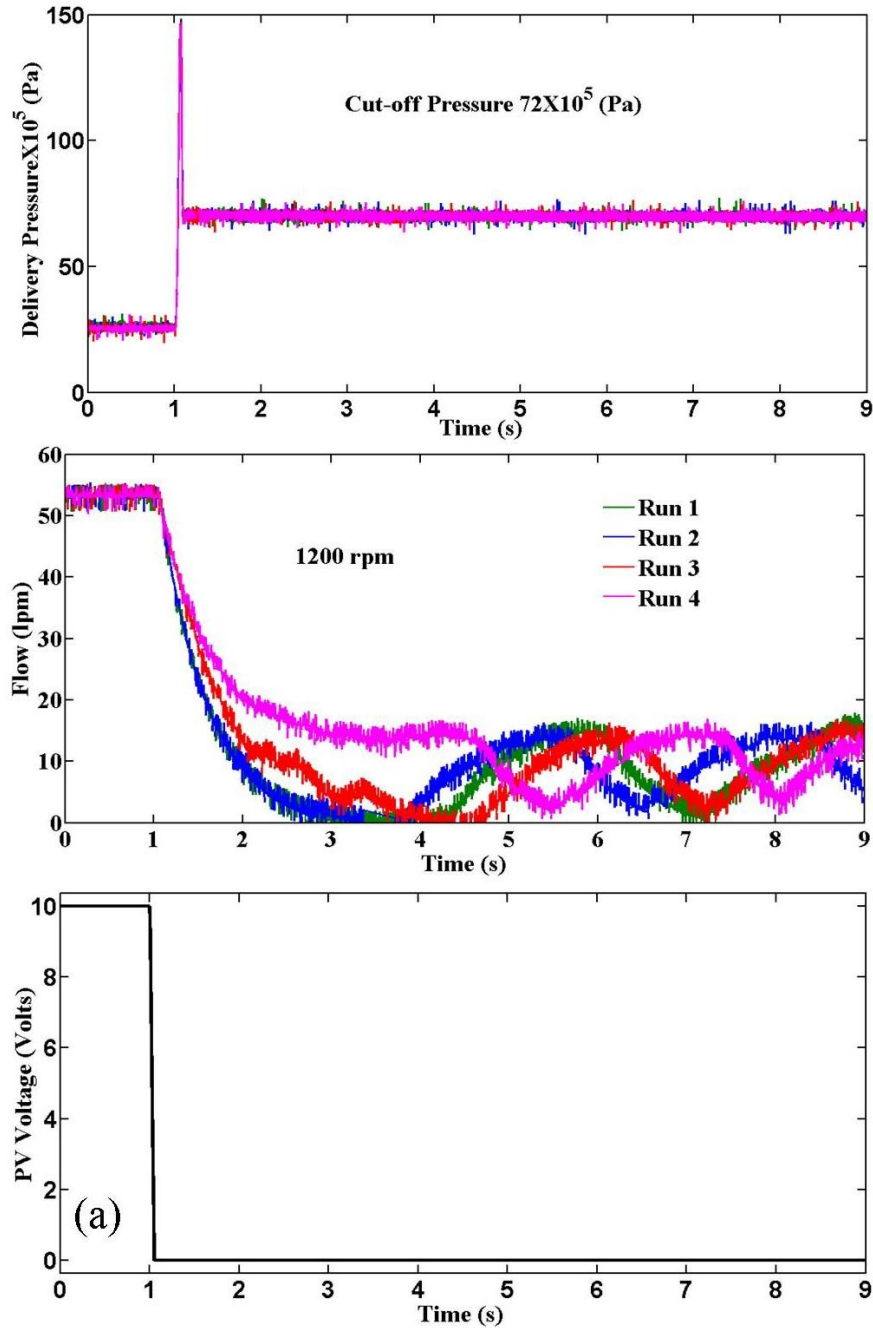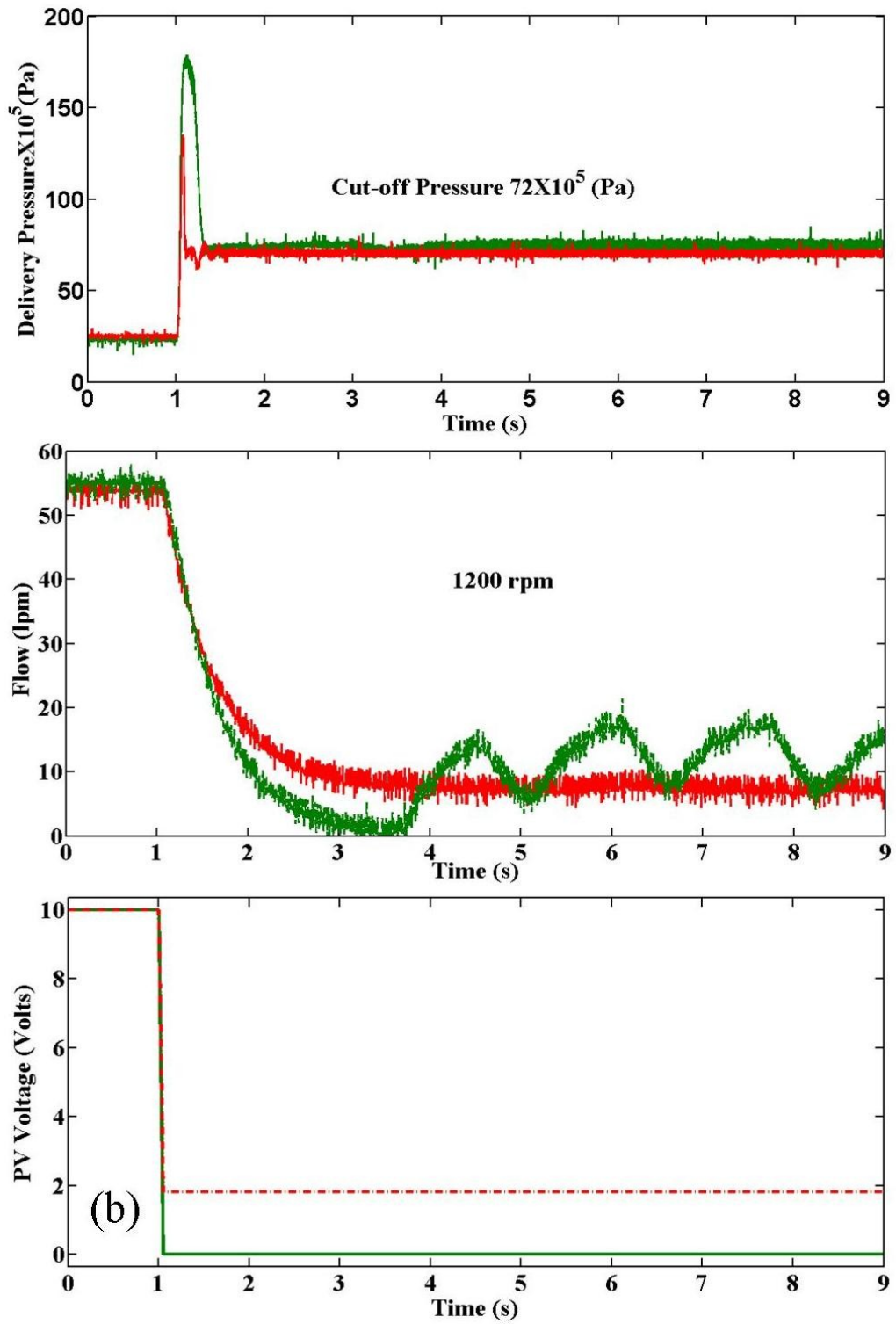
Figure 2.8: (b) Effect of deadband in PV on the pump performance – different PV voltage

2.3.3 Separation of PRV dynamics from pump dynamics

A pressure relief valve (PRV) is not necessary in the electrohydraulic system employing a variable displacement axial piston pump. However, while a real time study is carried out to test the characteristics of such pump, a pressure relief valve is engaged in the hydraulic circuit to avoid any kind of accident due to high pressure. For testing, it is essential to identify the margin between the reference setting pressure of the PRV and the cut-off pressure of the pump such that the dynamics of the PRV remain separated from the dynamics of the pump. Otherwise a dynamics of PRV could be reflected on the dynamics of the pump. For a fixed rotational speed of the motor 1200 rpm, two different cut-off pressure setting, the effect of PRV has been studied. For two different cut-off settings of the pump, experiments have been conducted with three different PRV setting for each. For 155 bar cut-off setting, using the same loading pattern (corresponds to 1.8 volts) as shown in Fig 2.8(b), it can be seen that the steady state delivery pressures for all three PRV setting remain fairly similar but there are substantial changes in the flow pattern. For 160 bar PRV setting, there is hardly any change in the flow rate after the closure of PV. This is due to the fact that in this case before change in the swash angle, the PRV gets cracked and the pump's flow is directed to the tank through the PRV. The flow meter FM captures the flow immediately after the pump. As the PRV setting is increased to 175 bar, the flow rate from the pump gets decreased but does not become minimum indicating a coupling of characteristics between the pump and the PRV. For the PRV setting of 175 bar the swash plate attains a steady state at some intermediate angle as there is a partial opening of PRV causing a limit in the pressure build up, which can be seen in the inset of pressure variation in Fig 2.9a. PRV setting of 210 bar provides his margin due to which the swash plate comes to its minimum angle resulting in minimum flow rate from the pump as seen in the figure. A similar phenomenon has been observed for cut-off setting of 72 bar as well shown in Fig 2.9(b). Here also, PRV setting of 145 bar completely separates itself from the characteristics of the pump. From this study it can be proposed that even if a PRV is employed for safety purpose in a circuit having variable displacement pump, the setting of the PRV should be kept at least twice the cut-off setting of the pump.
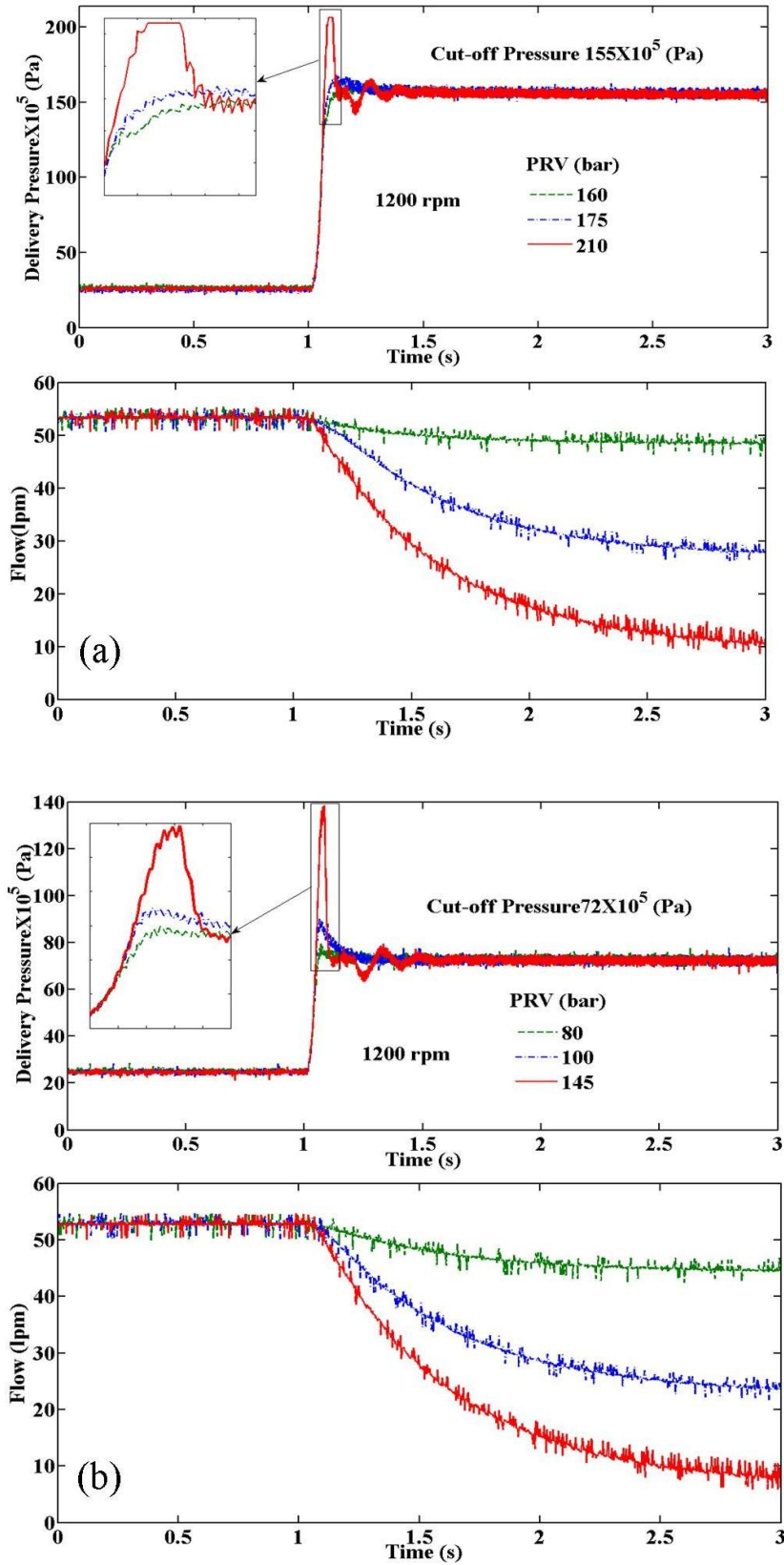
Figure 2.9: Effect of PRV on the pump performance at (a) 155 bar cut-off; (b) 72 bar cut-off

26

2.3.4 Identification of pressure and flow dynamics for different loading

Figure 2.10 represents the pressure and flow dynamics of the pump at a constant speed (1200 rpm) of the motor but at dissimilar area opening patterns of the load valve or PV. Here, 100 % area indicates as no load condition (corresponds to 10 volts input to PV) and 0 indicates full load condition (corresponds to 1.8 volts input to PV).

Figure 2.10: (a) Pressure and flow dynamics at various loads for short run time at 155 bar cut-off

27

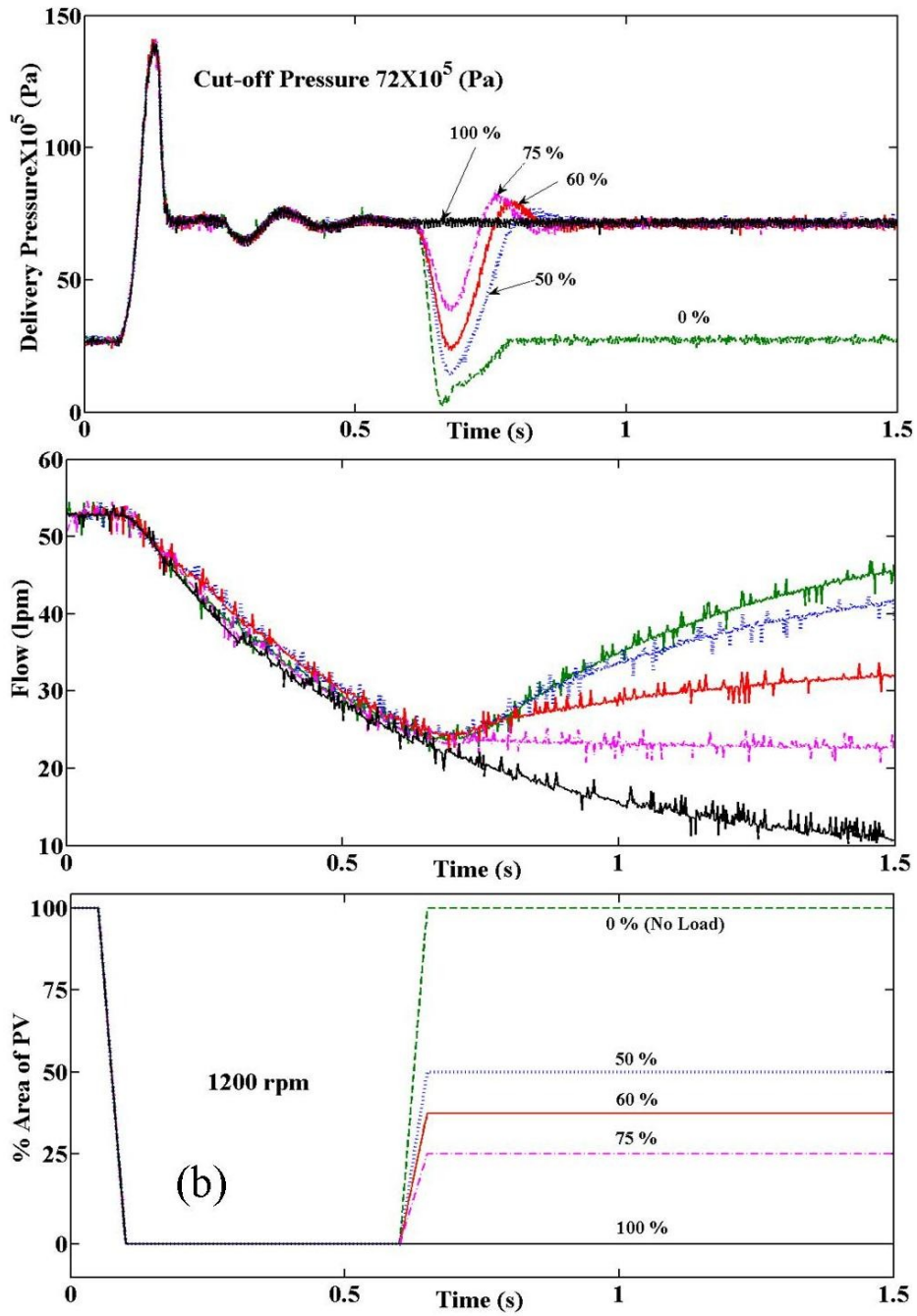
Figure 2.10: (b) Pressure and flow dynamics at various loads for short run time at 72 bar cut-off

In between 0 and 100, other numbers indicate intermediate loading to the pump. In the no load (full load) condition pressure of system is minimum (maximum) and flow is maximum (minimum). It can be seen that for the given loading patterns in both the cases of cut-off pressures, the flow rates were unable to reach to its minimum at full load

28

before being increased for different reduced loads. However, the pressure dynamics are found to be consistent in following the load variation. Increase in dwelling time at full load has enabled the flow rate to come to its minimum as evident in Fig. 2.11. From the result it can be said that in order to get a steady minimum flow rate from one operating point to other, at least 5 seconds time should be given as the flow dynamics is found to be much slower than the pressure dynamics.
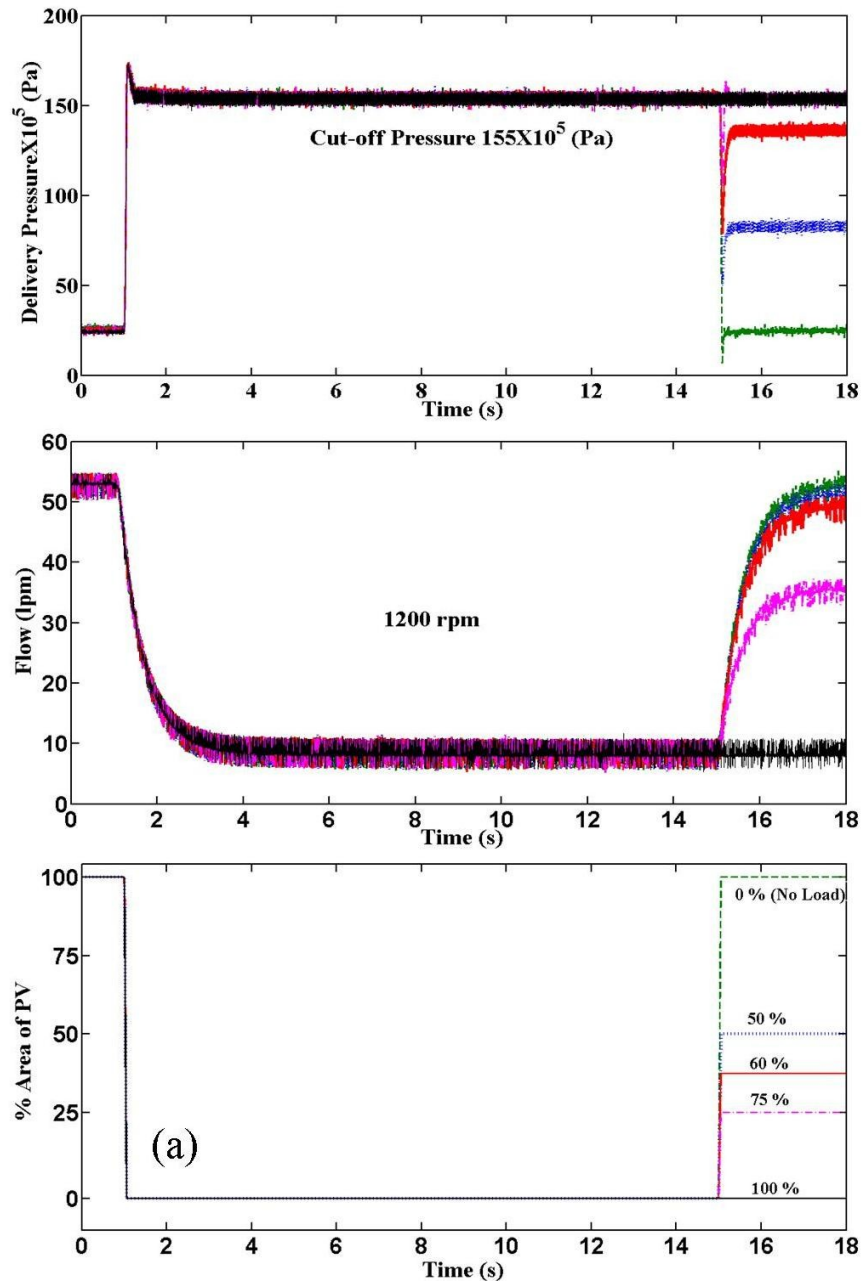
Figure 2.11: (a) Pressure and flow dynamics various loads for long run time at 155 bar cut-off
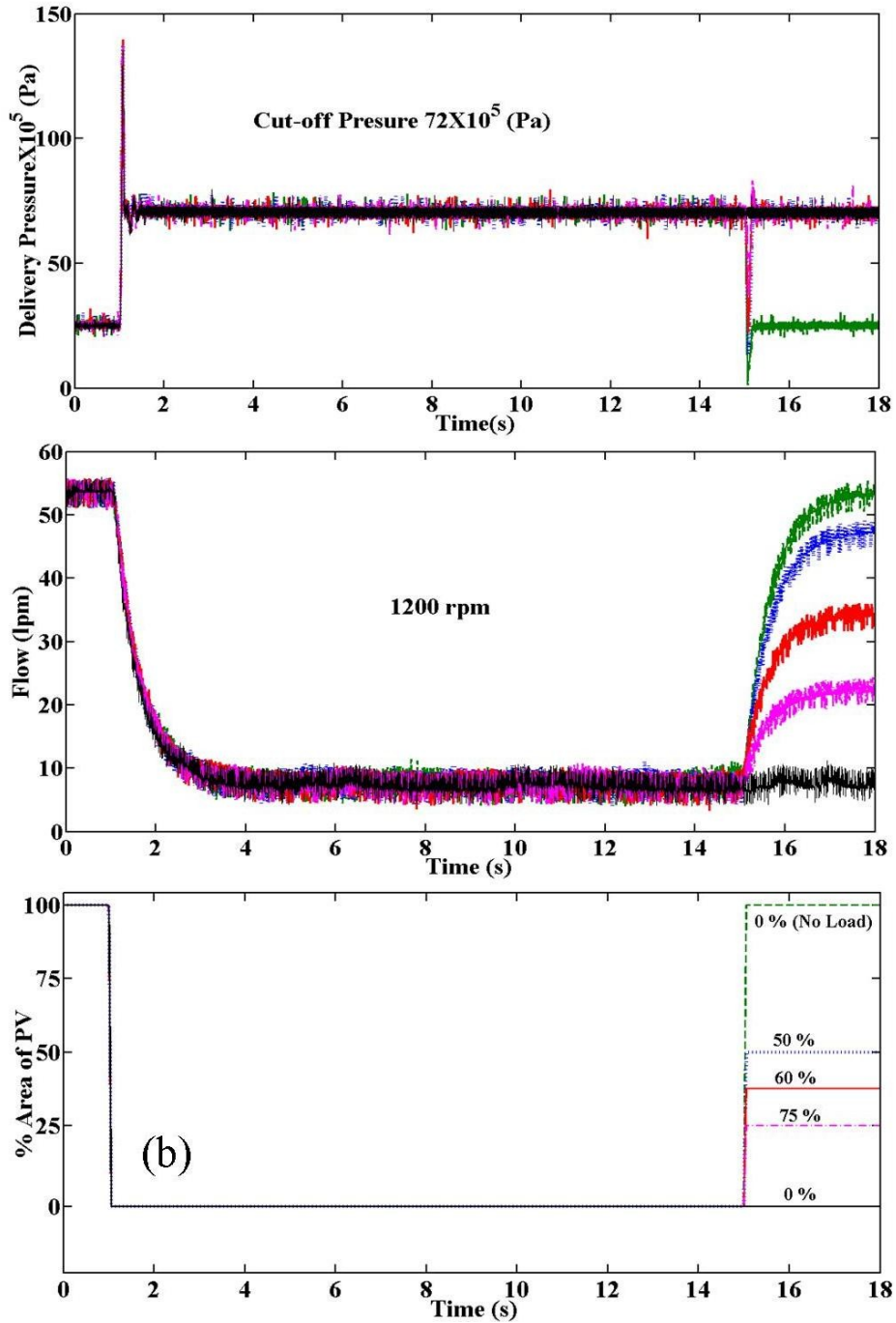
Figure 2.11: (b) Pressure and flow dynamics various loads for long run time at 72 bar cut-off

2.3.5 Effect of barrel rotation speed on pump dynamics

Figure 2.12 represents the pressure and flow dynamics of the pump for different rotation speed of the motor at a particular load valve opening pattern as 100-0-60 (no load-full load-60% load) at two different cut-off setting. The cut-off pressure of the pump

30

is set with the adjusting of the setscrews of the spool valve. Although for high cut-off setting, the flow and pressure dynamics are found to be different at the 60% load condition; in case of low cut-off setting both the pressure and flow dynamics remain almost unaffected irrespective of different rotational speed of the motor.
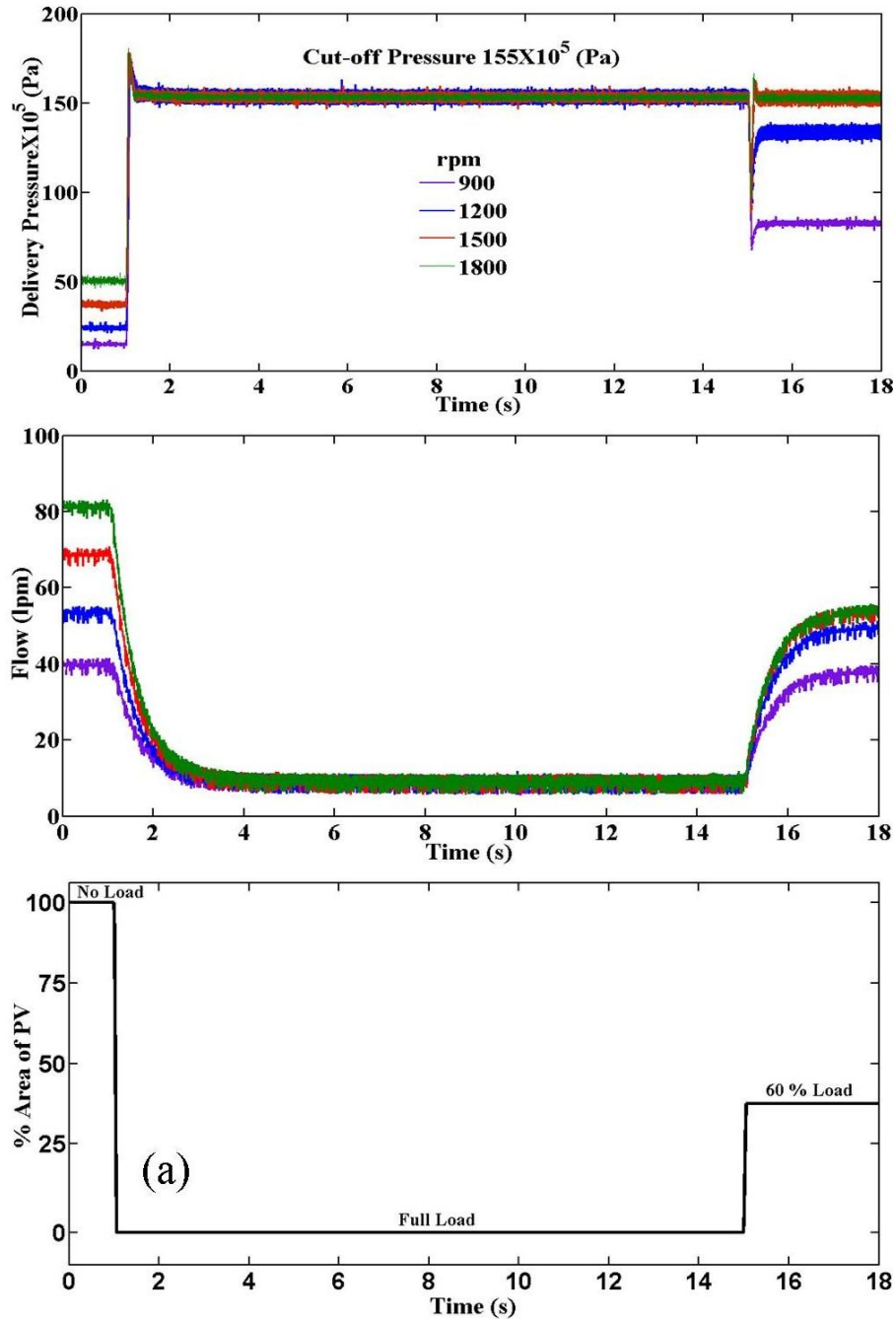
Figure 2.12: (a) Effect of rotating speed on pressure and flow dynamics for a typical load variation at 155 bar cut-off
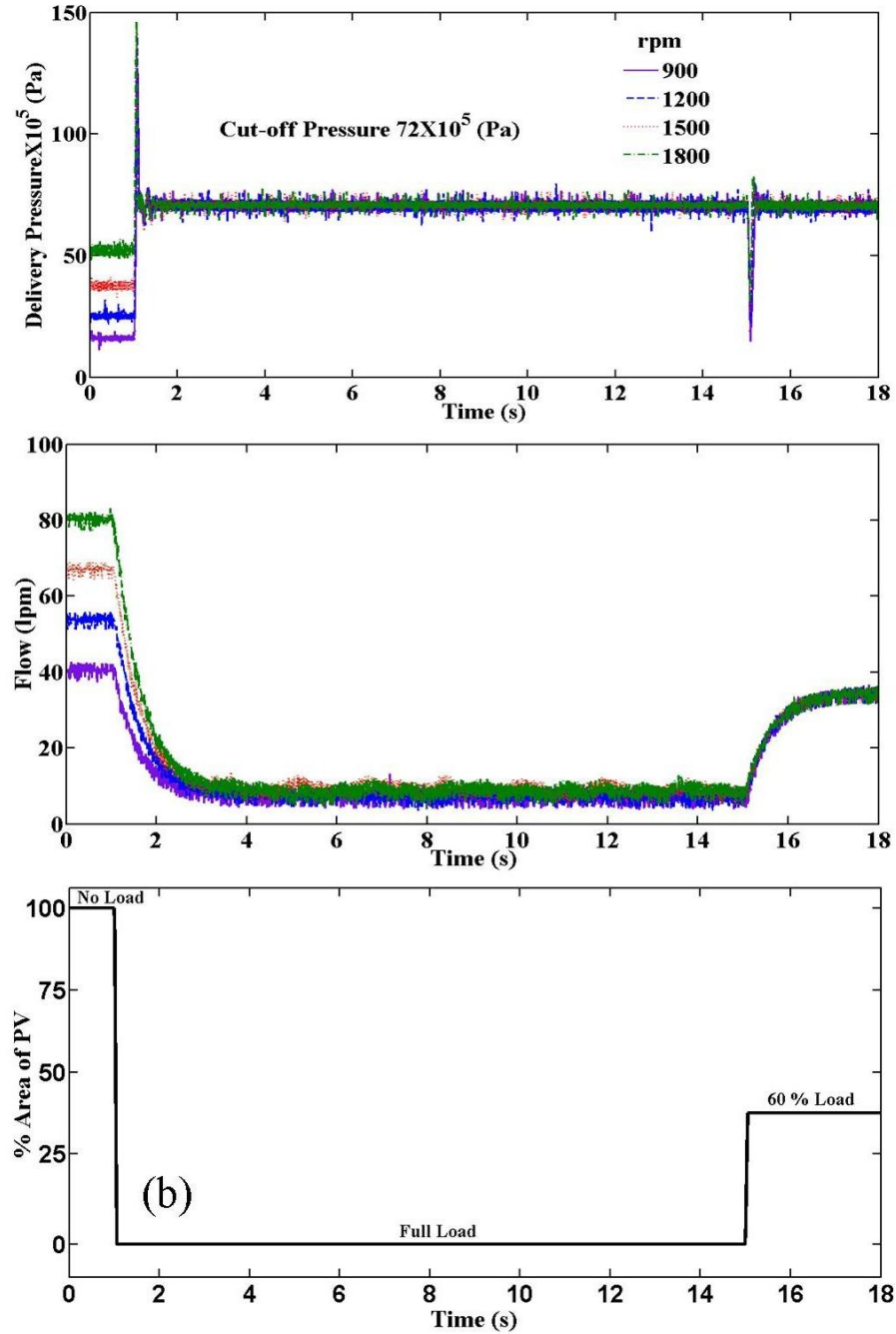
Figure 2.12: (b) Effect of rotating speed on pressure and flow dynamics for a typical load variation at 72 bar cut-off

2.3.6 Effect of rate of loading on pump dynamics

The dynamics of the delivery pressure and flow rate of the pump is linked to the rate of loading condition through the PV on the system. As shown in Fig. 2.13, the delivery pressure and flow dynamics is depended on the opening and closing time of the

load valve, the timing of the valve dynamic has a considerable influence on it. The span of pressure overshoot is directly proportional to the span of load valve closing time although the pressure over-shoot decreases with increasing of valve closing time. In case of valve opening time of the load valve the delivery pressure shows a typical dynamics. The delivery pressure stays at pressure close to the cut-off pressure at the initial stage of load valve transient region then it comes to the minimum pressure as evident Fig.2.13. The magnitude of pressure under shoot has been also regulated by the valve timing. The pressure overshoot is decreased with increase in the valve opening timing.
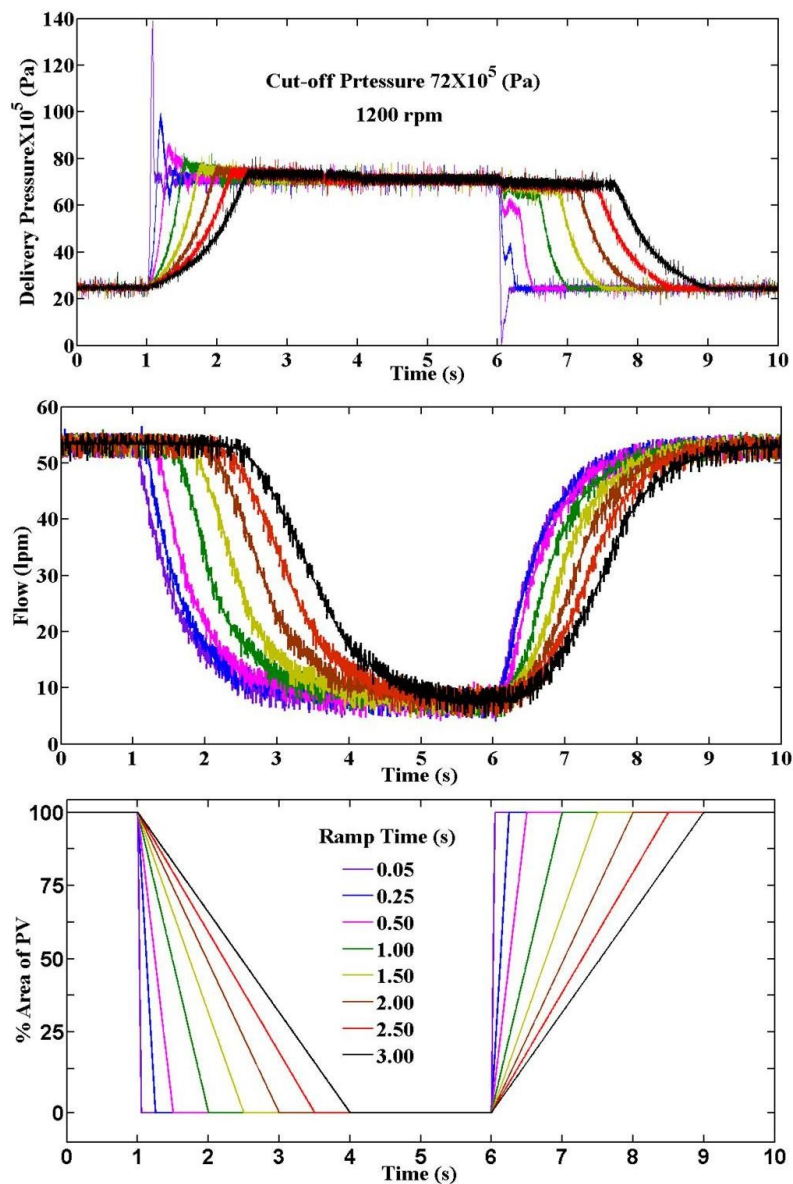
Figure 2.13: Effect of load valve opening and closing time on pump performance

33

2.4 Summary

This study has been focused on the experimental study of pressure and flow dynamics for a variable displacement axial piston pump on different demand and different operating condition. The effects of precompression of the top and bottom spool springs of the spool valve on the pump dynamics have been investigated experimentally.

The coupled effect of the deadband of the PV and the pump has been identified to become critical towards maximum loading to the pump, when the command voltage of the PV is set at zero. In order to separate the effect of deadband on the performance of the pump, it is recommended to reset the minimum command voltage to that value at which the flow rate becomes minimum and steady with nearly zero oscillation. The pressure setting of the PRV should be kept substantially away (at least twice) from the cut-off setting of the pump to avoid overshoot in the pressure dynamics of the pump.

It is found that control of the spring precompression percentage becomes a critical issue within the lower compression zone, especially when the precompression is adjusted manually. Hence, it becomes quite evident that the selection of the spring material and its design plays a vital role in determining the pump dynamics.

A set of experiment has been done to explore the effect of rotating speed of motor for a particular demand. The flow and pressure of the pump effectively depends on the rotation speed of the motor at no load condition but at full load the pressure and flow dynamics is controlled by the reference cut-off pressure setting.

The typical pressure overshoot occurring in the variable displacement pump is a consequence of sudden change in the load. For a slow change in the loading to the pump, the pressure overshoot gets reduced.

CHAPTER-3

DESIGN METHODOLOGY THROUGH MATHEMATICAL MODELLING

3.1 Overview

As evident from the previous chapter, the pressure compensator of a variable displacement pump acts as a flow controller, in which a small part of the main flow is passed through the passive spool valve for adjusting the orientation of swash plate to control the stroking volume of the pump. The adjustment of the flow is controlled by torque acting on the swash-plate due to the stroking cylinder, rate cylinder and barrel cylinders. Using the delivery pressure through a spool valve to a stroking or control cylinder and directly to a rate or bias cylinder, a control torque is produced to achieve a swivelling motion of the swash plate. Beyond the reference delivery pressure or cut-in pressure set by the precompression of the spring in the spool valve end, torque is developed due to the stroking cylinder. As the available torque increases with increase in delivery pressure above the cut-in limit, the steady inclination of the swash plate with respect to the plane normal to the axis of pump rotation attains a lower equilibrium value. With the decrease of the swash angle, the stroking volume of each piston becomes lesser leading to reduced delivery flow of the pump. At the cut-off pressure, the inclination of the swash plate approaches near zero and the effective delivery flow overcoming the internal leakages becomes negligible.

Satisfying the above functioning, a novel method has been formulated to design a pressure compensator of an axial piston pump that makes the pump variable displacement. The purpose of the work reported here is representing, through mathematical modelling, a complete design methodology of a pressure compensator for variable displacement axial piston pump based on some straightforward mechanistic ideology. Adopting a basic pump model, with the help of some simple static design steps the compensator of the pump has been developed for particular cut-in and cut-off pressure limits ensuring a balanced swivelling torque on the swash plate due to barrel piston rotation. Using the idea of a balanced swivelling torque design on the swash plate is one of the most important contributions of this research. Delivery pressure feedback to the rate cylinder has been acknowledged instead of employing a fully spring loaded cylinder (Mandal et al., 2014). In the second part, a comprehensive dynamic model of the pump including the compensator dynamics is developed.

3.2 Static modelling of the pump

3.2.1 Torque balance model of swash plate

Adopted from the description of the pump given in Section 1.4 of Chapter 1, Fig. 3.1 shows the arrangement of the different piston-cylinders on the swash plate in a schematic form. According the figure, at any static equilibrium of the swash plate other than the maximum or rated swash angle configuration, the net torque acting about the x axis should be mechanically balanced so that the net torque acting on the swash plate is zero. Mathematically it can be written as

$$T_s + T_{sp} + T_{rp} = 0,\qquad(3.1)$$

in which T_s is the net torque developed due to the rotating barrel known as swivelling torque, T_{sp} and T_{rp} are the torques due to the stroking piston and rate piston respectively. The expressions of the above torques are described next.
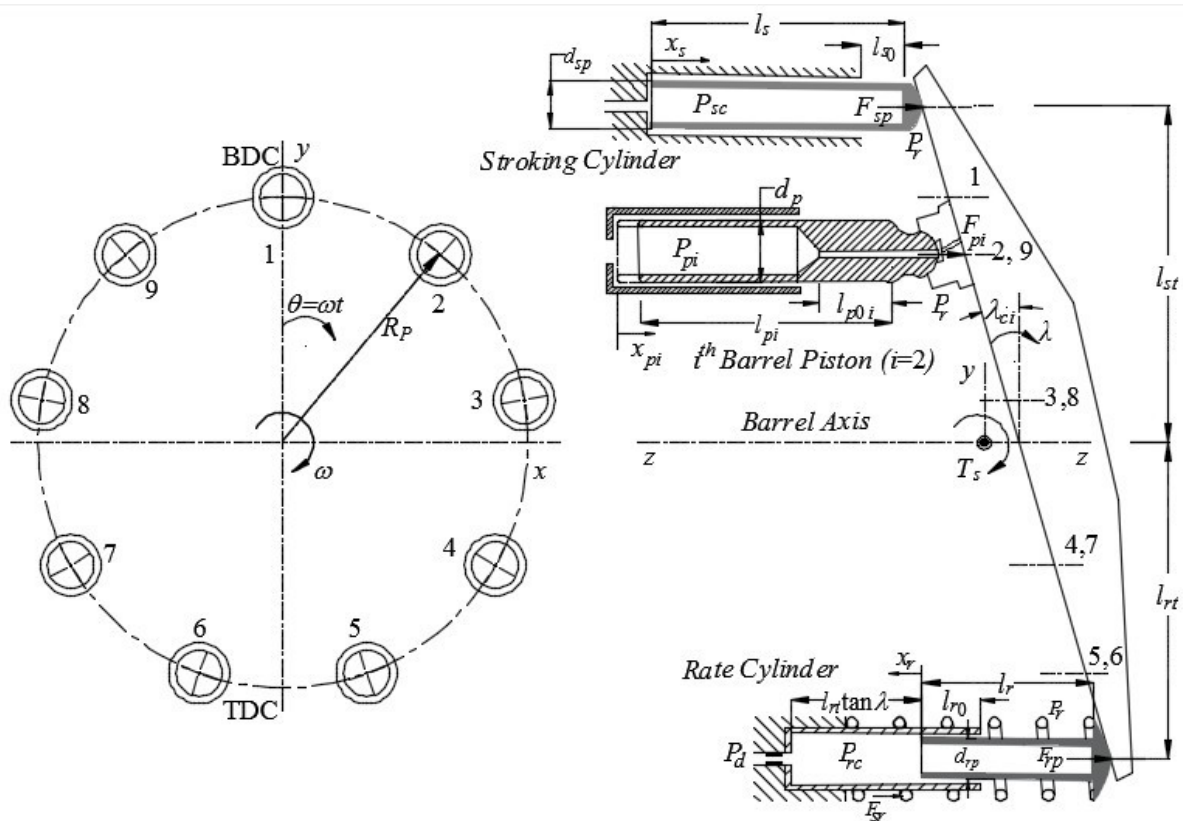
Figure 3.1: Distribution of different cylinders on the swash plate

37

As shown in Fig. 3.1, the ith barrel piston is exposed across the chamber pressure P_{pi} and case pressure P_r. This pressure drop causes a pressure force F_{pi} on the swash plate transmitted through the piston shoe. The summation of all piston forces produce a net torque to swivel the swash plate about x axis. If the barrel piston axis remains parallel to the barrel axis (which is ensured by the ball socket joint arrangement at the piston shoe) then the moment arm for the pressure force will be the perpendicular distance between the piston axis and barrel axis. This distance will depend on the respective location of the ith barrel piston represented by the angular position θ. Hence this swivelling torque is expressed in terms of the piston diameter d_p, pitch circle radius R_p and angular position of the piston on the manifold as

$$T_s = \sum_{i=1}^{9} [(P_{pi} - P_r)(\pi d_p^2 / 4)R_p \cos\{\theta + 2\pi(i-1)/9\}] . \qquad (3.2)$$

The pressure P_{sc} inside the stroking cylinder acts on the stroking piston to develop a force F_{sp} on the swash plate thereby producing the torque T_{sp} expressed in terms of the moment arm l_{st}, stroking piston diameter d_{sp} as

$$T_{sp} = (P_{sc} - P_r)(\pi d_{sp}^2 / 4)l_{st} . \qquad (3.3)$$

In addition to the force F_{rp} due to the pressure P_{rc} inside the rate cylinder, the compression of the spring of stiffness k_r also acts on the swash plate. These forces produce the torque T_{rp} that can be expressed in terms of the moment arm l_{rt}, rate piston diameter d_{rp} as

$$T_{rp} = -\{k_r(\delta_0 + x_r) + (P_{rc} - P_r)(\pi d_{rp}^2 / 4)\}l_{rt} , \qquad (3.4)$$

where x_r is the rate piston displacement that can be expressed in terms of l_{rt} and swash angle λ as $(l_{rt} \tan\lambda)$. The negative sign in equation (3.4) is due to the sign convention adopted for the moment as clockwise positive.

3.2.2 Steady state flow modelling for the pressure compensator and the pump

At the active condition of the pressure compensator, hydraulic oil flows through various constrictions in the pressure compensator components namely rate piston, stroking piston and the control spool valve. There are mainly three types of constrictions that can be recognized in Figs. 3.2 to 3.4. Those are fixed area or unmetered orifice, variable area or metered orifice and long orifice due to annulus space between piston and cylinder. As shown in Fig. 3.2, the entrance of the hydraulic oil in the rate cylinder is through a constant or fixed area orifice whereas the exit path of this oil is the radial clearance between the rate piston and cylinder. Of course depending on the pressure conditions, the entry and exit can be reversed, typically in case of retraction of the rate piston. In case of the stroking cylinder, the oil comes through a line from the control spool valve whereas the exit is through a similar annulus gap likes rate piston and cylinder.
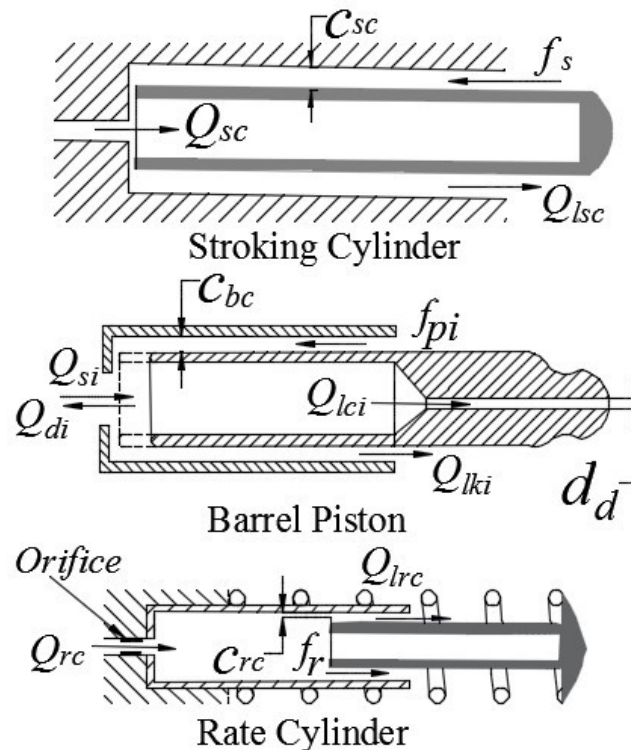

Figure 3.2: Details of different possible flow paths in the stroking cylinder, barrel piston and rate cylinder

Inside the pump, there are situations of variable-area orifice flow as well. Such situations arise during the engagement and disengagement of ith barrel cylinder with the respective manifolds. As apparent from the description in Section 1.4 and Fig.1.3, the angular displacement of a barrel cylinder over any bridge between the suction or delivery manifolds or any silencing groove makes the respective engaged areas with the kidney-shaped bore end of the barrel vary.

Apart from these main flows in the pump, in each barrel, as shown in Fig. 3.2, there is an annular orifice flow between each barrel piston and the cylinder. Also, through each piston there is a long straight orifice-flow passage up to the piston shoe for lubrication.

In the control valve, different orifices could be traced in Figs. 3.3 and 3.4, which have been obtained from Fig. 1.4. Through the respective fixed-area orifices, both the spool valves receive flow from Inlet Port **P** at delivery pressure P_d. By the positioning (neutral) of the land in each spool on the right of this fixed-area orifice, two metered orifices could form on the right and left flat faces of the land. While the left faces meter the outflow to the stroking cylinder line, the right faces meter the inflow from the same line. These lines are shown at pressures P_c and P_{sc} for the top and bottom spools respectively. The meter-in orifice on the right face of the top spool is shown at its maximum opening by an underlap length u_{r1}. An increase in delivery pressure to the cut-in value would reduce this opening to zero, thereafter blocking the return flow from the stroking cylinder to fixed-area Port **T**. Of course, the meter-out orifice on the left face would remain closed up to spool displacement below the overlap length o_{d1}, after which the flow passes to the stroking cylinder through Port **A**. These underlap and overlap in the metering land of the bottom spool are respectively equal to u_{r2} and o_{d2}. By virtue of higher precompression setting of the corresponding spring, the bottom spool would remain stationary up to a pressure greater than the cut-in pressure. Below the bottom spool valve, two tiny fixed orifices connect a bypass line between Ports **A** and **T**. Flow leakages occur through the annular orifices formed by the clearances between the moving spools and the bush, which for the present analysis those are neglected.
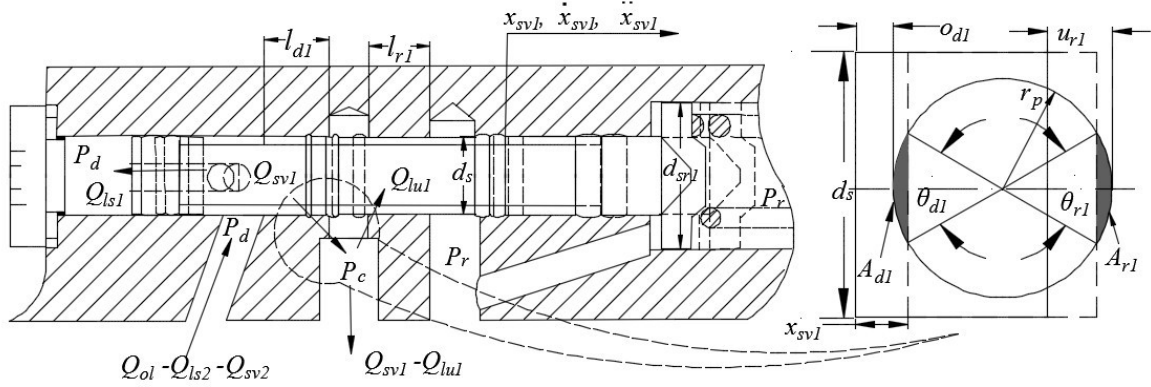
Figure 3.3: Details of flow paths, pressure nodes and port areas in top spool valve
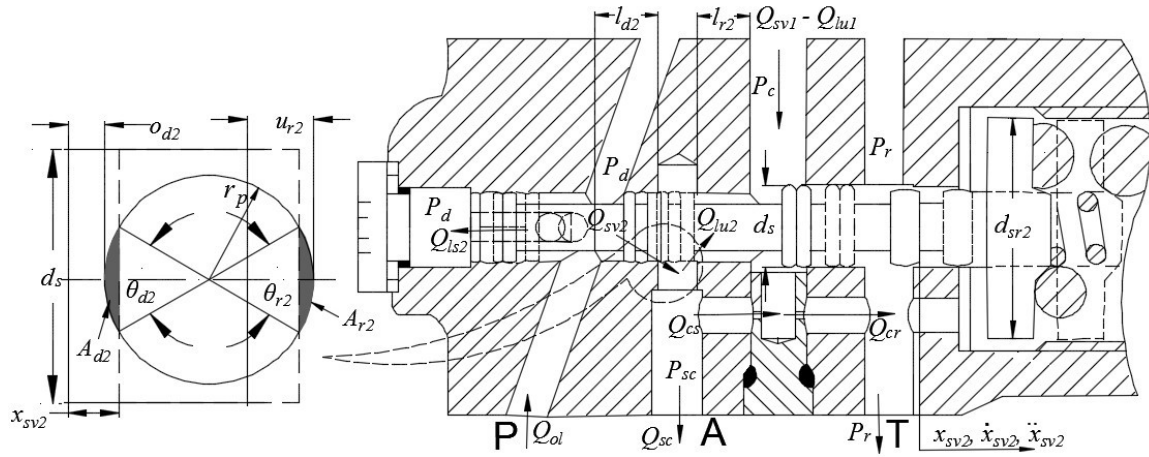
Figure 3.4: Details of flow paths, pressure nodes and port areas in bottom spool valve

With the identification of the flow through the various constrictions discussed above, the flow Q_o through the orifices, metered or unmetered, due to pressure drop ΔP_o across the orifice can be expressed by general orifice equation as,

$$Q_o = C_{do} A \sqrt{2|\Delta P_o|/\rho} \, \text{sgn}|\Delta P|, \tag{3.5}$$

where ρ is the density of oil, A is the area of the orifice and C_{do} in is the discharge coefficient that may vary for different orifices and the values for those can be estimated from any standard reference (Massey and Ward-smith 2006). The specific notations for the different orifices that can be modelled using Eq. (3.5) are furnished in Table 3.1 and the parameters involved in the respective subtended angle calculations for the metered orifices are furnished in Table 3.2. In case of variable-area orifice at a circular port with

41

n_p number of port cuts, port radius of r_p and subtended angle θ at the port opening, similar to the ones depicted in Figs. 3.3 and 3.4, the area can be represented as

$$A = n_p r_p^2 (\theta - \sin \theta)/2, \tag{3.6a}$$

where as in case of unmetered orifice of diameter d, the area is given by

$$A = (\pi/4)d^2, \tag{3.6b}$$

and the respective engaged areas A_{di} and A_{si} have been evaluated following earlier studies by Mandal et al. (2008, 2012, 2014) the details of which are elaborated in Appendix I

In Eq. (3.6a), n_p is the number of port cuts, r_p is the port radius and θ is the subtended angle of port opening due to the relative position of spool land and port which can be expressed in terms of the spool displacement, x_{svj} ($j=1$ for top spool and $j=2$ for bottom spool) and other parameters as,

$$\theta = 2\cos^{-1}\{1 - \max(x_{svj} - o, 0)/r_p\} \text{ for overlapped configuration} \tag{3.7a}$$

$$= 2\cos^{-1}\{1 - \max(u - x_{svj}, 0)/r_p\} \text{ for underlapped configuration} \tag{3.7b}$$

Table 3.1: Orifice flow-variable description at different locations

Location of orifice between	Type	Q	C_{do}	A	ΔP_o
P_d and P_{rc} at rate cylinder	Unmetered	Q_{rc}	C_{dr}	A_{or}	$P_d - P_{rc}$
P_d and P_c at top spool	Metered	Q_{sv1}	C_d	A_{d1}	$P_d - P_c$
P_c and P_r at top spool	Metered	Q_{lu1}	C_d	A_{r1}	$P_c - P_r$
P_d and P_{sc} at bottom Spool	Metered	Q_{sv2}	C_d	A_{d2}	$P_d - P_{sc}$
P_{sc} and P_c at bottom Spool	Metered	Q_{lu2}	C_d	A_{r2}	$P_{sc} - P_c$
P_{sc} and P_c below bottom Spool	Unmetered	Q_{cs}	C_{sv}	A_{oc}	$P_{sc} - P_c$
P_c and P_r below bottom Spool	Unmetered	Q_{cr}	C_{sv}	A_{oc}	$P_c - P_r$
P_{pi} and P_d at i^{th} barrel of pump	Metered	Q_{di}	C_d	A_{di}	$P_{pi} - P_d$
P_s and P_{pi} at i^{th} barrel of pump	Metered	Q_{si}	C_d	A_{si}	$P_s - P_{pi}$

Table 3.2: Parameters for the area evaluation

Area	Lap condition (*o* or *u*)	Subtended angle of opening (θ)
A_{d1}	o_{d1} : overlap in land (P_d side) of top spool	θ_{d1} : towards the P_d side
A_{r1}	u_{r1} : underlap in land (P_r side) of top spool	θ_{r1} : towards the P_r side
A_{d2}	o_{d2} : overlap in land (P_d side) of bottom spool	θ_{d2} : towards the P_d side
A_{r2}	u_{r2} : underlap in land (P_c side) of bottom spool	θ_{r2} : towards the P_c side

For the annulus gaps or radial clearance in the pressure compensator components and in the pump, considering fully developed laminar flow through these passages, the flow rate Q_a obtained from (Massey and Ward-smith 2006, Ivantysyn, J. and Ivantysynova 2003) can be expressed in general as,

$$Q_a = \pi d_{pn} c_r^3 \Delta P_a / \{12\mu(l_{in} + x)\}, \tag{3.8}$$

where x is the displacement of the piston, d_{pn} is the diameter of the piton, c_r is the radial clearance between cylinder and piston and l_{in} is the initial length of the annulus gap and ΔP_a is the pressure drop across the annulus gap. The specific notations for the different locations of the annulus are furnished in Table 3.3.

Table 3.3: Annulus flow-variable description at different locations

Location of annulus	Q_a	c_r	d_{pn}	l_{in}	x	ΔP_a
Rate cylinder	Q_{lrc}	c_{rc}	d_{rp}	l_{r0}	x_r	$P_{rc} - P_r$
Stroking cylinder	Q_{lsc}	c_{sc}	d_{sp}	$l_s - l_{r0}$	$-x_s$	$P_{sc} - P_r$
Barrel cylinder	Q_{lki}	c_{bc}	d_p	$l_{pi} - l_{p0i}$	$-x_{pi}$	$P_{pi} - P_r$

Considering Poiseuille flow inside the barrel piston for the long circular flow passage of diameter d_d and length l_b, the flow rate can be expressed as

$$Q_{lci} = (\pi d_d^4)(P_{pi} - P_r)/(128\mu l_b). \tag{3.9}$$

3.2.3 Static force balance in the spools of the control valve

According to the configuration of variable displacement pump as stated in Section 1.4, the delivery line of the pump is directly connected to the left side of both spools end resulting action of pressure force due to P_d on the left face of both the spools. The right faces of both the spools, remain at the case pressure P_r, are supported by compression spring which opposes the pressure force. Although the intermediate chambers of both the spool valves are exposed to different pressures, due to symmetry, the intermediate faces will not experience any resultant force. However, beyond cut-in pressure, due to the entry and exit of flow through the metered orifices in each spool, there will be a force known as the steady flow force (Merritt 1967) acting on the spool, the nature of which is in opposition with the pressure force. Therefore, under the action of these forces on each spool the static force balance equation, applicable for cut-in and beyond, can be expressed in general form for the jth spool (j=1 for top and j=2 for bottom) as

$$\pi(P_d d_{sj}^2 - P_r d_{srj}^2)/4 - k_{sj}(\delta_{sj} + x_{svj}) - F_{sj} = 0 \tag{3.10}$$

where d_{sj} and d_{srj} are respectively the diameters of the left and right side of the jth spool, δ_{sj} and k_{sj} are respectively the precompression and stiffness of the spring at j^{th} spool. In the above equation, F_{sj} is the steady state flow force acting on the jth spool expressed from Merrit (Merritt 1967) as

$$\begin{aligned}
F_{sj} &= 2C_d C_{vj}\{A_{dj}(P_d - P_c)\cos\theta_{mdj} + A_{ri}(P_c - P_r)\cos\theta_{mrj}\} && \text{for } j = 1 \\
&= 2C_d C_{vj}\{A_{dj}(P_d - P_{sc})\cos\theta_{mdj} + A_{rj}(P_{sc} - P_c)\cos\theta_{mrj}\} && \text{for } j = 2
\end{aligned} \tag{3.11}$$

Where for the jth spool, C_{vj} is the coefficient of velocity, θ_{mdj} and θ_{mrj} are respectively the jet angles of the metered flows Q_{svj} and Q_{luj} described in equation (3.5) with Table 3.1. Assuming near-zero radial clearance, all the jet angles are assigned as 69^0 from Merrit (1967).

3.3 Design methodology of the pressure compensator from static model

The static design is targeted to achieve the performance of an A10VSO45 series pump from Bosch Rexroth driven by an electric motor rotating at a speed ω equal to 1500rpm. From the technical specifications and the formulae given in the literature (Rexroth Bosch Group, 2004), the rated flow, torque and power have been calculated for the above speed theoretically. Of course, the torque and power vary with the operating pressure of the pump, although the rated flow remains moderately constant for a constant speed of rotation of the motor driving the pump.

3.3.1 Estimation of maximum swivelling torque

For the instantaneous dispositions of Pistons 5 to 9 on the delivery manifold shown in Fig. 3.5, the contributions of the torque from the last two are adverse as these attempts a reduction of the swash angle λ, whereas those from the first three are favourable since their effect is to increase this angle.
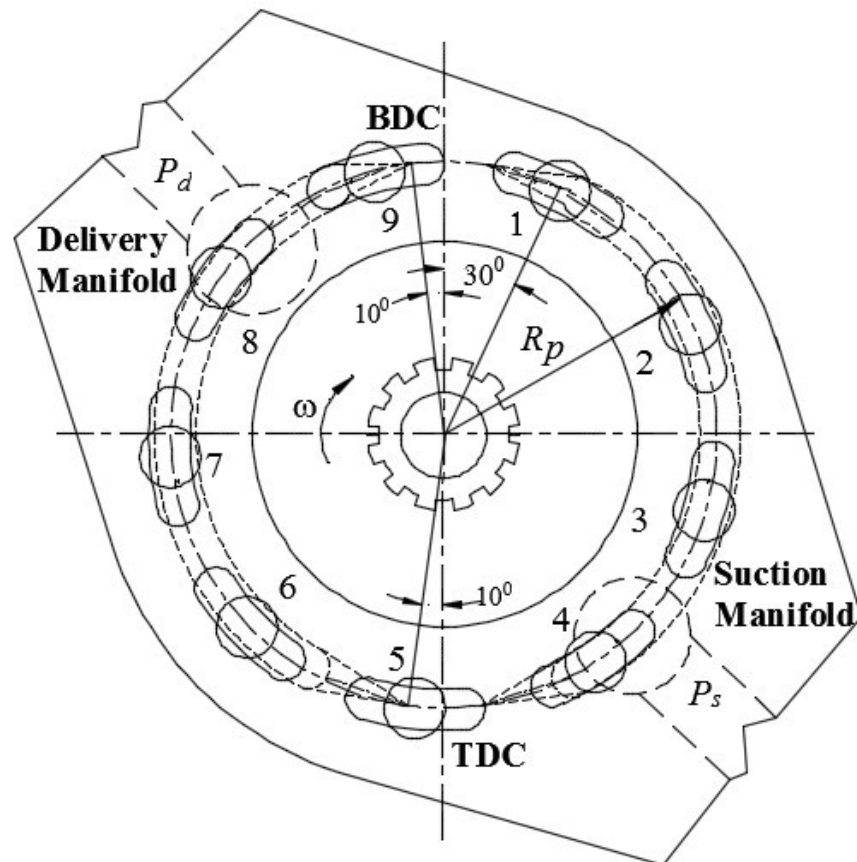

Figure 3.5: Instantaneous dispositions of pistons over the manifold of the pump

45

The adverse swivelling torque would indeed be the maximum, when a piston would be on the verge of leaving the delivery manifold near the BDC. This is because the length of the moment arm would be maximum at the BDC. For instance, when Piston 9 leaves the manifold, this torque suddenly decreases consequent to the decrease in number of pistons producing the adverse torque. During the period of rotation between leaving the manifold by two consecutive pistons, this torque keeps on increasing. Three simplifications have been adopted for estimating the maximum swivelling torque in static design. With reference to Fig. 3.5, these are stated next.

First, according to the Fig.3.5 the delivery manifold of the pump extends from 10^0 clockwise angular position after the TDC to 10^0 before the BDC. For a nine piston arrangement, these two positions are taken up by Pistons 5 and 9 respectively, when Piston 1 location is given by θ equal to 30^0 after the BDC. Secondly, the pressures on Pistons 5 to 9 are equal to the delivery pressure P_d as those are allocated in the side of delivery manifold. Thirdly, the pressures acting on Pistons 1 to 4 are equal to the suction manifold pressure P_s that in turn is assumed to be equal to the reservoir or case pressure P_r. These simplifications allow an approximate design-level estimation of the swivelling torque by neglecting the difference of the piston chamber pressures P_{pi} from the corresponding manifold pressures. Therefore, for the static design of the pressure compensator, the maximum swivelling torques T_{sci} and T_{sco} for cut-in and cut-off delivery pressures P_{dci} and P_{dco} can respectively be found through a simplified form of Eq. (3.2) in terms of the barrel piston diameter d_p, pitch circle radius R_p and the corresponding position of the barrel pistons as

$$T_{sci} = \sum_{i=5}^{9} [(P_{dci} - P_r)(\pi d_p^2/4)R_p \cos\{\theta + 2\pi(i-1)/9\}]$$ (3.12a)

$$\text{and } T_{sco} = \sum_{i=5}^{9} [(P_{dco} - P_r)(\pi d_p^2/4)R_p \cos\{\theta + 2\pi(i-1)/9\}].$$ (3.12b)

The application of these equations in designing the rate and stroking cylinders corresponding to cut-in and cut-off delivery pressures are described next.

3.3.2 Design of diameter and radial clearance of rate piston

When the pump operates at the cut-in delivery pressure, the delivery pressure P_d shown in Fig. 3.1, becomes equal to P_{dci}. It is evident from equation (3.1) that the corresponding torque T_{rp} gets counterbalanced by the cut-in swivelling torque T_{sci}, in this case the contribution of the stroking piston in terms of torque is negligible because the pressure inside it remains much below the cut-in pressure. So under the cut-in condition the stroking cylinder has no role on the torque distribution. In order to find out the diameter of the rate piston, the following assumptions have been made.

  a) There is no precompression of rate piston spring at the cut-in situation.

  b) The rate piston displacement x_r is zero at cut-in.

  c) With reference to equation (3.5) and Table 3.1, the pressure drop ΔP_o across the rate piston orifice is 2 bar or 2×10^5 Pa so that with pressure inside the rate cylinder in Pa, $P_{rc} = P_{dci} - 2\times10^5$.

Therefore for a selection of l_{rt}, from equation (3.1) along with the above assumptions, the rate piston diameter d_{rp} is obtained as

$$d_{rp} = [\{(4/\pi)T_{sci}\}/\{(P_{dci}-2\times10^5)l_{rt}\}]^{1/2}. \tag{3.13}$$

Since the rate piston should remain stationary up to the cut-in condition, the steady state flow continuity would mean the flow Q_{or}, that can be estimated from equation (3.5) and Table 3.1, to be equal to the annulus leakage flow Q_{lrc} that can be obtained from equation (3.8) and Table 3.3. For a known rate cylinder orifice diameter d_{or}, initial engaged length l_{r0}, the radial clearance can be evaluated by solving equations (3.5) and (3.8) as

$$c_{rc} = [\{600\mu l_{r0}c_{dr}d_{dr}^2\sqrt{10/\rho}\}/\{d_{rp}(P_{dci}-2\times10^5-P_r)\}]^{1/3}. \tag{3.14}$$

The spring on the rate piston is selected based on the rate piston diameter. For the chosen mean diameter D of the spring compatible with d_{rp}, number of active turns n_r of the spring and spring index D/d_r the stiffness is found from the standard relation

$$k_r = G_r d_r^4 /(8D^3 n_r). \tag{3.15}$$

Where G_r the modulus of rigidity of the spring material is, d_r is the wire diameter of the spring (Bhandari 2010).

3.3.3 Spring design of the spool valve

There are two springs in the spool valve. The main fundamental concept of static force balance is used to design the springs. The following are the assumptions for the design of top and bottom springs of the spool valve.

a) A small but realistic selection of the diameter of both the spool land is taken as d_s by choice.

b) The top spool displacement starts at cut-in pressure P_{dci}, and attains the maximum at $P_{dci} + \Delta P_{dci}$, during which the bottom spool remains closed.

c) The bottom spool displacement starts at $P_{dci} + \Delta P_{dci}$, and attains the maximum at P_{dco}, which is also the system cut-off pressure.

d) The flow forces F_{si} on both the spools are neglected.

Therefore at the onset of the top spool displacement, equation (3.10) along with chosen spring precompression δ_{s1} yields the spring stiffness as

$$k_{s1} = (P_{dci} - P_r)(\pi d_s^2 / 4) / \delta_{s1}. \tag{3.16}$$

A realistic size of the spring in terms of mean coil diameter, wire diameter and number of coil turns has been chosen using the relation depicted in equation (3.15) so as to match the estimated stiffness. The free length has been estimated by the addition of solid length of the spring, total axial gap and chosen spring pre-compression δ_{s1}. The total axial gap is equal to the product of (number of total turns -1) and gap between two consecutive coils (Bhandari 2010). In order to accommodate the accessible spring in the right side of the spool chamber, necessary modifications in terms of increase in the return side spool land diameter, d_{sr1} and the chamber length have been done.

The maximum spool displacement of the top spool is obtained from the static force balance at the stated condition of this spool as

$$x_{sv1max} = [\pi\{(P_{dci} + \Delta P_{dci})d_s^2 - P_r d_{sr1}^2\}/4]/k_{s1} - \delta_{s1}. \tag{3.17}$$

Similarly for bottom spool with two concentric springs, the spring stiffness has been designed for a chosen precompression δ_{s2} as

$$k_{s2} = (P_{dci} + \Delta P_{dci} - P_r)(\pi d_s^2 / 4) / \delta_{s2}. \tag{3.18}$$

Two feasible sizes of the spring in terms of same free length but different coil diameters, wire diameters and number of coil turns have been obtained in a similar way as the top spool so as to match the estimated equivalent stiffness.

The maximum spool displacement of the bottom spool is obtained from the static force balance at cut-off condition incorporating the modified return side diameter d_{sr2} of the spool as

$$x_{sv2\max} = \{\pi(P_{dco}d_s^2 - P_r d_{sr2}^2)/4\}/k_{s2} - \delta_{s2}. \tag{3.19}$$

3.3.4 Design of diameter and radial clearance of stroking piston

The cut-off condition is used to find out the stroking piston diameter. During cut-off, the following assumptions have been made.

a) The swash angle becomes zero ($\lambda_{co} = 0$) resulting the maximum rate piston and stroking piston displacements respectively equal to ($l_{rt} \tan\lambda_{ci}$) and ($l_{st} \tan\lambda_{ci}$), λ_{ci} being the cut-in swash angle and l_{rt}, l_{st} are the distances of the rate piston axis and stroking piston axis from the barrel axis respectively.

b) The bottom spool is fully opened.

c) With reference to equation (3.5) and Table 3.1, pressure drop ΔP_o for the metered orifice (between P_d and P_{sc}) at bottom spool is 5 bar or 5×10^5Pa so that with pressure in Pa, $P_{sc} = P_{dco} - 5\times10^5$.

At the cut-off condition, the equilibrium condition expressed by equation (3.1) would mean counterbalancing of the sum of the corresponding cut-off swivelling torque T_{sco} and the stroking piston torque T_{sp} by the rate piston torque T_{rp} so as to maintain zero swash angle. Invoking equations (3.1), (3.3), (3.4) along with the above considerations, the stroking piston diameter can be found for a specified l_{st} as

$$d_{sp} = [\{-T_{sco} + (P_{dco} - 5 \times 10^5)(\pi d_{rp}^2 / 4)l_{rt} + k_r l_{rt}^2 \tan \lambda_{ci}\}$$
$$/\{(\pi / 4)(P_{dco} - 5 \times 10^5)l_{st}\}]^{1/2}. \tag{3.20}$$

At the cut-off condition, the metered port at the left face of the bottom spool controlling the flow received at Port P shown in Fig. 3.4 becomes fully open, whereas the metered port on the right face gets fully closed. For the above stated considerations, the maximum flow through the open orifice can be found. Putting the numerical value of $P_d - P_{sc} = P_{dco} - (P_{dco} - 5 \times 10^5)$, in equation (3.5) along with Table 3.1, it can be found in terms of coefficient of discharge, area of opening and density as

$$Q_{sv2max} = 1000 C_d A_{d2max} \sqrt{1/\rho}, \tag{3.21a}$$

with the maximum area of opening A_{d2max} from equation. (3.6a) determined as

$$A_{d2max} = n_p r_p^2 (\theta_{d2max} - \sin \theta_{d2max})/2, \tag{3.21b}$$

in which θ_{d2max} is obtained from equation (3.7a) for a chosen overlap o_{d2} as

$$\theta_{d2max} = 2 \cos^{-1}\{1 - (x_{sv2max} - o_{d2})/r_p\}. \tag{3.21c}$$

For displacement of the bottom spool greater than u_{r2}, the flow Q_{sv2max} enters the stroking cylinder and leaves through the annulus at a rate Q_{lsc} described by equation (3.8) along with Table 3.3. Equating Q_{lsc} with Q_{sv2max} to satisfy flow continuity, the radial clearance c_{sc} can be determined for a given length of the stroking cylinder l_s as

$$c_{sc} = 1000[(C_d A_{d2max} \sqrt{1/\rho})\{12\mu(l_s - l_{st} \tan \lambda_{ci})\}$$
$$/\{\pi d_{sp}(P_{dco} - 5 \times 10^5 - P_r)\}]^{1/3}. \tag{3.22}$$

Using the methodology described above, the result of a pressure compensator design for a typical maximum cut-in and cut-off settings respectively equal to 19MPa and 20MPa is shown in Table 3.4. The table lists some parameters with chosen values, the basis of which are from the manufacturer literature (Bosch Rexroth, 2004) and from the previous works (Mandal et at. 2008, 2012, 2014). Putting the chosen values through equations (3.12) to (3.22) the values of the parameters listed as 'values (obtained)' have been determined.

Table 3.4: Parameter values for the designed pressure compensator

Parameters	Value (chosen)	Parameters	Value (chosen)
l_{rt}, l_{st}	50×10^{-3} m	u_{r1}, u_{r2}	90 μm
A_o	1.767×10^{-6} m^2	d_s	6.5×10^{-3} m
l_r	35×10^{-3} m	**Parameters**	**Value (obtained)**
l_s	48×10^{-3} m	d_{rp}	9×10^{-3} m
l_{r0}	10×10^{-3} m	k_r	463 N/m
l_{s0}	5×10^{-3} m	c_{sc}	39 μm
δ_0	2×10^{-3} m	d_{sp}	12.85×10^{-3} m
λ_{ci}	22°	c_{rc}	70 μm
δ_{s1}	11.51×10^{-3} m	k_{s1}	54174 N/m
δ_{s2}	5×10^{-3} m	k_{s2}	128074.8 N/m
r_p	1.335×10^{-3} m	d_{sr1}	19×10^{-3} m
θ_{d1}, θ_{d2}	79.24^{o},51 at x_{svmax}, 0,0 at $x_{sv}=0$	d_{sr2}	26×10^{-3} m
θ_{r1}, θ_{r2}	0,0 at x_{svmax}, 42.3,42.3 at $x_{sv}=0$	x_{sv1max}	3.067×10^{-4} m
o_{d1}, o_{d2}	10 μm	x_{sv2max}	1.3×10^{-4} m

3.4 Dynamic modelling of the pump-compensator for designing of parameters through simulation

3.4.1 Model of the spool valve dynamics

The left side of the spool valve is connected to the delivery side of the pump at pressure P_d and the other side is connected to the reservoir at pressure P_r as shown in Fig. 3.3 and Fig.3.4. With reference to the free body diagram shown in Fig. 3.6, the equation of motion of the jth spool can be written as

$$F_{pj} - F_{dj} - F_{sj} - F_{spj} = m_{svj}\ddot{x}_{svj}. \tag{3.23a}$$

Using the above relation and the expressions for F_{pj} and F_{spj} shown in Fig. 3.6, during the operation of the pump, the jth spool displacement equation can be written as

$$x_{svj} = 0 \text{ for } F_{pj} \leq k_{sj}\delta_{sj},$$
(3.23b)

$$m_{svj}\,\ddot{x}_{svj} + k_{sj}(\delta_{sj} + x_{svj}) = (\pi/4)(P_d d_s^2 - P_r d_{srj}^2) - F_{dj} - F_{sj} \text{ for } F_{pj} > k_{sj}\delta_{sj},$$
(3.23c)

where F_{sj} can be obtained from equation (3.11) and F_{dj} is the transient flow force and can be expressed from Merrit (1967) as

$$F_{dj} = \rho(l_{dj}\dot{Q}_{svj} - l_{rj}\dot{Q}_{luj}).$$
(3.24)

$$F_{pj} = (\pi/4)(P_d d_s^2 - P_r d_{srj}^2) \qquad F_{spj} = k_{sj}(\delta_{sj} + x_{svj})$$
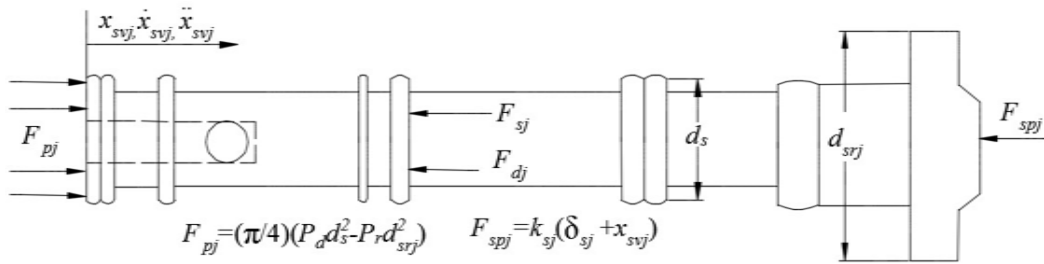
Figure 3.6: Free body diagram of jth spool

The flow rate Q_{ol} from the pump delivery enters the control valve to sustain motion of the spools and the stroking cylinder. With reference to Fig. 3.3 and Fig.3.4, the flow continuity condition in the pertaining flow passage starting from Port P up to the top spool can be expressed as

$$Q_{ol} = Q_{ls1} + Q_{ls2} + Q_{sv1} + Q_{sv2},$$
(3.25)

in which Q_{sv1} and Q_{sv2} can be found at any time instant from equations (3.5) to (3.7) with appropriate use of Tables 3.1 and 3.2. Considering incompressible flow condition in the left side chambers of both the spools, the flow rates Q_{lsj} in the chamber can be expressed in terms of the velocity of the jth spool as

$$Q_{lsj} = \pi(d_s^2/4)\dot{x}_{svj}.$$
(3.26)

Considering compressibility effect inside the chamber of volume V_c having pressure P_c as shown in Fig. 3.3, the pressure dynamics of P_c can be found using the definition of bulk modulus (Merrit, 1967) with flow networks as illustrated in Fig. 3.3 and Fig. 3.4 as

$$\dot{P}_c = \beta\{Q_{sv1} - Q_{lu1} + Q_{lu2} - Q_{cs} - Q_{cr}\}/V_c, \tag{3.27}$$

where β is the bulk modulus of the hydraulic oil, V_c is the volume of the chamber connected between top spool and bottom spool with reference to Fig. 3.3 and Fig. 3.4. Of course, there is a direct interaction of the spool valve dynamics with the swivelling dynamics of the swash plate including the rate and stroking cylinders.

3.4.2 Modelling of swash plate and associated motion dynamics

In order to develop the swivelling dynamics of the swash plate as an extension of equation (3.1), inertia and viscous friction forces are considered in all the pistons possessing physical connectivity with the swash plate as shown in Fig. 3.1 and Fig. 3.2. For convenience of expressing the dynamics, the angular acceleration of the swashplate $\ddot{\lambda}$ and the linear acceleration of the rate piston $\ddot{x}_r$ are expressed in terms of the linear acceleration of the stroking piston $\ddot{x}_s$. Taking moments of all the forces about x-x axis as shown in Fig. 3.1, and considering I_s as the mass moment of inertia of the swash plate, m_s, m_r and m_p as the respective masses of the stroking, rate and each barrel pistons, the equation of the active swivelling dynamics can be derived as

$$[\{I_s/l_{st}\} + \{m_s l_{st} + m_r l_{rt}\}]\ddot{x}_s$$
$$= F_{sp}l_{st} - F_{rp}l_{rt} + \sum_{i=1}^{9}[(F_{pi} - m_p\ddot{x}_{pi})\{R_p \cos(\omega t + 2\pi(i-1)/9)\}], \tag{3.28a}$$

with the swash angle related to the stroking piston displacement as

$$\lambda = \tan^{-1}(x_s/l_{st}) \tag{3.28b}$$

and $\ddot{x}_{pi}$ is the acceleration of the ith barrel piston that can be obtained from the instantaneous position of the piston expressed in terms of the variable swash angle λ and the speed of barrel rotation ω as

$$x_{pi} = R_p[1 - \cos\{\omega t + 2\pi(i-1)/9\}]\tan\lambda. \tag{3.29}$$

F_{sp}, F_{rp} and F_{pi} are respectively the resultant forces acting on the stroking, rate and each barrel piston given as

$$F_{sp} = (P_{sc} - P_r)(\pi d_{sp}^2 / 4) - f_s \qquad (3.30a)$$

$$F_{rp} = -k_r(\delta_0 + x_r) - (P_{rc} - P_r)(\pi d_{rp}^2 / 4) + f_r \qquad (3.30b)$$

and $\quad F_{pi} = (P_{pi} - P_r)(\pi d_p^2 / 4) + f_{pi} \qquad (3.30c)$

in which f_s, f_r and f_{pi} are the viscous friction forces acting respectively on the stroking, rate and i^{th} barrel piston given as

$$f_s = \pi \mu d_{sp}(l_s - l_{s0} - x_s)\dot{x}_s / c_{sc} \qquad (3.31a)$$

$$f_r = \pi \mu d_{rp}(l_{r0} + x_r)\dot{x}_r / c_{rc} \qquad (3.31b)$$

and $f_{pi} = \pi \mu d_p \dot{x}_{pi}(l_{pi} - l_{p0i} - x_{pi}) / c_{bc} \qquad (3.31c)$

These friction forces oppose the piston motion and are due to the flows through the annular passages between the respective piston and cylinder.

3.4.3 Modelling of pressure dynamics inside the cylinders

In equation (3.30) the pressures, other than the case pressure, associated with the respective pistons have their own dynamics. Such dynamics can be expressed with reference to the earlier studies (Mandal et at. 2008, 2012, 2014) by considering only the effect of compressibility within the respective control volumes so as to write

$$\dot{P}_{sc} = \beta\{Q_{sc} - Q_{lsc} - (\pi / 4)d_{sp}^2 \dot{x}_s\} / V_{sc}, \qquad (3.32a)$$

$$\dot{P}_{rc} = \beta\{(\pi d_{rp}^2 / 4)\dot{x}_s - Q_{lrc} + Q_{rc}\} / V_{rc}, \qquad (3.32b)$$

and $\dot{P}_{pi} = \beta\{(\pi d_p^2 / 4)\dot{x}_{pi} - Q_{lci} - Q_{lki} - (Q_{di} - Q_{si})\} / V_{bc}, \qquad (3.32c)$

where V_{sc}, V_{rc} and V_{bc} are the respective variable volumes of the stroking, rate and each barrel cylinder expressed in terms of variable swash angle λ, and other relevant geometries with reference to Fig. 3.1 as

$$V_{sc} = (\pi d_{sp}^2 / 4)(l_s + x_s), \qquad (3.33a)$$

$$V_{rc} = (\pi d_{rp}^2 / 4)(l_r + l_{rt} \tan \lambda_{ci} - x_r), \qquad (3.33b)$$

54

and $V_{bc} = (\pi d_p^2 / 4)(l_{pi} - l_{p0i} + x_{pi})$. (3.33c)

Different flow rates involved in equations (3.32a) to (3.32c) can be obtained from equations (3.5) to (3.9) along with using Table 3.1 to 3.3 appropriately.

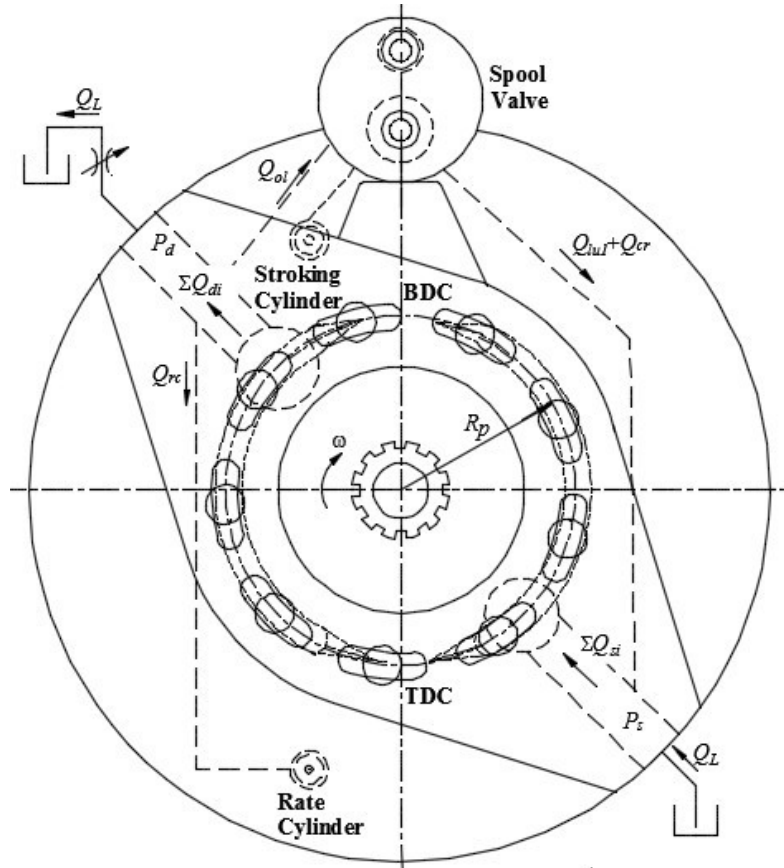### 3.4.4 Modelling of pressure and flow external to the pump

Figure 3.7: Main flow path of the pump and pressure compensator

With reference to Fig.3.7, the dynamics of pressures P_d and P_s in the respective delivery and suction manifolds can be obtained by considering compressibility effect in the volume V_{pd} between delivery port and load orifice upstream and the volume V_{ps} of reservoir and suction port together. Assuming no leakage outside the pump, it is considered that the flow coming out from the load orifice, Q_L re-enters to the pump

through the suction manifold. Hence, the pressure rates can be expressed as

$$\dot{P}_d = \beta[(\sum_{i=1}^{n} Q_{di} - Q_L - Q_{rc} - Q_{ol}]/V_{pd},$$ (3.34a)

$$\text{and } \dot{P}_s = \beta[Q_L + Q_{lu1} + Q_{cr} - \sum_{i=1}^{n} Q_{si}]/V_{ps},$$ (3.34b)

in which the flow through the load orifice can be expressed as

$$Q_L = C_d A_L \sqrt{2(P_d - P_r)/\rho} .$$ (3.35)

Equations (3.23), (3.28), (3.27), (3.32) and (3.34) respectively involve the dynamics of different displacements and pressures. Simultaneous solution of those equations along with other static equations will lead to prediction of the dynamic performance of the system under study. While those parameters evaluated from the static design compiled in Table 3.4 are used in the dynamic simulation, certain other parameters to be identified through dynamic simulation described in the next Chapter.

3.5 Summary

A mathematical model followed by a static design methodology for the pressure compensator with two stage spool valve of a variable displacement swash plate type axial piston pump at a fixed cut-in and cut-off setting has been reported here. The design principle is based on the torque balance condition for the chosen cut-in and cut-off setting with an objective to check the working of the pump at various other cut-in and cut-off settings.

CHAPTER-4

DESIGN ANALYSIS AND EXPERIMENTAL VERIFICATION OF THE PRESSURE COMPENSATOR

4.1 Overview

After the development of the mathematical model of pressure compensator for the variable axial piston pump along with framing a design methodology under static condition, an exhaustive dynamic simulation has been performed in this chapter for analyzing the design to obtain the best sizes of some important parameters. Such parameters of the pressure compensator have a critical role in the pump performance. The sizes have been obtained by tuning the simulation prediction to meet the desirable performance. A commercially available pump (Bosch Rexroth, 2004) has been taken up as the reference for the proposed design methodology. The simulated performance of developed model has been compared with the experimental result obtained from the commercial pump.

4.2 General procedure and conditions for simulation

The flow chart in Fig. 4.1 shows the procedure, how the pressure compensator design has been accomplished starting from the selection of cut-in and cut-off pressure for the pump. The output of the Design Module from the static consideration is marked as Tuneable Parameters, which are analyzed through the Simulation Module. Through the Design Analysis study, described in the following, the design of the pressure compensator has been finalized, which subsequently has been verified with experiment through the Experimental Module for same loading condition represented in the figure as Load Area Variation block. Also for verification, the actual pump speed has been fed to the Simulation Module. Other than this, the static and dynamic models along with the chosen parameters are utilized in the Simulation Module. While those parameters evaluated from the static design compiled in Table 3.4 are used in the dynamic simulation, certain other parameters, explicitly required for the simulation, are furnished in Table 4.1.

The mathematical (both static and dynamic) model developed above has been coded in MATLAB-Simulink version 8.0, R2011a and solved by using ODE4 (Runge-Kutta) solver with fixed time step of 2.5×10^{-7}s. The detailed model has been furnished in Appendix II.

58

For the simulation study, following assumptions are to be noted.

1. The temperature, density, and the bulk modulus of the hydraulic oil remain constant.

2. The discharge coefficients for the different constrictions remain constant.

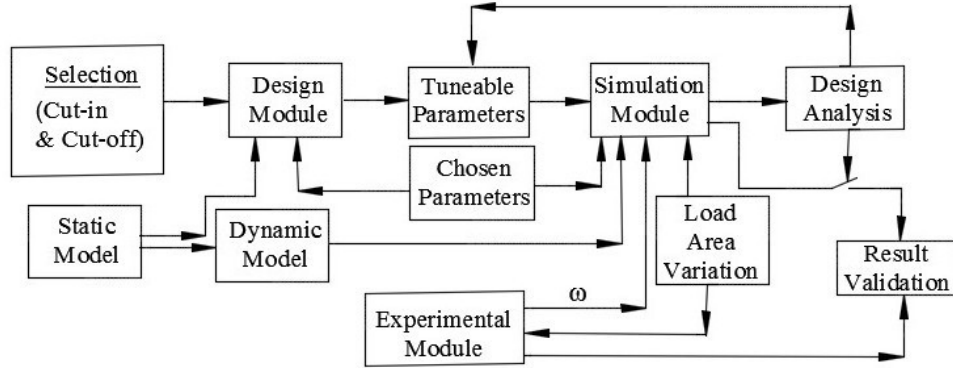3. Only viscous friction forces are considered during dynamic simulation.

Figure 4.1: Flow chart for design analysis and result validation

Table 4.1: Additional parameters required for dynamic simulation

Parameters	Value	Parameters	Value
l_d, l_r	15x10^{-3} m	l_{sr}	41.5x10^{-3} m
I_s	985.992x10^{-9} kg-m^2	R_p	35x10^{-3} m
m_s	0.041 kg	l_{pi}	65.5x10^{-3} m
m_r	0.052 kg	l_{p0i}	10 x 10^{-3} m
m_p	0.0306 kg	C_{bc}	11x10^{-6} m
m_{sv1}, m_{sv2}	0.0143kg,0.0182 kg	V_{pd}, V_{ps}	1.44x10^{-4}m^3,0.714 m^3
d_{dr}	1.5x10^{-3} m	A_L	8.55e-6 m^3
d_d	0.9 x10^{-3} m	l_b	15 x10^{-3} m

In the following part of the chapter, the results are presented in two parts. In the first part, starting from Section 4.2 to Section 4.6, the design sensitivity analysis through dynamic simulation has been reported for the critical parameters of the pressure compensator. Those are the diameters and radial clearances for the rate and stroking

piston, the lap conditions for both the top and bottom spools and the diameter of the clearance orifice at the bottom of the spool valve. In the above set, the parameters for the rate and stroking piston have been obtained from the static design process, whereas, the others have been chosen arbitrarily. The objective of the dynamic simulation is to check the success of the static design concept and to tune the chosen parameters so as to minimize the arbitrariness and to achieve reasonable sizes. All the designs pertain to barrel rotational speed of 1500rpm, case drain pressure of 0.2MPa. The second part of the result presented in Section 4.7, deals with the experimental verification of the pressure compensator design.

4.3 Sensitivity analysis of the rate and stroking piston diameters

Figure 4.2 presents the sensitivity analysis of the swashing dynamics for three combinations of diameters (d_{rp} and d_{sp}) for rate the and stroking cylinder in terms of delivery pressure, pressure inside the stroking cylinder, swash angle and flow rate. The nominal design refers to the one obtained following the steps through torque balance described in Section 3.2. In Off-Nominal1 design, a lower than nominal diameter for the rate piston is selected and a corresponding stroking piston diameter is obtained from equation (3.20), keeping the size of all other components of the compensator same with the nominal design. In the same way, Off-Nominal2 design has been obtained considering the rate piston diameter more than that for nominal design. The pump dynamics have been studied for a typical external load variation achieved by changing the area of the load orifice. Initially, up to 30ms, the load orifice area A_L is set at a value that corresponds to the near cut-in delivery pressure of 19MPa. For the next 40ms, the area is decreased linearly towards full closure and maintaining it for 40ms targeting the cut-off condition. After that the area is increased in a same linear manner such that the pump returns back to its cut-in condition. The pattern is shown in Fig.4.2a in the scale of 0-1, where 1 indicates cut-in and 0 indicates cut-off condition. The same area pattern is followed for all the dynamic simulation studies unless mentioned.

Apparently, for the three sets of rate and stroking pistons, the performances in terms of attaining the cut-off pressure followed by return back to the cut-in pressure are more or less acceptable. However, as shown in Fig. 4.2b, the penalty for having off

nominal design can be felt in the pressure dynamics inside the stroking piston, where Off-Nominal1 design predicts strong negative pressure spikes that may lead to cavitation. In this design, higher swash-plate oscillation during cut-off operation is revealed in Fig. 4.2c. This could be attributed to lower torque produced by the pressure inside this cylinder acting on a smaller area for the rate piston with smaller diameter. Even within the cut-in limit, because of torque imbalance, the swivelling torque drives the swash plate. The negative pressure is due to the movement of the stroking piston by the swash plate while the supply to the stroking cylinder is through the case only. This is because the spool valve during cut-in remains closed. Thus, no flow from the pump delivery enters in the stroking cylinder chamber. Increase in the size of both the pistons beyond nominal design, as done in Off-Nominal2 design, reduces the negative pressure spikes in the stroking piston. However, for compact sizing of the pump, the nominal design remains a better choice.
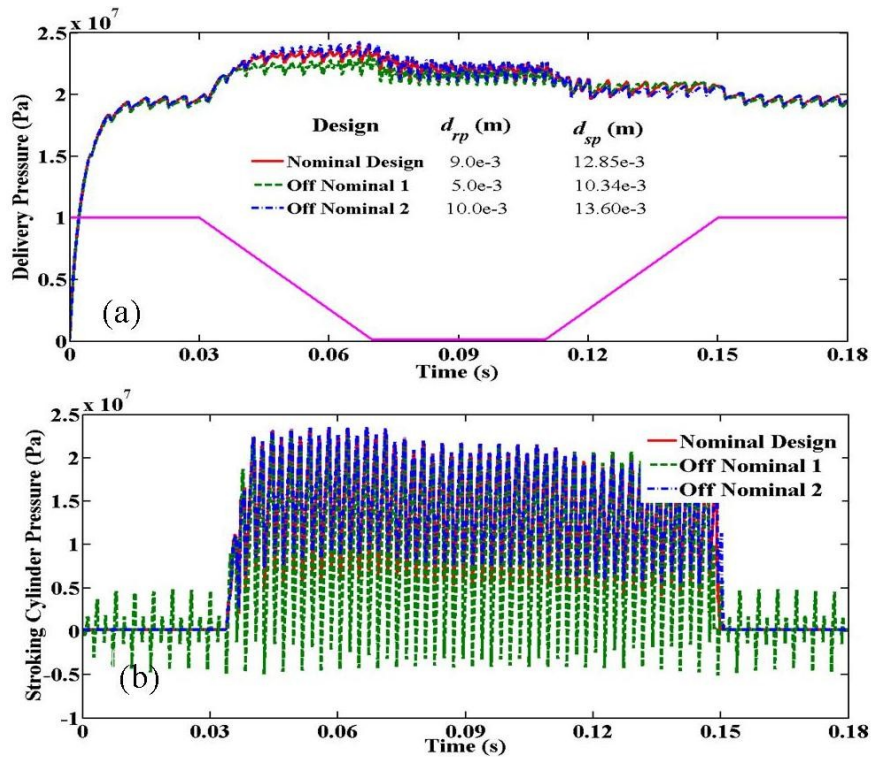
Figure 4.2: Sensitivity study for different pump designs – (a) delivery pressure dynamics; (b) stroking cylinder pressure dynamics

61
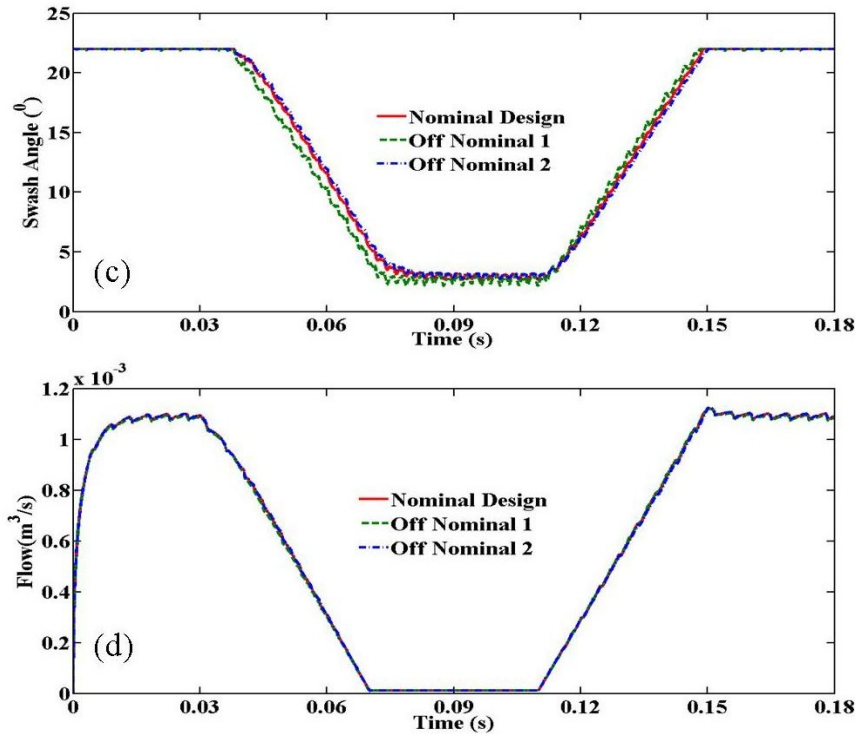
Figure 4.2: Sensitivity study for different pump designs – (c) swash angle dynamics; (d) flow dynamics

4.4 Effect of radial clearance between the rate cylinder and piston

Figure 4.3 depicts the performance of the pump for different radial clearances other than nominal between the rate piston and the cylinder. From the static design process, the nominal value is obtained as 70μm. It can be observed that for lower radial clearance (30μm) there is no perceptible change in the delivery pressure or swash angle dynamics. However, maintaining low radial clearance of this order calls for higher manufacturing cost. So in the next phase, the radial clearance has been increased from the nominal value. The simulated results show that beyond 200μm clearance, the pressure dynamics is degraded, particularly during the phase of changing from cut-off to cut-in pressures. In fact for radial clearance 200μm, the swash angle dynamics is found to behave differently with respect to the nominal situation. The behavior gets worse for 300μm. The trend indicates that the radial clearance between the rate piston and cylinder may be kept within 100μm for strict adherence to the nominal performance, whereas it

may be kept within 200µm with a possibility of slight departure from the nominal performance.
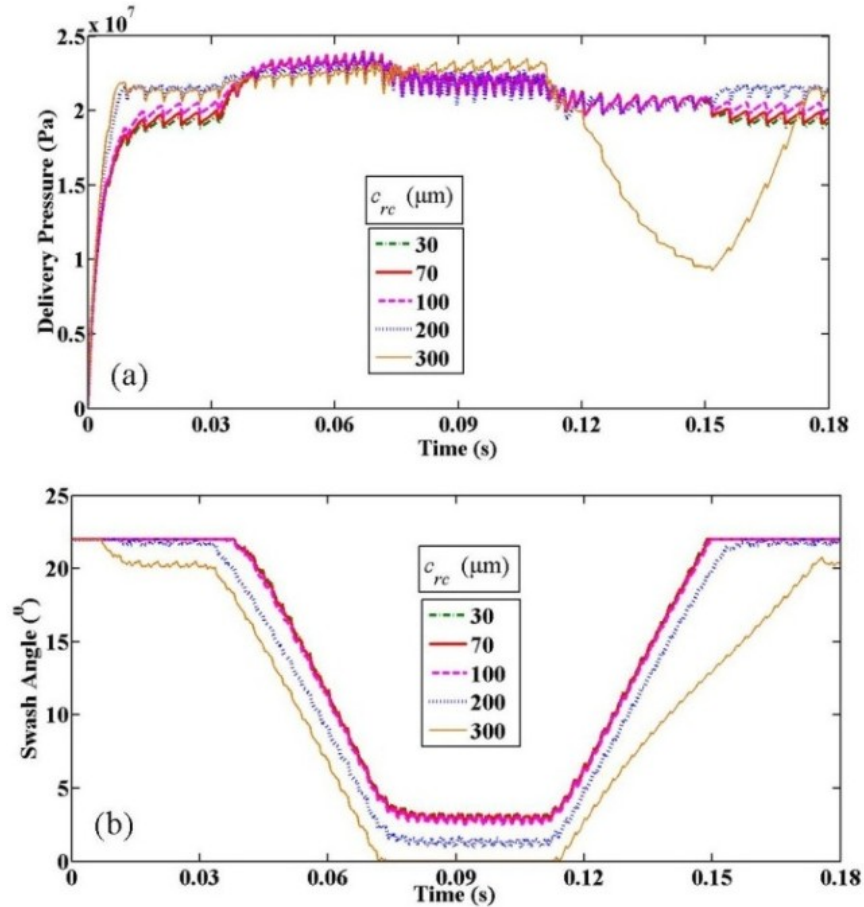
Figure 4.3: **Effect of radial clearance of rate cylinder on dynamic performance of the pump**

4.5 Effect of radial clearance between the rate cylinder and piston

The radial clearance between the stroking piston and the cylinder is varied about the nominal value of 39µm obtained from the static design process. Similar to the rate cylinder, in this case also reduction in the radial clearance (20µm) does not alter the pressure and swash angle dynamics at all as shown in Fig. 4.4. Increase in the radial clearance to 100µm causes minimal change in the performance of the pump. However, radial clearances of 200µm and above result significant degradation in the performance in terms of rise in delivery pressure much beyond the cut-off pressure. In fact for 300µm radial clearance, during the closure of the load orifice (refer Fig. 4.2a), the swash plate is unable to deflect towards minimum angle (refer Fig. 4.4b). This is due to the fact that with increased amount of annulus gap, the bulk of the flow coming from the spool valve

63

leaks through this gap. Therefore, pressure does not build up inside the stroking cylinder, so as to produce the necessary torque for swash plate deflection. The study reveals that the radial clearance of the stroking piston has to be maintained within 100μm.
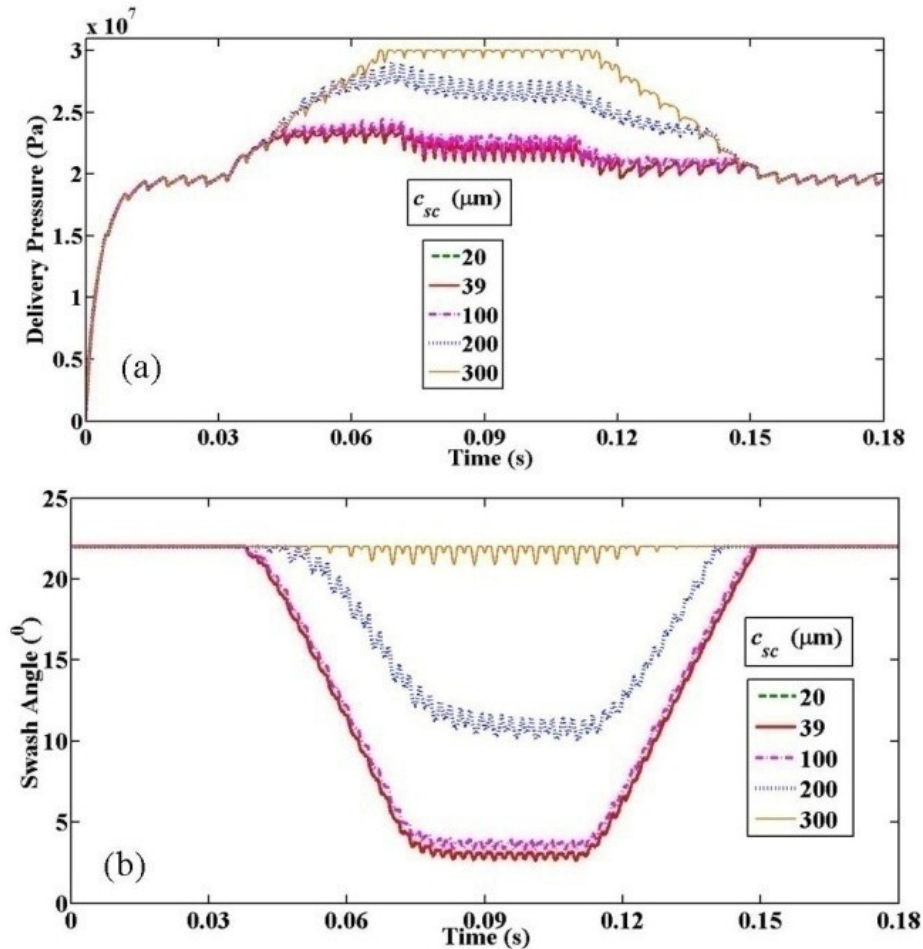
Figure 4.4: Effect of radial clearance of stroking cylinder on dynamic performance of the pump

4.6 Effect of lap conditions of the spool valve on pump performance

The role of lap condition of the spool valve is important in achieving the stability of the swash plate. During the modelling in Section 3.2.2, both the spool valve is considered to have overlap at the respective left chambers and underlap at the right chambers. The nominal values of those for the static design have been chosen as 10μm and 90μm respectively. In one study, the lap condition is swapped by having underlap at the left chamber and overlap at the right chamber, denoted by negative sign in the values of overlap o_d and underlap u_r shown in Fig. 4.5. It is evident that the swapping would

64

not provide the desired performance of the pump. Due to underlap at the left chamber, which is connecting the stroking cylinder with the delivery pressure, the stroking cylinder receives flow even when the spools do not get deflected against the spring. Thus even before the delivery pressure reaches cut-in condition the swash plate starts rotating towards zero as seen in Fig. 4.5b for higher underlap. This observation establishes the requirement for having overlap at the left spool and underlap at the right spool.
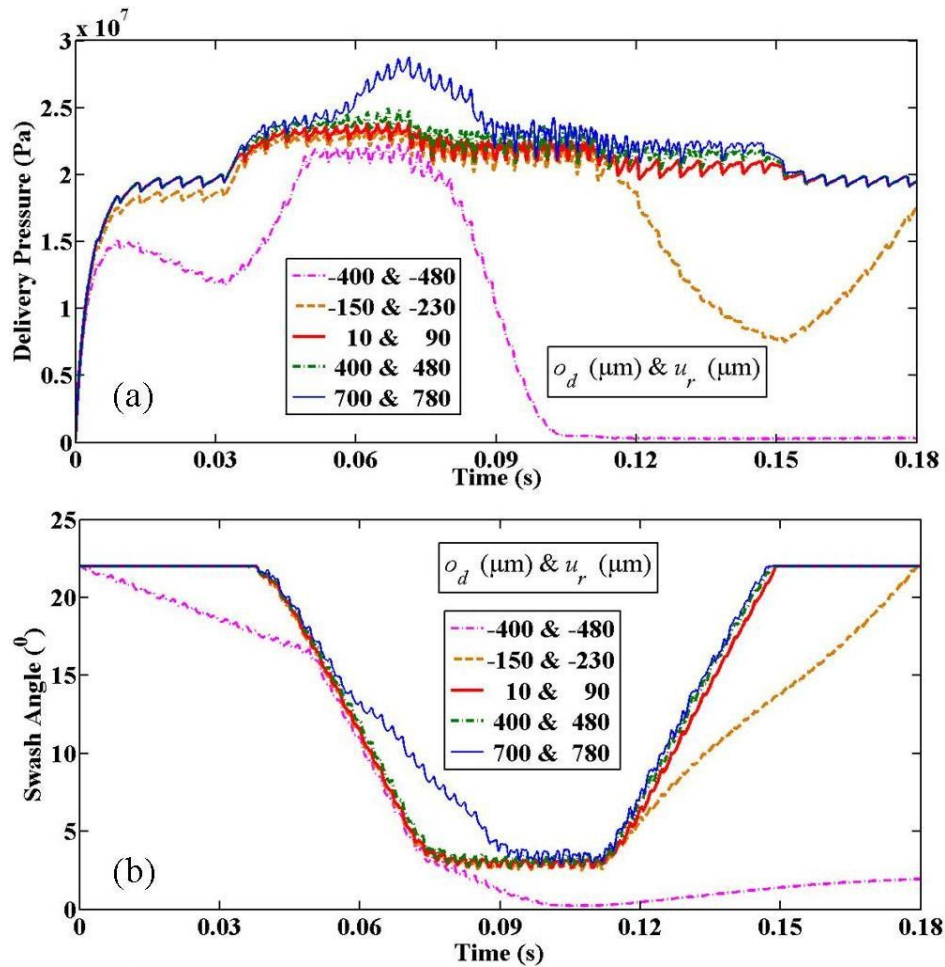
Figure 4.5: Effect of lap conditions of the spool valve on dynamic performance of the pump

Figure 4.5 also depicts the results for increased lap sizes. It can be seen that for 400μm overlap and 480μm underlap, the pressure dynamics and swash angle dynamics remain more or less close to the desired performance. However, for 700μm overlap and 780μm underlap, the delivery pressure is raised much beyond the cut-off setting, which is detrimental for the operation of variable displacement pump in a system without pressure

relief valve. Much increase in the overlap calls for more compression in the spool spring causing overshoot in the delivery pressure. From this study, it can be said that the overlap and underlap of both the spools should be kept within 400μm.

4.7 Effect of bypass orifice in the control spool valve

The role of the bypass orifice situated below the bottom of the spool valve connecting ports A and T, as shown in Fig. 3.4, is now analyzed. The bypass is typically required during the retraction of the stroking piston, while the spool valve remains closed due to fall in the system pressure below cut-in. Therefore, choice of the orifice size (diameter, d_{oc}) may be a crucial issue in achieving this performance of the pump. In this study, from no orifice (zero diameter) to different sizes of orifices have been used for a typical variation of the load, which is different than in case of the previous studies. The load variation shown in Fig. 4.6a, has been achieved by varying the load orifice area. Initially, for the first 30ms the load orifice remains fully open (corresponds to no load condition). Then for the next 40ms the area is decreased to minimum that corresponds to the cut-off condition. This area is maintained for the next 50ms and for the subsequent 40ms the load orifice area is increased up to 50% of the full opening and held constant for the next 40ms. Figure 4.6 shows the dynamic performances of the pump for above mentioned condition for different orifice sizes. The results clearly show the requirement of the bypass orifice, typically during transition from higher pressure to low pressure operating condition. As far as the pressure build up is concerned (Fig. 4.6b), there is hardly any difference in the performance of the pump from no orifice to any other sizes of the orifice. But there are substantial differences in the performance during the latter part of the load area variation. In case of no orifice, at cut-off, the swash angle becomes zero. But when the load is reduced by increasing the opening of the load area orifice, the swash plate is unable to rotate back as evident from the characteristics of swash angle in Fig. 4.6c. During low pressure below cut-in, as both the spool valve gets closed, the oil from the stroking cylinder does not get any exit route. Because of this sealing of oil inside the stroking cylinder, the swivelling torque and the torque due to the rate piston are unable to rotate the swash plate. Hence, the delivery pressure remains minimum even there is a substantial load within cut-in limit. With increase in the orifice size, the

66

performance gets improved for this part and it has been found that from orifice diameter 1mm onwards the steady state value of the delivery pressure and swash angle remains same with variation in the dynamics. Therefore, from this study, an orifice size of 1mm can be denoted as a critical size. However, the pump could be operated without bypass orifice by introducing underlap in the left spool as depicted in Fig. 4.5. In such case the stroking piston could be depressurized with degradation in the dynamic performance.
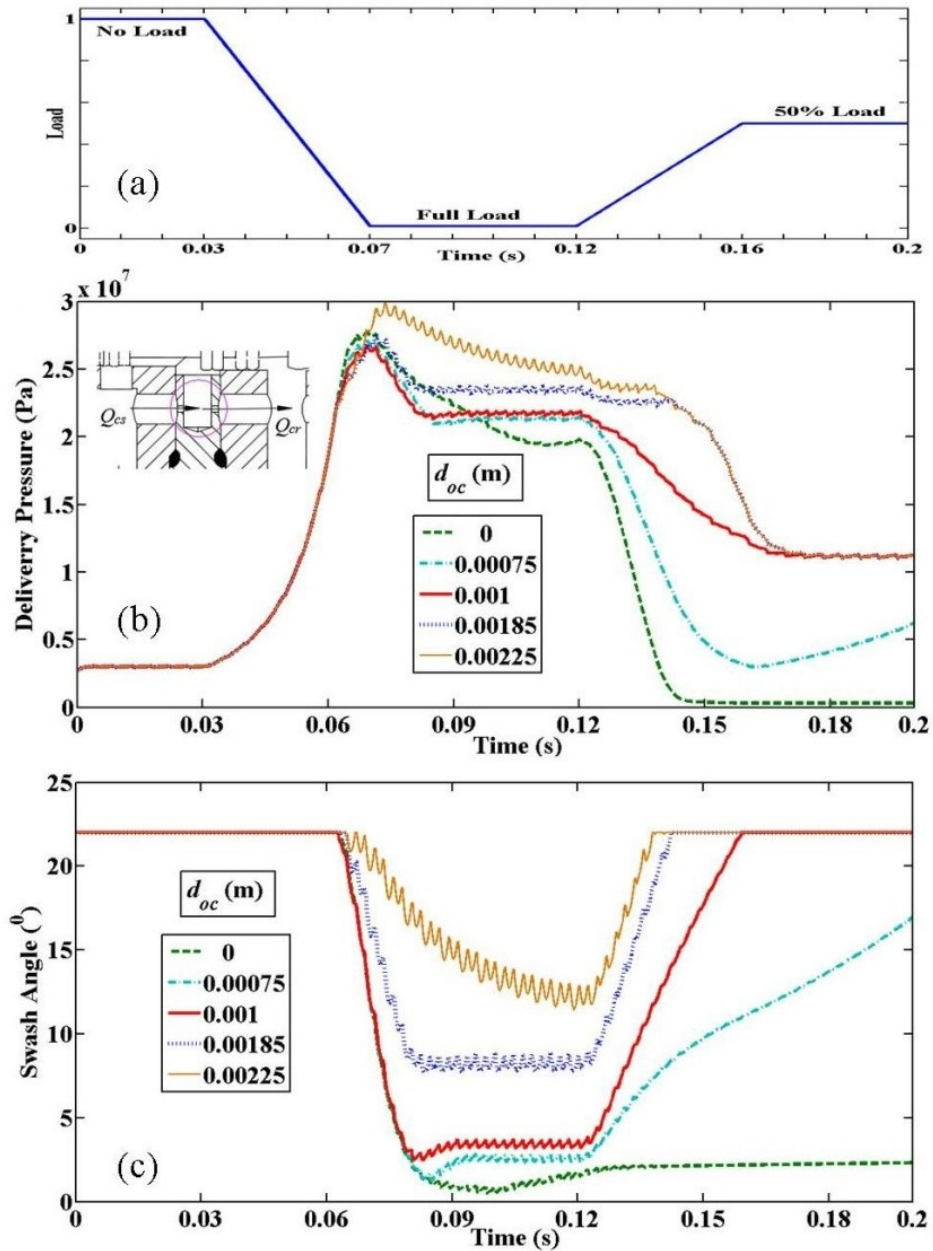
Figure 4.6: Effect of orifice size at bottom of the spool valve on the dynamic performance of the pump

67

4.8 Experimental verification of the compensator design

The pressure compensator model has been verified here by comparing the simulation predictions with the experimental result in two stages. In the first stage, the spring precompression setting of the bottom spool is kept fixed at 0.00415m, while that for the top spool is varied in order to achieve the matching result with the experimental one. Figure 4.7 shows that for a top spool spring precompression setting of 0.0086m, the simulation result matches fairly well with the experimental result. In the second stage keeping the top spool spring precompression fixed at 0.0086m, the precompression of the bottom spool spring is varied.
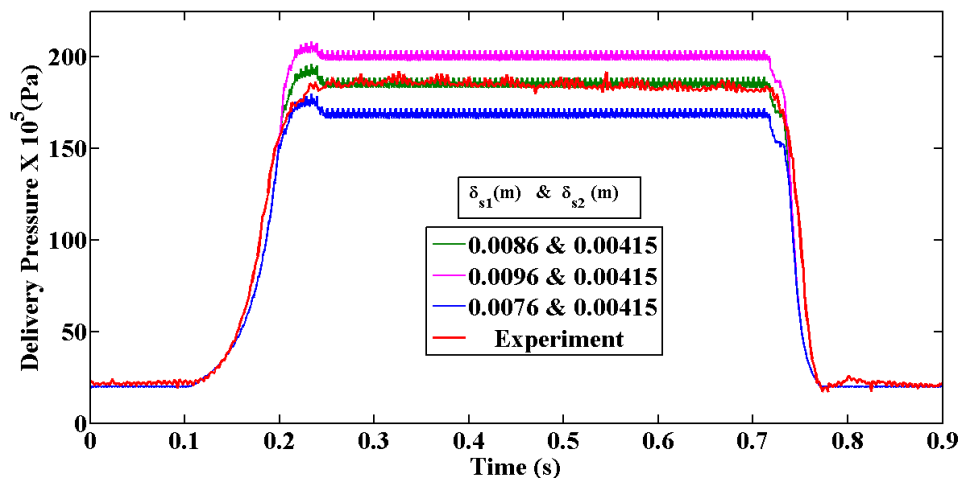
Figure 4.7: **Experimental validation of pressure dynamics for different precompressions of top spool**
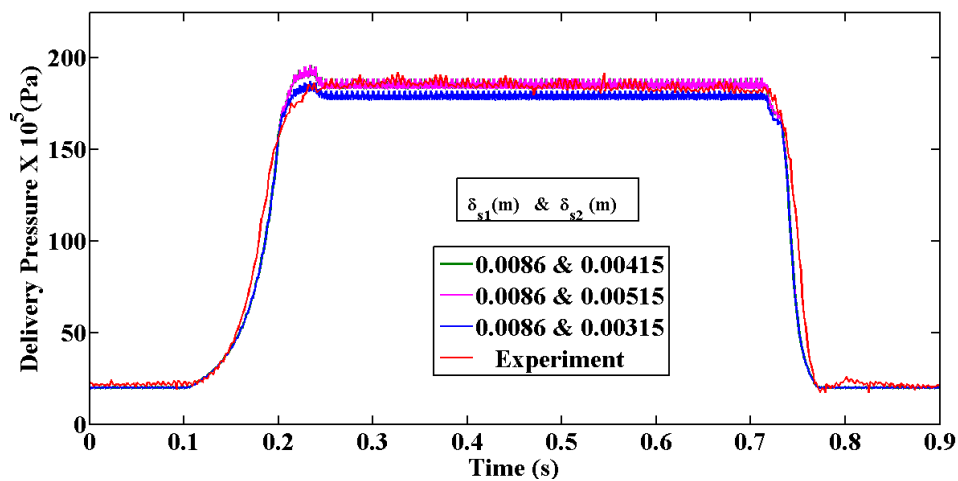
Figure 4.8: **Experimental validation of pressure dynamics for different precompressions of bottom spool**

It can be seen from Fig. 4.8 that for a combination of 0.0086m and 0.00415m spring precompression of top and bottom spool respectively, the simulation matches best with the experimental one. As the bottom spool spring is of higher stiffness than the top, it is observed from Fig. 4.8 that change in bottom spool spring precompression within a range of ±0.001m causes ±0.65MPa change in the cut-off pressure. It may be mentioned that although the compensator design has been performed for 19.5MPa cut-off pressure, it has been used in the verification study with a factory set cut-off value of 18.5MPa. Clearly, the study establishes the robustness of the balanced torque design apart from validating the model.

4.9 Summary

In this study, some critical design parameters have been tuned through dynamic simulation, which have very important role in the pump performance. The sensitivity analysis of nominal and off-nominal dimensions through dynamic simulation and the subsequent experimental verification have established the potential of the design approach. It has been found that the nominal diameters of the rate and stroking pistons provide the most compact dimensions without any significant swash plate oscillation during load transience. Predictions with respectively up to 50% and 250% increase in nominal clearances between the rate and stroking piston-cylinder pairs exhibited acceptable pump performance. But, further increase in clearances within stroking cylinder bore has indicated major degradation of the pump performance. The metering out and metering in of the flow to and from the stroking cylinder through both the spools in the pressure compensator valve have been observed to be a strong requirement. The role of the bypass line between the stroking-cylinder port and the tank port has been identified as for achieving acceptable dynamics of the swashing angle during the return phase corresponding to load within cut-in limit.

CHAPTER-5

A PROPOSITION FOR A SIMPLE SPOOL VALVE FOR THE PRESSURE COMPENSATOR

5.1 Overview

Following the methodology discussed in Chapter 3, in this chapter a detail design analysis of a rather simple single stage control spool valve has been taken up with an aim to replace the commercially used two stage valve as shown in Fig. 5.1. The design involves evaluation of the spool size and selection of spring from static equilibrium condition to satisfy cut-in and cut-off pressure. After modifying the dynamic model of the system, a design sensitivity analysis of the spool valve has been carried out through simulation to identify the critical sizes of the parameters, which affect the pump performance. Results obtained from simulation for the present design has been compared with the commercial pump (A10VSO45 series pump from Rexroth) having compensator with double spool in order to study the effectiveness of the simplified compensator design.
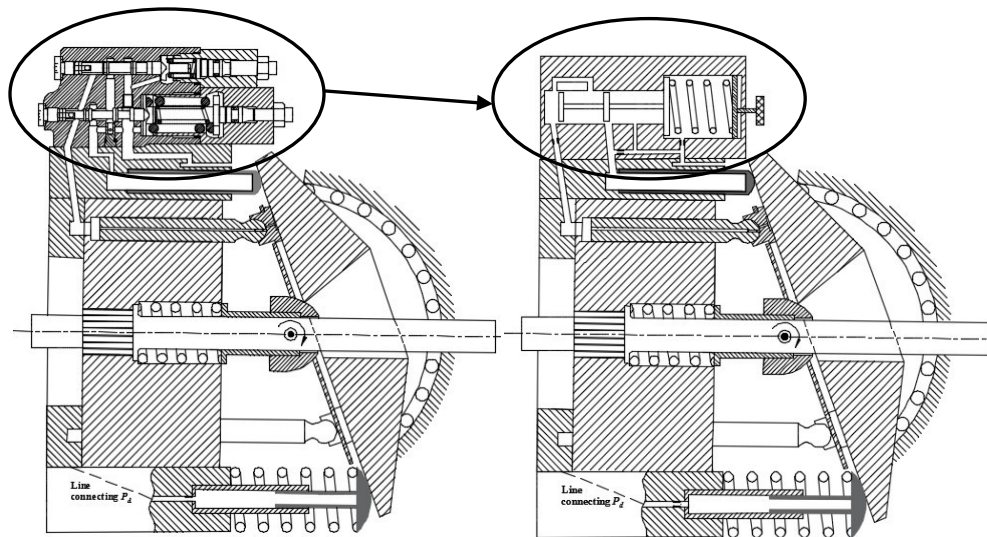
Figure 5.1: Replacement of control spool valve

5.2 Design of spool valve from static condition

The control spool has been designed through some considerations. Following are the considerations for the design of spring and spool land of the spool valve, the schematic of which is shown in Fig. 5.2.

a) The spool displacement starts at cut-in pressure P_{dci}, and attains its maximum displacement at the cut-off pressure P_{dco}.

b) The flow force F_s, acting on the spool is neglected under static condition.

c) The effect of radial clearance is neglected.

In static condition at the cut-in limit, the active pressure P_d^* acting at the left side of the spool remains at P_{dci}, whereas the back pressure P_l acting on the right side of the spool remains at the case pressure P_r. Under this situation the hydraulic force on the spool should be balanced by the spring force due to a spring precompression δ_{s0} leading to the relation

$$(P_{dci} - P_r)(\pi d_s^2 / 4) = k_s \delta_{s0} . \tag{5.1a}$$

For a realistic choice, following the previous approach done in Section 3.3.3, both the spool land diameter, d_s and spring pre-compression, δ_{s0}, the spring stiffness k_s has been estimated. A feasible size of the spring in terms of coil diameter, wire diameter, number of coil turns has been selected using a well-known relation (Bhandari, 2010) so as to match the estimated stiffness. The equation is

$$k_s = \frac{G d^4}{8 D^3 n}, \tag{5.1b}$$

where G is the modulus of rigidity of the spring material, d is the wire diameter, D is the mean coil diameter and n is the number of turns.

In order to accommodate the available spring, necessary modifications in terms of increase in the right side spool land diameter and the chamber length have been done. It can be observed that this diameter d_{sr} could be larger than the diameters (d_s) of the other two lands. However, this increase in size would not alter the force balance equation as long as both sides of this land experience the case pressure P_r, typically for the situation under static condition. The maximum spool displacement, which is also the maximum spring compression, is obtained from the static force balance at cut-off condition given by

$$P_{dco}(\pi d_s^2 / 4) - P_r(\pi d_{sr}^2 / 4) = k_s (\delta_{s0} + x_{svmax}) . \tag{5.2}$$

Table 5.1 lists the parameters related to the spool valve designed, while those related to the other components of pump are kept same as furnished in Table 3.4 of Chapter 3.
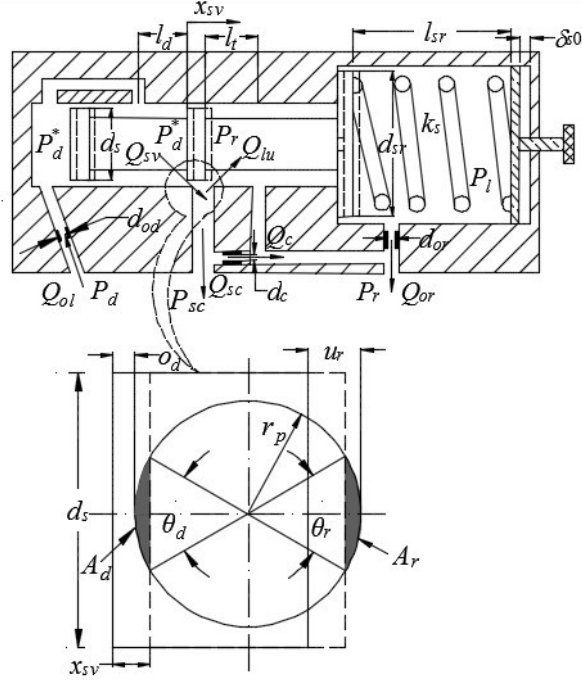
Figure 5.2: Schematic of the single-stage control spool valve

$$F_{sf}=k(\delta_{s0}+x_{sv})$$

$$F_p=P_d^*(\pi d_s^2/4)+\pi P_r/4(d_{sr}^2-d_r^2)-P_l(\pi d_s^2/4)$$
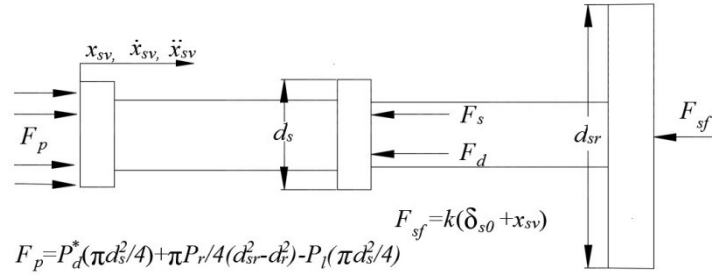
Figure 5.3: Free body diagram of the spool

Table 5.1: Parameter values for the designed pressure compensator

Parameters (Chosen)	Value	Parameters (obtained)	Value
d_s	6.5×10^{-3} m	k_s	68786 N/m
δ_{s0}	8.6×10^{-3} m	x_{svmax}	2.408×10^{-4} m
G	79.3×10^{9} Pa	d_{sr}	20.5 m
d	4×10^{-3} m	D	16×10^{-3} m
n	8		

5.3 Modification in the dynamic model of the compensator system

As shown in Fig.5.2, the left chamber of the control spool valve is connected to the delivery line of the pump through an entry orifice of diameter d_{od}, the pressure inside the entry chamber remains at P_d^* instead of delivery pressure P_d due to the pressure drop through the orifice. The right end chamber of the spool is connected to the reservoir through an orifice of diameter d_{or}, due to which the pressure remains at P_l instead of reservoir pressure P_r. The chamber between the middle and right land of the spool valve is directly connected to the reservoir, thereby considered to experience the same reservoir pressure. This pressure acting on both the opposing surfaces will not result any net force acting on the spool. Under these considerations and with reference to Fig. 5.3, the spool displacement equation, in terms of the conditions between the net hydraulic pressure force F_p and the spring force F_{sf}, can be written as

$$\ddot{x}_{sv} = 0 \text{ for } F_p \le k_s \delta_{s0}, \tag{5.3a}$$

$$\ddot{x}_{sv} = (F_p - F_d - F_s - F_{sf})/m_{sv} \text{ for } F_p > k_s \delta_{s0}, \tag{5.3b}$$

where F_d is the transient flow force and F_s is the steady flow force acting on the spool expressed respectively from Merrit (Merritt,1967) as

$$F_d = \rho(l_d \dot{Q}_{sv} - l_t \dot{Q}_{lu}), \tag{5.4a}$$

$$F_s = 2C_d C_v \{A_d (P_d^* - P_{sc}) \cos \theta_{jd} + A_r (P_{sc} - P_r) \cos \theta_{jr}\}, \tag{5.4b}$$

where C_d and C_v are the coefficients of discharge and velocity respectively, l_d and l_t are the two damping lengths in the spool valve as shown in Fig. 5.2. The two metered flows Q_{sv} from the spool valve to the stroking cylinder and Q_{lu} to the return chamber from the stroking cylinder can be expressed in terms of the respective pressure drops as

$$Q_{sv} = C_d A_d \sqrt{2(P_d^* - P_{sc})/\rho} \operatorname{sgn}|P_d^* - P_{sc}|, \tag{5.4c}$$

$$\text{and } Q_{lu} = C_d A_r \sqrt{2(P_{sc} - P_r)/\rho} \operatorname{sgn}|P_{sc} - P_r|, \tag{5.4d}$$

where θ_{jd} and θ_{jr} are respectively the jet angles of the metered flows Q_{sv} and Q_{lu}. Assuming near-zero radial clearance both the jet angles are assigned as 69^0 from Merrit (1967). From the geometry shown in Fig. 5.2, the variable opening areas A_d and A_r due to the spool displacement can be expressed as

$$A_d = n_p r_p^2 \{\theta_d - (\sin\theta_d)\}/2,$$ (5.5a)

and $A_r = n_p r_p^2 \{\theta_r - (\sin\theta_r)\}/2,$ (5.5b)

for n_p numbers of circular port cuts of radius r_p, where as θ_d and θ_r are the angles subtended by the intersections of the spool land with the circular port cut at the delivery and return sides respectively as shown in the expanded view in Fig. 5.2. For a spool displacement x_{sv}, overlap o_d at the delivery side and underlap u_r at the return side, these angles can be obtained as

$$\theta_d = 2\cos^{-1}\{1 - \max(x_{sv} - o_d, 0)/r_p\},$$ (5.6a)

and $\theta_r = 2\cos^{-1}\{1 - \max(u_r - x_{sv}, 0)/r_p\}.$ (5.6b)

Taking into consideration the compressibility effect, the dynamics of the pressure P_d^* in the entry chamber of the control spool valve can be expressed in terms of the velocity of the spool, flow rate through the entry orifice, bulk modulus of the working fluid and dead volume of the chamber as

$$\dot{P}_d^* = \beta\{Q_{ol} - \pi(d_s^2/4)\dot{x}_{sv}\}/v_0 + \pi(d_s^2/4)x_{sv}\},$$ (5.7a)

in which the flow rate Q_{ol} through the entry orifice of diameter d_{od} can be expressed as

$$Q_{ol} = C_d(\pi d_{od}^2/4)\sqrt{2(P_d - P_d^*)/\rho}\ \mathrm{sgn}\left|P_d - P_d^*\right|.$$ (5.7b)

In case, the pressure in the left chamber of the spool valve is considered same as the delivery pressure of the valve, the flow rate Q_{ol} can be found using continuity equation inside the chamber considering incompressible flow as

$$Q_{ol} = \pi(d_s^2/4)\dot{x}_{sv}.$$ (5.7c)

In a ploy to achieve damping in the spool motion, an orifice of diameter d_{or} is provided in the drain side of the spool valve as shown in Fig. 5.2, such that a back pressure P_l is developed at the return side chamber due to which a force acts on the rightmost spool land opposing the spool motion as written in equation (5.3b). In terms of the spool motion and bulk modulus β, the dynamics of this back pressure is expressed as

$$\dot{P}_l = \beta\{\pi(d_{or}^2/4)\dot{x}_{sv} - Q_{or})\}/\{\pi(d_{or}^2/4)(l_{sr} - x_{sv})\},$$ (5.8a)

where l_{sr} is the length of the rightmost spool chamber after the precompression that can be evaluated from the knowledge of the free length of the spring selected through static

design and the amount of precompression and Q_{or} is the flow through this damping orifice given by

$$Q_{or} = C_d(\pi d_{or}^2/4)\sqrt{2(P_l-P_r)/\rho}\operatorname{sgn}\left|P_l-P_r\right|,\qquad(5.8b)$$

In case, the back pressure is considered same as the case pressure of P_r, the flow rate Q_{or} can be found using continuity equation inside the chamber considering incompressible flow as

$$Q_{or} = \pi(d_{or}^2/4)\dot{x}_{sv}.\qquad(5.8c)$$

Satisfying continuity across the valve, the flow Q_{sc} entering to the stroking cylinder from the spool valve that can be written from Fig. 2 as,

$$Q_{sc} = Q_{sv} - Q_{lu} - Q_c,\qquad(5.9a)$$

where Q_c is the flow through the clearance orifice of diameter d_c of the spool valve that can be expressed as

$$Q_c = c_d(\pi d_c^2/4)\sqrt{2(P_{sc}-P_r)/\rho}\operatorname{sgn}\left|P_{sc}-P_r\right|,\qquad(5.9b)$$

while, Q_{sv} and Q_{lu} have already modelled in equations (5.4c) and (5.4d).

Of course, there is a direct interaction of the spool valve dynamics with the swivelling dynamics of the swash plate including the rate and stroking cylinders of the pressure compensator. The mathematical model for the dynamics of swash plate, other components of the pressure compensator and the pump are kept intact as developed in Chapter 3.

5.4 Parameter sizing through simulation

Following the same methodology illustrated in Fig. 4.1 in Chapter 4, the dynamic model of the pressure compensated pump system, which has single stage spool valve in the compensator represented mathematically through equations (5.3) to (5.9) along with those related to the pump dynamics (adopted from chapter 3) have been coded as a Matlab/Simulink (version 8.0). The conditions for running the model are kept same as in the previous model.

Apart from using the parameter values listed in Table 5.1 and 5.2, the other parameters for simulation are adopted from Table 3.4 and Table 4.1. The input required

to run the simulation are the speed of barrel rotation ω, set at 1500 rpm and the loading condition of the pump represented by the area A_L of the load orifice in equation (3.19). Unless otherwise mentioned, for all the simulation and experiment exercises, the variation of load orifice area is maintained same as shown in Fig. 4.2a. For convenience the pattern has been elaborated again. The orifice area has been set initially at a value that corresponds to the near cut-in delivery pressure of 19MPa. This area is retained for up to 30ms after which for the next 40ms, the area is decreased linearly towards full closure and maintaining it for 40ms targeting the cut-off condition. After that the area is increased in a same linear manner such that the pump will return back to its cut-in condition. Figure 5.4 shows the typical variation of the load orifice area, which has been input to the simulation model.

Table 5.2: Additional parameters required for dynamic simulation

Parameters	Value	Parameters	Value
A_0	1.767×10^{-6} m^2	l_{r0}	10×10^{-3} m
A_L	8.66×10^{-5} m^2	l_s	48×10^{-3} m
C_{rc}	70 μm	l_{s0}	5×10^{-3} m
C_{sc}	39 μm	l_{st}, l_{rt}	50×10^{-3} m
d_{rp}	9×10^{-3} m	m_{sv}	0.02 kg
d_{sp}	12.85×10^{-3} m	O_d, u_r	10 μm, 90 μm
l_r	35×10^{-3} m	l_d, l_t	15×10^{-3} m
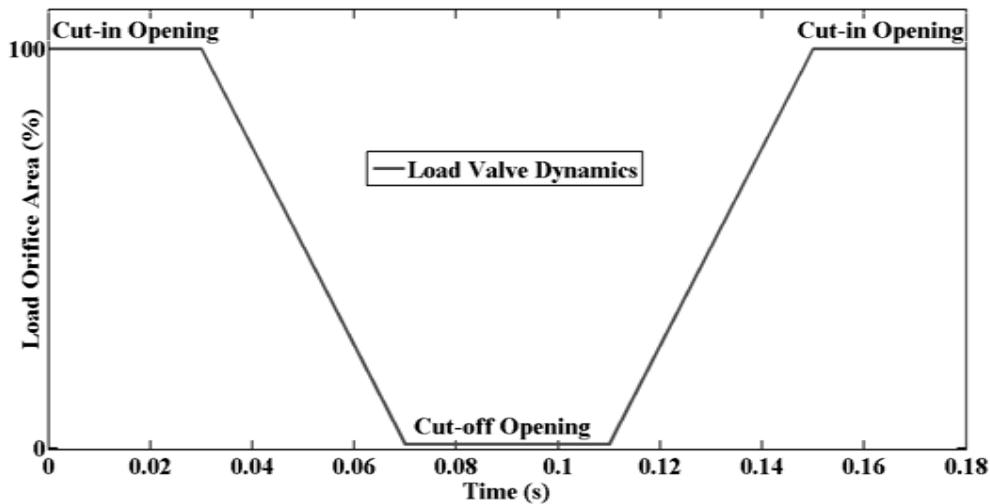
Figure 5.4: Loading pattern to the axial piston pump by changing orifice area

5.4.1 Effect of compressibility model at the delivery chamber of spool valve

Before the parametric study, the need of considering separate pressure node P_d^* at the delivery chamber of the spool valve has been studied. Such consideration calls for inclusion of equations (5.7a) and (5.7b) in the simulation and termed as compressible model while if the delivery chamber of the valve is considered to remain same as delivery pressure P_d, of the pump, the same is termed as incompressible. In such case, equations (5.7a) and (5.7b) need to be replaced by equation (5.7c) in the simulation. The study has been done in terms of observing the predictions of delivery pressure, spool displacement and pressure inside the stroking cylinder for the loading pattern mentioned above. Figure 5.5 shows the comparison between the two modelling approaches. It can be seen that there are hardly any differences in the predictions following the two different methods. However, in order to evaluate the size of the entry orifice, depicted in the next section, the compressible model has been used.

5.4.2 Evaluation of the size of entry orifice to the spool valve

Figure 5.6 depicts the performance of the pump for different delivery orifice at the spool valve. This orifice acts as a bridge element between the pump and the spool valve. The delivery line of the pump is connected to the spool valve through this orifice. The diameter of the orifice has been varied from zero to 1 mm and the performance of the pump has been predicted in terms of delivery pressure, swash angle and flow rate characteristics of the pump for the same loading pattern shown in Fig. 5.4. Of course in Fig.5.6 zero size orifice is indicated as 'no orifice' in which the left spool chamber is directly connected with the pump. It is clear from the figure that there is very little difference in terms of the performance of the pump with or without having an orifice at the entry of the spool valve. Hence, for the spool valve, no entry orifice has been suggested and accordingly for the rest of the study, incompressible model has been used for it takes less simulation runtime.
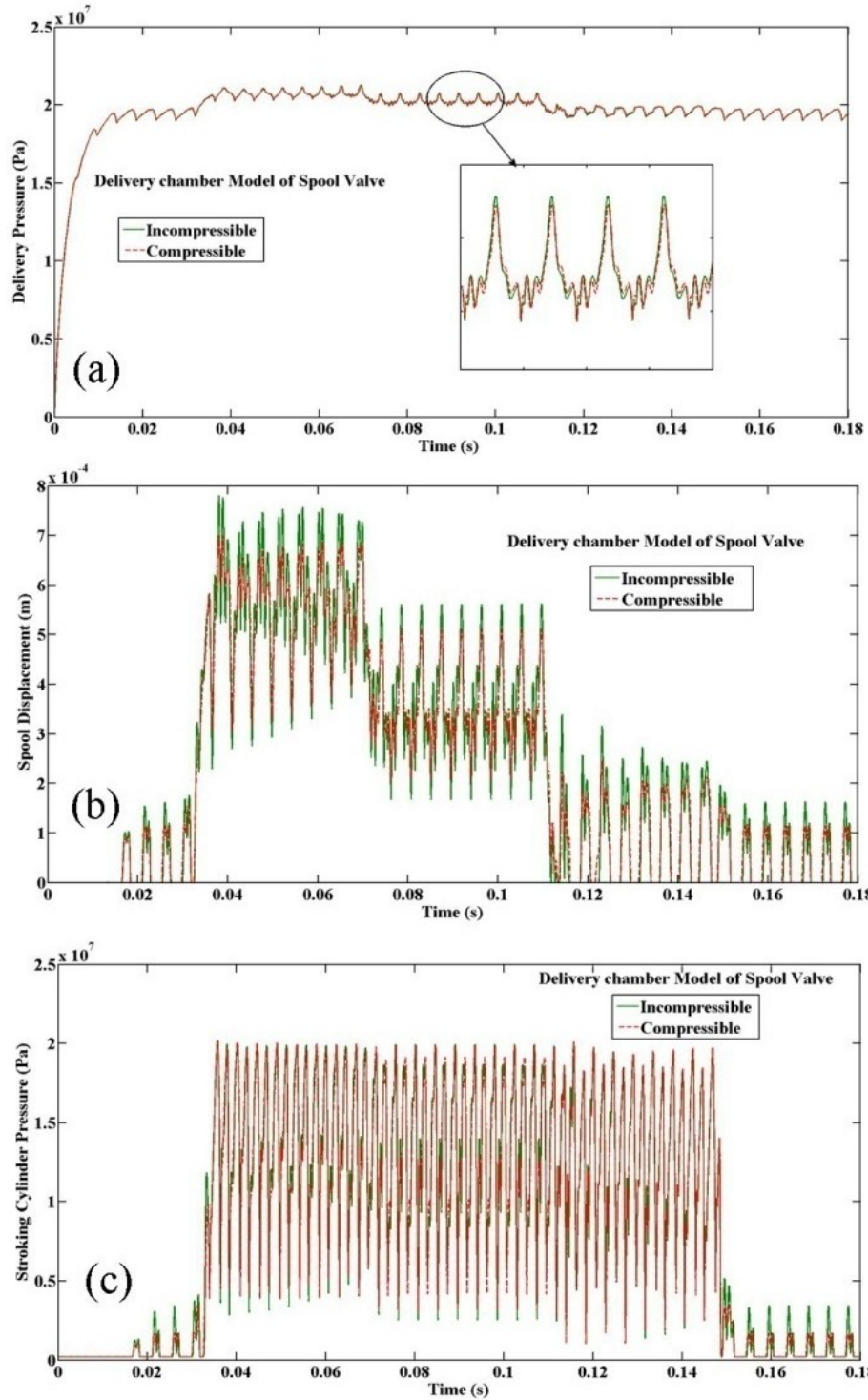
Figure 5.5: Effect of compressible model in the extreme left chamber of the spool valve
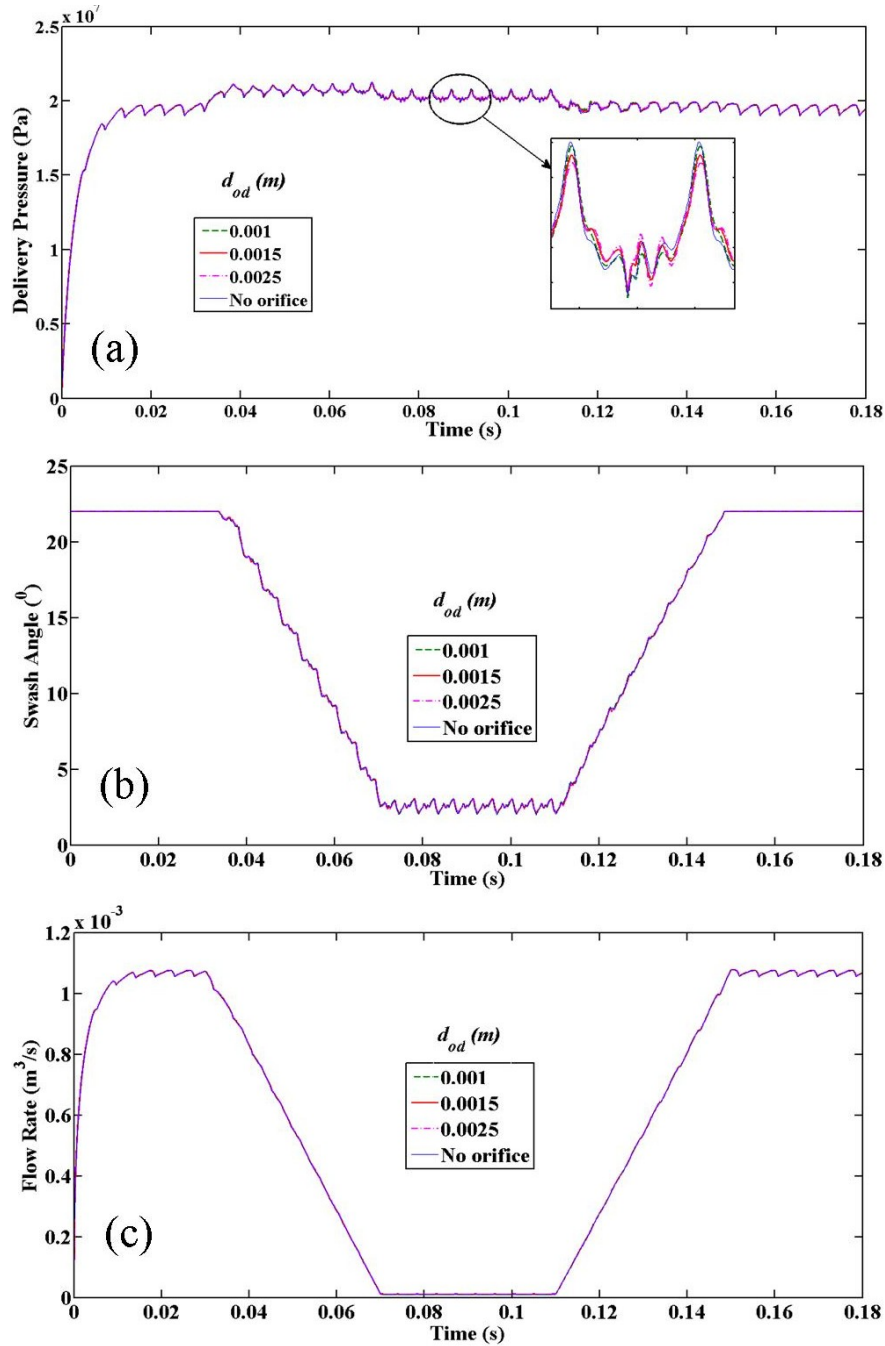
Figure 5.6: Effect of entry orifice the spool valve

5.4.3 Evaluation of the size of drain side orifice of the spool valve

A similar study has been conducted by varying the drain orifice diameter from 1mm to 3mm in which equations (5.8b) and (5.8c) have been invoked, while for no drain orifice case, equation (5.8c) has been used. Figure 5.7 illustrates the comparison of the performances in terms of delivery pressure, swash angle and delivery flow rate

characteristics for load variation depicted in Fig. 5.4.

The study reveals that direct drain connection between the spool end chamber and reservoir is the best option. Introduction of orifice creates back pressure due to which during increase in loading on the pump more amount of force was required to move the spool against the spring force. As a result the delivery pressure shoots up beyond the designed cut-off pressure, particularly for orifices of 1mm and 2mm sizes. For these orifices, the internal dynamics of the pump take longer time to stabilize the swash plate for near zero delivery flow rate due to full closure of the load orifice. Consequently, after withdrawal of the loading, it takes more time for the flow and delivery pressure to recover to the cut-in setting. Increasing the diameter of the orifice (3mm) close to the no orifice situation shows better performance of the pump. Therefore, it is suggested that no orifice may be used at the drain side of the valve. In absence of orifice, for the rest of the study, equation (5.8c) has been used as a model of drain flow rate.

5.4.4 Effect of over-lap and under-lap of the spool valve in the pump performance

The lap condition of the central spool land has a great influence on the pump dynamics. In the studies conducted in the previous sections, the central spool land was considered to have overlap o_d of 10μm at the left side and underlap u_r of 90μm at the right side of it with respect to the metered port shown in Fig. 5.2. Now a set of lap combinations have been studied without altering the main configuration of the spool valve. In fact the study has been extended for reverse lap condition in which the central spool land is under lapped at left side and overlapped at right side. Figure 5.8 shows the result of the study, where both are denoted with negative signs. All the performance predictions have been made against same area pattern of load orifice shown in Fig. 5.4. It can be observed that within a range of the lap conditions of the spool valve, the performance of the pump remains satisfactory. The study also reveals that reversed lap condition in the order of 25μm underlap and 105μm overlap may be admissible. Up to the lap condition in the order of 100μm overlap and 180μm underlap, the pump operates within the designed cut-in and cut-off condition. The degradation in the performance for larger reversed lap is due to the fact that at the beginning of the pump operation, the stroking cylinder is directly connected to the pump delivery line, which affects the cut-in

pressure of the pump. On the other hand, for the larger overlap at the left side of the spool, the cut-off pressure is increased because more pressure force is required to overcome the overlap length. The corresponding dynamic characteristics of spool valve displacement, swash angle of the pump are also shown in Fig. 5.8(b) and 5.8(c).
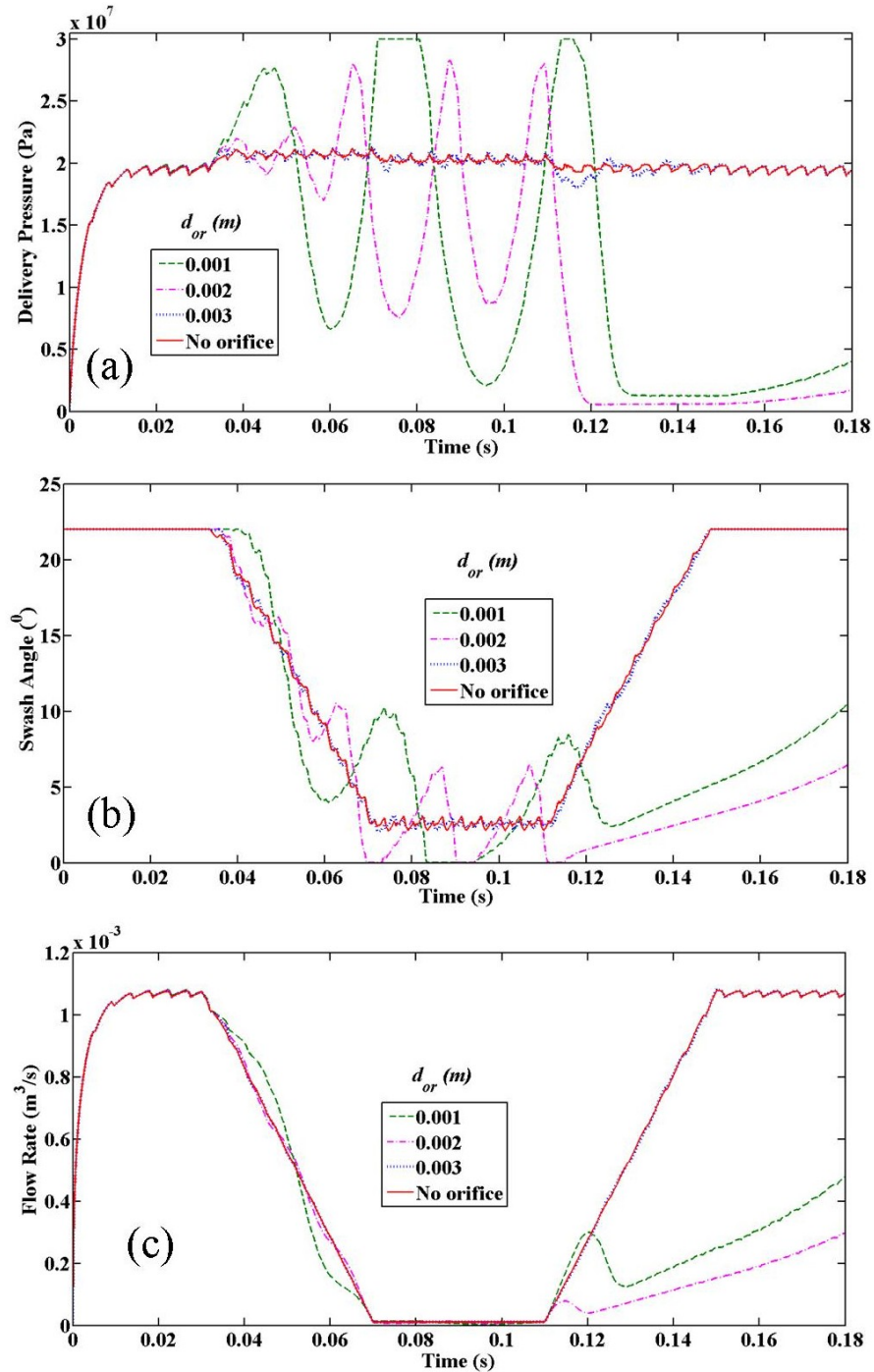
Figure 5.7: Effect of drain side orifice of the spool valve

82
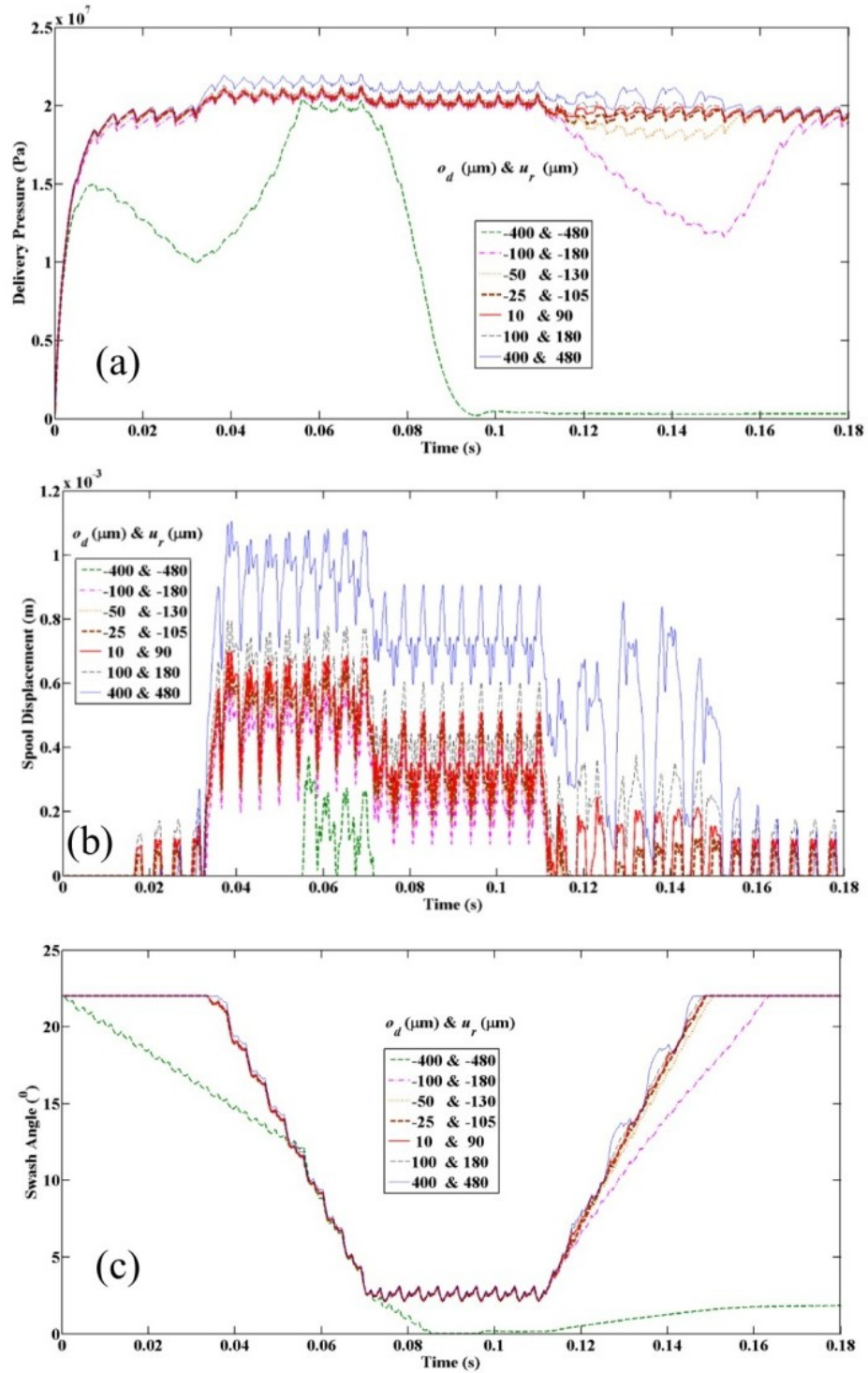
Figure 5.8: Effect of over-lap and under-lap of the spool valve

5.4.5 Evaluation of the size of clearance orifice

As shown in Fig. 5.2, the additional orifice added between the spool valve and stroking cylinder plays an important role particularly during transition from cut-off to cut-in operating condition. It has a small influence on the cut-off pressure setting, but it is really important when the load valve comes back from its cut-off area setting to cut-in area setting and stays steadily within the cut-in area zone. This orifice acts as a bypass route of the pressurized fluid of stroking cylinder when the load of the pump is being reduced from cut-off to cut-in condition and even below that.
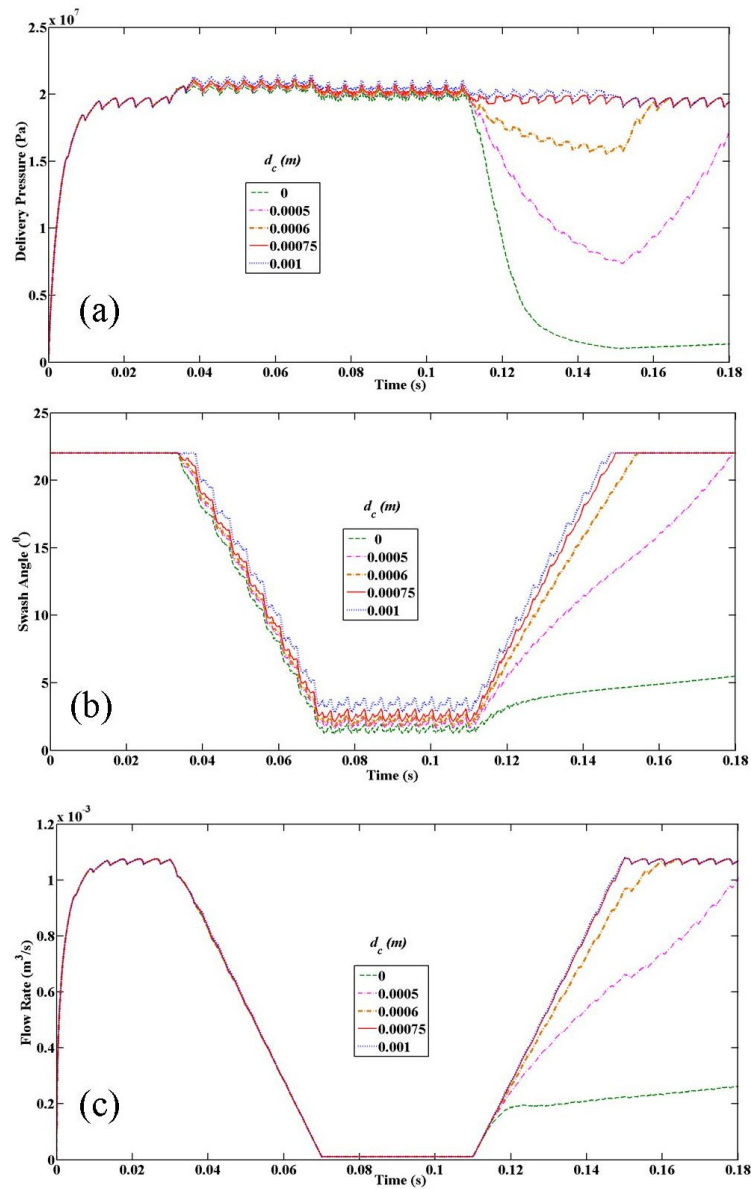
Figure 5.9: Effect of clearance orifice of the spool valve

The precompression of the spring of the spool valve causes closure of the metered port once the load is reduced. For depressurization of the stroking cylinder, the entrapped oil needs to be leaked to the case drain. The radial clearance and the underlap of the spool land may not be sufficient to provide the leakage necessary for the depressurization so that the swash plate can able to come back to its rated orientation. This is evident from Fig. 5.9, where the performance of the pump has been studied for different sizes of the clearance orifice starting from zero size orifice, equivalent to no orifice. The same loading pattern as shown in Fig. 5.4 has also been used for this study and apart from varying the diameter of the clearance orifice, all other parameters are kept at their nominal values. It can be seen that for a diameter of 750μm, the recovery of cut-in pressure from cut-off pressure occurs in the pump in a smooth manner. The behaviours of swash angle and the delivery flow rate also have been found to satisfactory. Below this size of orifice, the return of the swash angle to its rated value gets delayed as can be observed from the figure thereby the delivery pressure and flow rate of the pump get affected. Orifice size of 1mm has resulted higher pressure ripple due to oscillations in the swash dynamics. Therefore, from this study, the size of the clearance orifice has been recommended as 750μm. The sizing of the spool valve obtained from dynamic simulation has been furnished in Table 5.3.

Table 5.3: Parameters obtained from dynamic simulation

Parameters	Value	Parameters	Value
d_{od}	Not required	u_d	105 μm to 180 μm
d_{or}	Not required	d_c	0.75 m
O_d	-25 μm to 100 μm		

5.5 Performance analysis between double spool compensator with single spool compensator

Figure 5.10 presents the comparison of the dynamics performance of the present pressure compensator with another one having a two stage spool valve. In both the cases apart from the spool valves all other components of the pump remain same. The pump

85

dynamics has been studied for the same load dynamics as shown in Fig. 5.4. It can be observed from Fig. 5.10(a) that a pressure overshoot appears when the orifice goes from cut-in area to cut-off area in both types of pressure compensators. However peak overshoot is more in the case of the compensator with two stage spool valve. The primary reason behind this feature may be attributed to the combined effect of the two springs associated with the spool ends, although both the designs of pressure compensator maintain the same cut-in pressure but the cut-off pressure is high in case of compensator with double spool. Figure 5.10(b) illustrates that the pressure ripples in the rate cylinder at the valve transient region and the full load region is slightly more in case of single spool compensator design. The stroking cylinder pressure dynamics has been shown in the Fig.5.10(c). Figures 5.10(d) and 5.10(e) demonstrate the features of swash plate dynamics and the flow dynamics of the system. At the cut-off region, the flow is nearly zero for both the cases, but the swash angle is less in case of compensator with two stage spool valve than compensator with single stage spool valve.
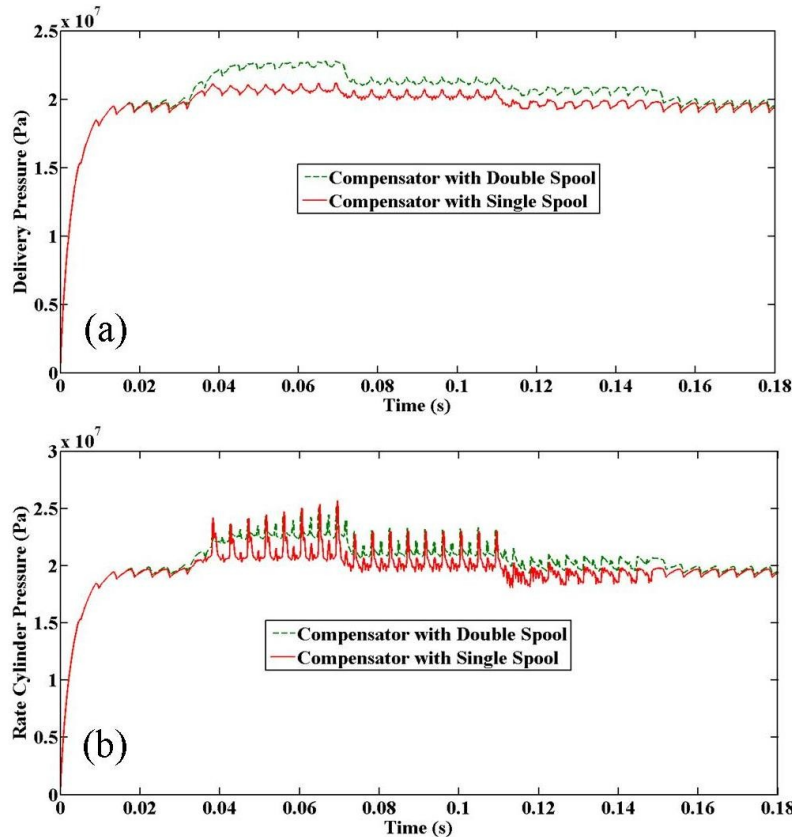
Figure 5.10: Performance comparisons between two compensators - (a) delivery pressure; (b) rate cylinder pressure
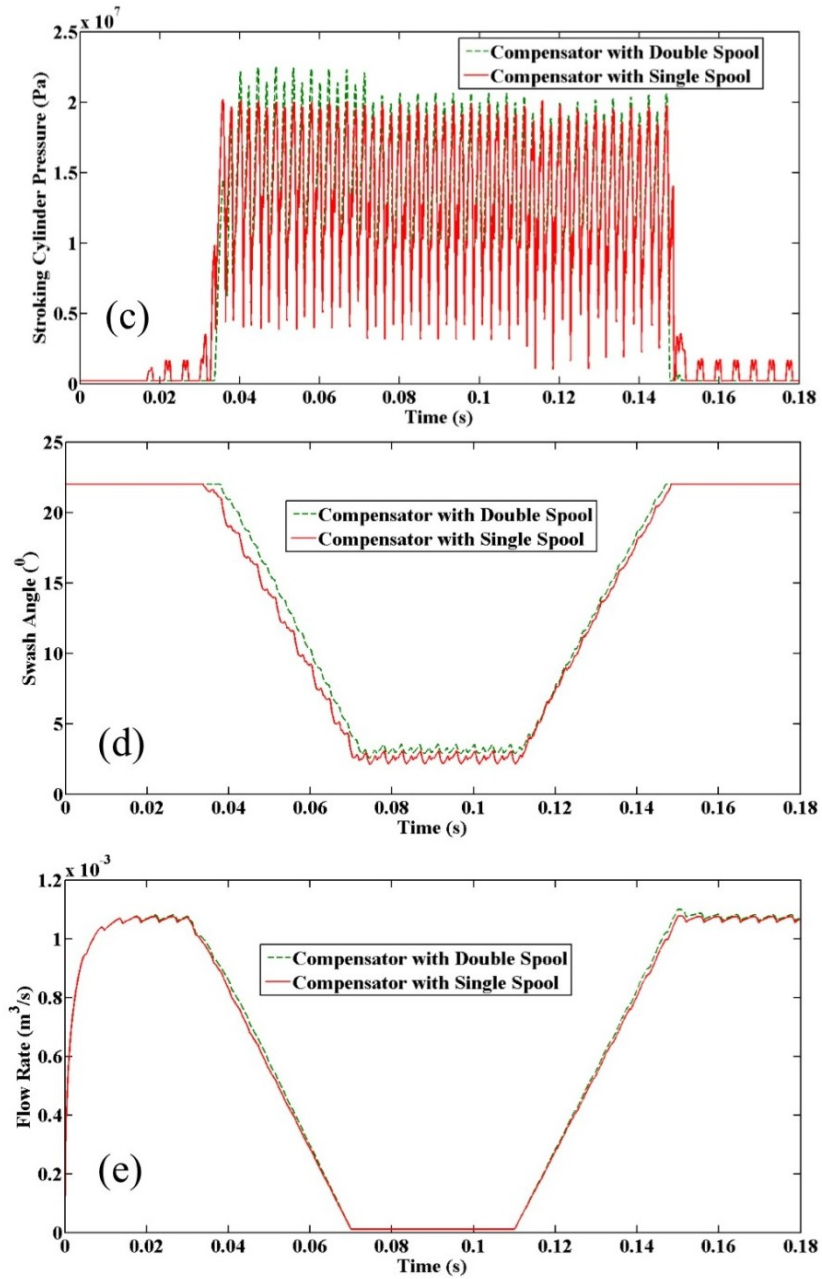
Figure 5.10: Performance comparisons between two compensators - (c) stroking cylinder pressure; (d) swash angle; (e) flow rate

5.6 Performance comparison with a real pump

The objective of this section is to verify whether the simulated performance of the axial piston pump having the designed single spool compensator matches with a

commercially available similar pump but having double spool compensator. In the earlier study, the same experimental test setup had been used to verify the correctness of the simulation software and the design methodology.

The pressure compensator model which consists of a single stage spool valve has been verified with the experimental result and simulation of system with two stage spool valve subjected to same loading pattern. The loading has been obtained by varying the command signal to the PV as shown in Fig. 5.11a. Figure 5.11b shows the performance comparison result in terms of the delivery pressure characteristics against the loading pattern. The spring precompression setting of the single spool valve has been adjusted to 0.0072m to have a satisfactory matching with the experimental one. In case of compensator with double spool, the spring precompression setting of the bottom spool is kept fixed at 0.00415m, while that for the top spool is set at 0.0086m to match with the experimental result as shown in Fig. 5.11b. It may be mentioned that although the compensator design with single spool valve has been performed for 20MPa cut-off pressure, it has been used in the verification study with a factory set cut-off value of 18.5MPa.
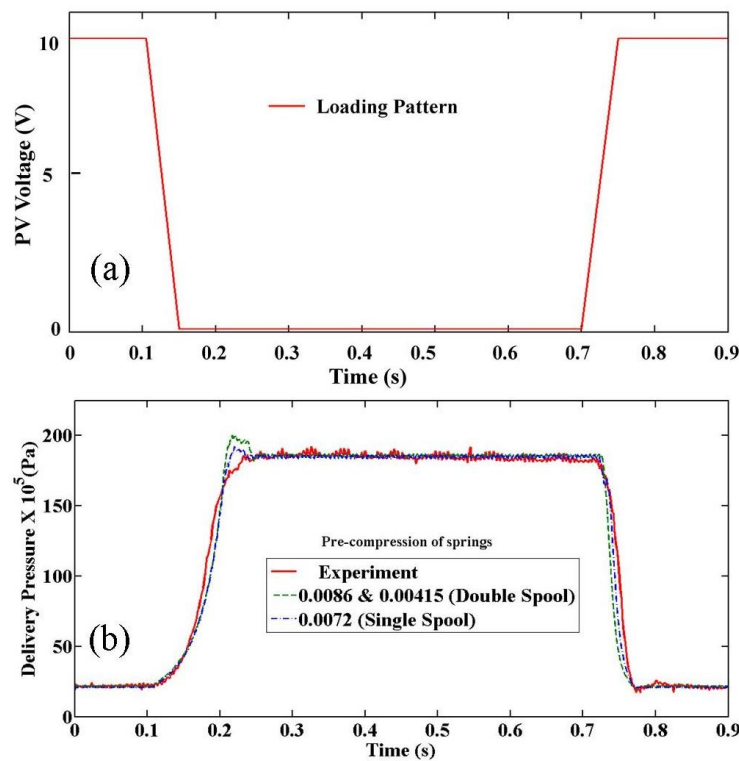
Figure 5.11: Experimental and simulation validation for a load variation

88

5.7 Summary

A simplified spool valve instead of a two stage spool valve has been theoretically incorporated in the pressure compensator of a variable displacement axial piston pump in order to perform a comparative study with a commercial pump. The design sensitivity of the spool valve has been carried out through simulation to identify the critical size of the parameters, which affects the pump performance. The designed compensator system has been compared first with the one having two stage spool valve through simulation and then both have been compared with the experimental result obtained from the commercial pump.

CHAPTER-6

EPILOGUE

6.1 Salient features of the overall work

A comprehensive study on the different aspects of a pressure compensated variable displacement axial piston pump through experiments and analysis has been done in the present work. In the experimental side, a set up is developed for different performance study of the pump. The setup is capable of capturing dynamic characteristics of the pump. Large scale experiments have been carried out at various conditions and demands to understand the effect of all other components of the electrohydraulic circuit on the dynamic performance of the pump. The effects of changing the rotational speed without altering the cut-off pressure of the pump have also been studied experimentally.

From the understanding of the experimental results, a need for designing a pressure compensator became imperative. In particular identification of the philosophy of designing the two cylinders of the pressure compensator is an important feature of the present work. A comprehensive mathematical model of the pump-compensator system has been developed that could predict the dynamics of the pump in terms of pressure and flow at different locations, angular position of the swash plate and spool positions. Followed by static design, some critical parameters of the pressure compensator have been evaluated through dynamic simulation. The performance of the simulation model with the tuned parameters has been verified with experimental results.

A simplified single stage alternate control spool valve for the pressure compensator without changing the others components of the pump has been proposed. Finally, a large scale simulation study has been carried out to check the permissible tolerance of various parameters related to the control spool valve.

6.2 Conclusion

Establishment of a test setup to analyze the pump performance and study the effects of some electrohydraulic components on the dynamics of the pump is a significant contribution in the area of positive displacement pump. Thorough experimental study has revealed the coupled effects of pressure relief valve and the proportional valve (used as load valve) on the performance of pump. The required margin of pressure required to isolate the effect of pressure relief valve has been identified. Also experimental study has

revealed the effect of load transience on the dynamics of pressure. It is found that faster load transience would result large overshoot in the pressure transience.

Followed by the experimental study, a novel design methodology for a pressure compensator of a variable displacement axial piston pump has been established. The most notable contribution of the methodology is to arrive at a nominal design from simple mechanistic consideration of static balance of torque on the swash plate both at cut-in and cut off conditions of the pump. The sensitivity analysis of nominal and off-nominal dimensions through dynamic simulation and the subsequent experimental verification have established the potential of the design approach. It has been found that the nominal diameters of the rate and stroking pistons provide the most compact dimensions without any significant swash plate oscillation during load transience. Predictions with up to 50% and 250% increase in nominal clearances between the rate and stroking piston-cylinder pairs exhibited acceptable pump performance. But, further increase in clearances within stroking cylinder bore has indicated major degradation of the pump performance. The metering out and metering in of the flow to and from the stroking cylinder through both the spools in the pressure compensator valve have been established as a strong requirement. But, wide permissible tolerance for the corresponding lap sizes is a positive finding for the pump manufacturers. The role of the bypass line between the stroking-cylinder port and the tank port has been established for achieving acceptable build-up dynamics of the swashing angle during the phase of corresponding variation of the external load.

By systematic design, it is possible to have a single stage spool valve controlled pressure compensator that can produce performance of the variable displacement axial piston pump at par with a similar commercially available pump.

6.3 Future scope of work

The developed setup can be used for any other positive displacement pump. An optimization study could be planned considering the critical parameters for minimizing cavitation inside the pump chamber and maximizing the performance of the pump without much overshoot at the transience.

Design realization of the proposed single stage control spool valve through fabrication of a prototype and subsequent performance testing using the developed setup could be aimed at in future.

A detailed study about the leakage flow and pressure on the various parts of the pump and pressure compensator may be attempted to improve the design and performance of the pump.

References:

Achten, P., 2013. Dynamic high-frequency behaviour of the swash plate in a variable displacement axial piston pump. Proceedings of the Institution of Mechanical Engineers, Part I: Journal of Systems and Control Engineering, 227(6), pp.529-540.

Achten, P., Van Den Brink, T. and Schellekens, M., 2005, June. Design of Variable-Displacement Floating Cup Pump. In The Ninth Scandinavian Conference on Fluid Power, SCIFP(Vol. 5, pp. 1-3).

Akers, A. and Lin, S.J., 1988. Optimal control theory applied to a pump with single-stage electrohydraulic servovalve. Journal of dynamic systems, measurement, and control, 110(2), pp.120-125.

Baz, A., 1983. Optimization of the dynamics of pressure-compensated axial piston pumps. Fluidics quarterly, 15(2), pp.64-81.

Bergada, J.M., Haynes, J.M. and Watton, J., 2008. Leakage and groove pressure of an axial piston pump slipper with multiple lands. Tribology transactions, 51(4), pp.469-482.

Bergada, J.M., Kumar, S., Davies, D.L. and Watton, J., 2012. A complete analysis of axial piston pump leakage and output flow ripples. Applied Mathematical Modelling, 36(4), pp.1731-1751.

Bhandari, V.B., 2010. Design of machine elements. Tata McGraw-Hill Education.

Chaudhuri, S., Dasmahapatra, S., Chatterjee, A., Saha, R., Mookherjee, S. and Sanyal, D., 2017. Adaptive Fuzzy—Sliding Mode Control with Fixed Bias Compensator for an Electrohydraulic Actuation System with Hard Nonlinearities. In Fluid Mechanics and Fluid Power–Contemporary Research (pp. 1223-1232). Springer, New Delhi.

Cho, S.H. and Burton, R., 2011. Position control of high performance hydrostatic actuation system using a simple adaptive control (SAC) method. Mechatronics, 21(1), pp.109-115.

Daher, N. and Ivantysynova, M., 2014. Energy analysis of an original steering technology that saves fuel and boosts efficiency. Energy conversion and management, 86, pp.1059-1068.

Ericson, L., 2013, November. Movement of the swash plate in variable in-line pumps at decreased displacement setting angle. In Proceedings of the 22nd International

Congress of Mechanical Engineering (COBEM 2013), Ribeirão Preto, SP, Brazil (pp. 3-7).

Ericson, L., 2014, March. Swash plate oscillations due to piston forces in variable in-line pumps. In Proceedings of 9th International Fluid Power Conference, Aachen, Germany.

Gao, F., Ouyang, X., Yang, H. and Xu, X., 2013. A novel pulsation attenuator for aircraft piston pump. Mechatronics, 23(6), pp.566-572.

Gilardino, L., Mancò, S., Nervegna, N. and Viotto, F., 1999. An experience in simulation: The case of a variable displacement axial piston pump. In *Proceedings of the JFPS International Symposium on Fluid Power* (Vol. 1999, No. 4, pp. 85-91). The Japan Fluid Power System Society.

Goto, K., Suzuki, S., Hoshino, N. and Hoshino, T., Toyota Industries Corp, 1994. Variable displacement hydraulic piston pump with torque limiter. U.S. Patent 5,295,796.

Ivantysyn, J. and Ivantysynova, M., 2003. 1st ed., Physical Fundamentals, Akademia Books International, New Delhi, India, pp. 32-33.

Kaliafetis, P. and Costopoulos, T., 1995. Modelling and simulation of an axial piston variable displacement pump with pressure control. Mechanism and machine theory, 30(4), pp.599-612.

Kemmetmüller, W., Fuchshumer, F. and Kugi, A., 2010. Nonlinear pressure control of self-supplied variable displacement axial piston pumps. Control Engineering Practice, 18(1), pp.84-93.

Khalil, M.B., Svoboda, J. and Bhat, R.B., 2004. Modelling of swash plate axial piston pumps with conical cylinder blocks. Transactions-American Society of Mechanical Engineers Journal of Mechanical Design, 126(1), pp.196-200.

Lin, S. and Hu, J., 2015. Tribo-dynamic model of slipper bearings. Applied Mathematical Modelling, 39(2), pp.548-558.

Mandal, N.P., Saha, R. and Sanyal, D., 2008. Theoretical simulation of ripples for different leading-side groove volumes on manifolds in fixed-displacement axial-piston pump. Proceedings of the Institution of Mechanical Engineers, Part I: Journal of Systems and Control Engineering, 222(6), pp.557-570.

Mandal, N.P., Saha, R. and Sanyal, D., 2012. Effects of flow inertia modelling and valve-plate geometry on swash-plate axial-piston pump performance. Proceedings of the Institution of Mechanical Engineers, Part I: Journal of Systems and Control Engineering, 226(4), pp.451-465.

Mandal, N.P., Saha, R., Mookherjee, S. and Sanyal, D., 2014. Pressure compensator design for a swash plate axial piston pump. Journal of Dynamic Systems, Measurement, and Control, 136(2), p.021001.

Manring, N.D., 1999. The control and containment forces on the swash plate of an axial-piston pump. Journal of dynamic systems, measurement, and control, 121(4), pp.599-605.

Manring, N.D., 2000. The discharge flow ripple of an axial-piston swash-plate type hydrostatic pump. Journal of dynamic systems, measurement, and control, 122(2), pp.263-268.

Manring, N.D. and Damtew, F.A., 2001. The control torque on the swash plate of an axial-piston pump utilizing piston-bore springs. Journal of Dynamic Systems, Measurement, and Control, 123(3), pp.471-478.

Manring, N.D., 2002. The control and containment forces on the swash plate of an axial piston pump utilizing a secondary swash-plate angle. In Proceedings of the 2002 American Control Conference (IEEE Cat. No. CH37301) (Vol. 6, pp. 4837-4842).

Massey, B.S. and Ward-Smith, J., 2006. Mechanics of fluids 8th ed. Taylor & Francis, (2006) 201-205.

Merritt, H., 1967. Hydraulic control systems. John Wiley & Sons.

Norhirni, M.Z., Hamdi, M., Musa, S.N., Saw, L.H., Mardi, N.A. and Hilman, N., 2011. Load and stress analysis for the swash plate of an axial piston pump/motor. Journal of Dynamic Systems, Measurement, and Control, 133(6), p.064505.

Park, S.H., Lee, J.M. and Kim, J.S., 2013. Modelling and performance improvement of the constant power regulator systems in variable displacement axial piston pump. The Scientific World Journal, 2013.

Rexroth Bosch Group, 2004 – Industrial Hydraulics Catalogue. Variable Axial Piston Pump, Type - A10VSO, series–31/DR, RA92711,

http://www.pneumax.co.th/catalogue/hyd/rexroth/ pump/A10VSO.pdf /, 2004, (accessed 07.04.17).

Rundo, M. and Pavanetto, M.A., 2018, August.Comprehensive Simulation Model of a High Pressure Variable Displacement Vane Pump for Industrial Applications.In *ASME 2018 International Design Engineering Technical Conferences and Computers and Information in Engineering Conference*.American Society of Mechanical Engineers Digital Collection.

Schoenau, G.J., Burton, R.T. and Kavanagh, G.P., 1990. Dynamic analysis of a variable displacement pump. Journal of Dynamic Systems, Measurement, and Control, 112(1), pp.122-132.

Sarkar, B.K., Das, J., Saha, R., Mookherjee, S. and Sanyal, D., 2013. Approaching servoclass tracking performance by a proportional valve-controlled system. IEEE/ASME Transactions on Mechatronics, 18(4), pp.1425-1430.

Seeniraj, G.K. and Ivantysynova, M., 2006, January. Impact of valve plate design on noise, volumetric efficiency and control effort in an axial piston pump. In ASME 2006 International Mechanical Engineering Congress and Exposition (pp. 77-84). American Society of Mechanical Engineers.

Tang, H., Ren, Y. and Xiang, J., 2017. A novel model for predicting thermoelastohydrodynamic lubrication characteristics of slipper pair in axial piston pump. International Journal of Mechanical Sciences, 124, pp.109-121.

Zaki, H. and Baz, A., 1979. On the dynamics of axial piston pumps. J. Fluid. Q, 11, pp.73-87.

Zeiger, G. and Akers, A., 1985. Torque on the swashplate of an axial piston pump. Journal of dynamic systems, measurement, and control, 107(3), pp.220-226.

Zeiger, G. and Akers, A., 1986. Dynamic analysis of an axial piston pump swashplate control. Proceedings of the Institution of Mechanical Engineers, Part C: Journal of Mechanical Engineering Science, 200(1), pp.49-58.

APPENDIX-I

FORMULATION OF

GROOVE AND MANIFOLD AREAS FOR SYMMETRIC GROOVE CONFIGURATION
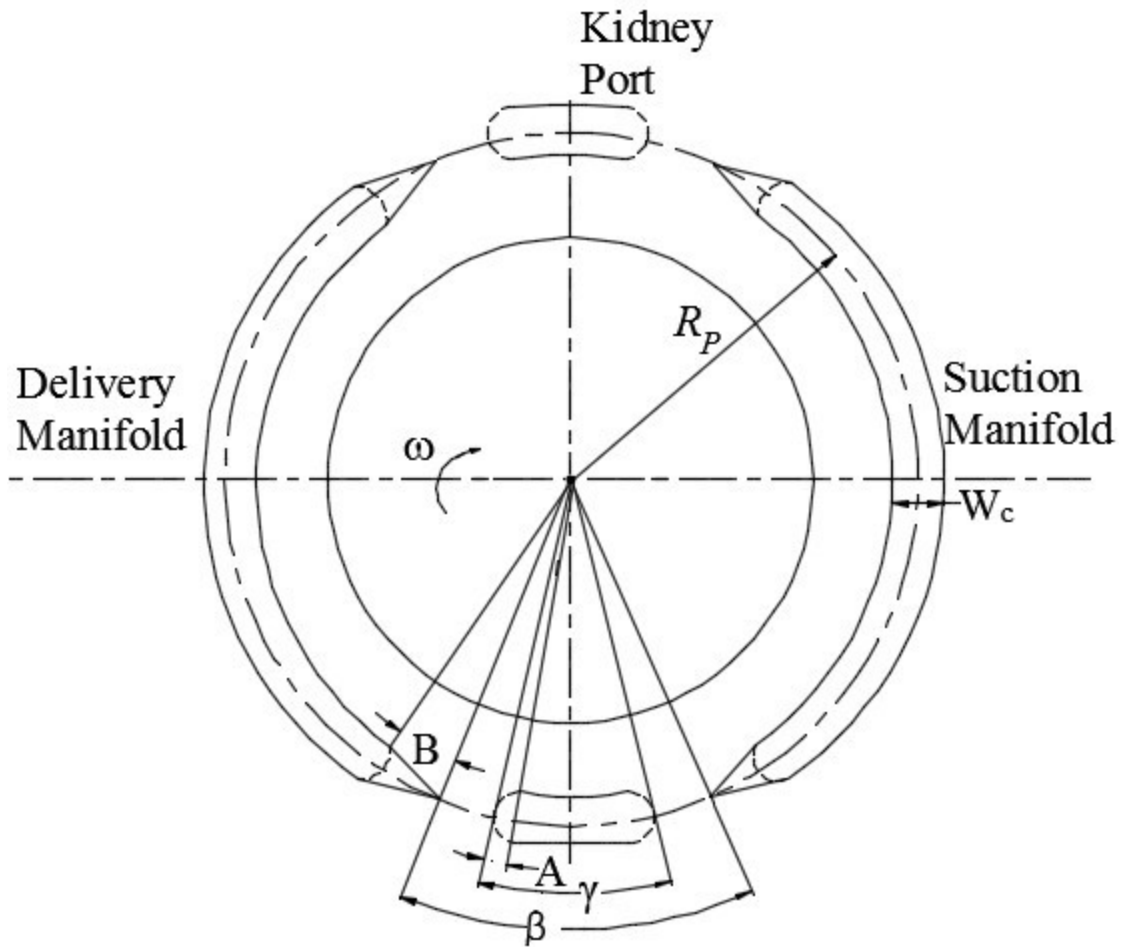
Figure A1.1: Kidney port and manifold geometry of the pump

The area formulation of the suction manifold and delivery manifold has been illustrated through geometric consideration. The primary geometrical configuration has been drawn on the Fig. A1.1. The geometric details required for the formulation of area covered by the kidney port due to its various instantaneous position has been configured in the Figs. A1.4 and A1.5. Total area covered by the kidney port due to 360° has been formulated in the table A1.
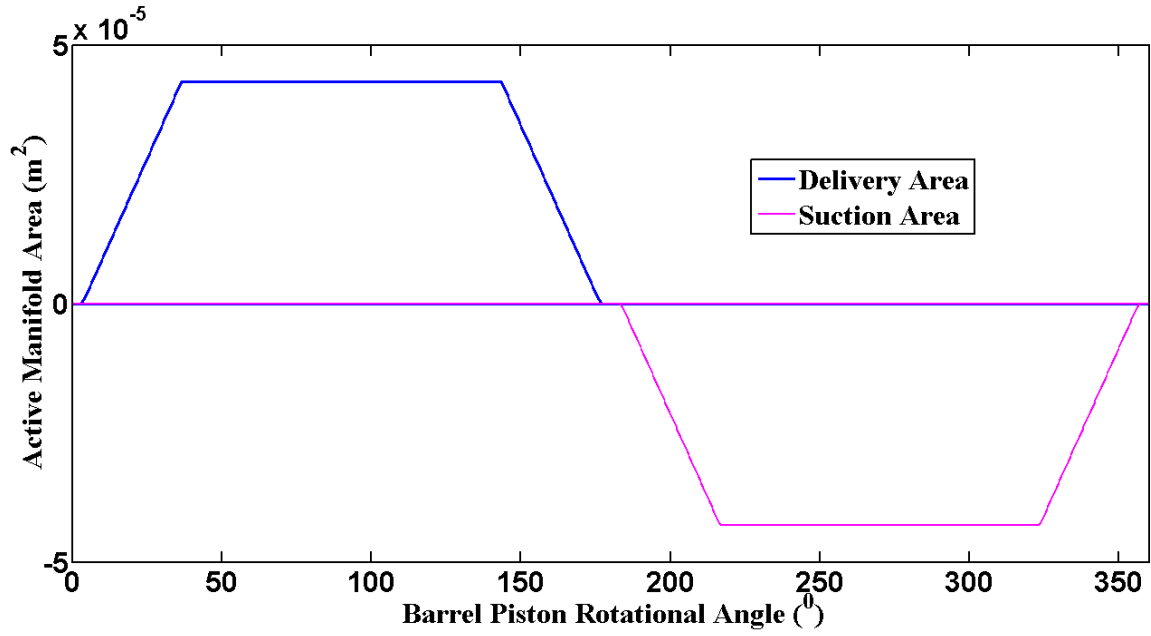
Figure A1.2: Area variation with angle of rotation

Actual
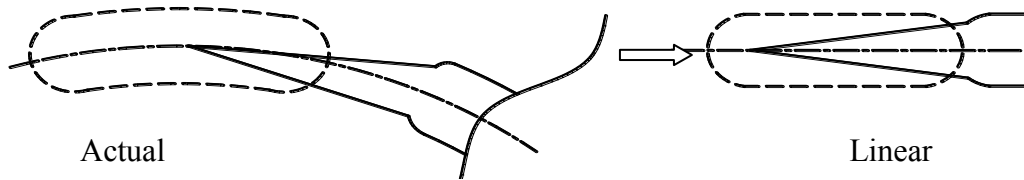
Linear

Figure A1.3: Linearization of Kidney port manifold combination

100
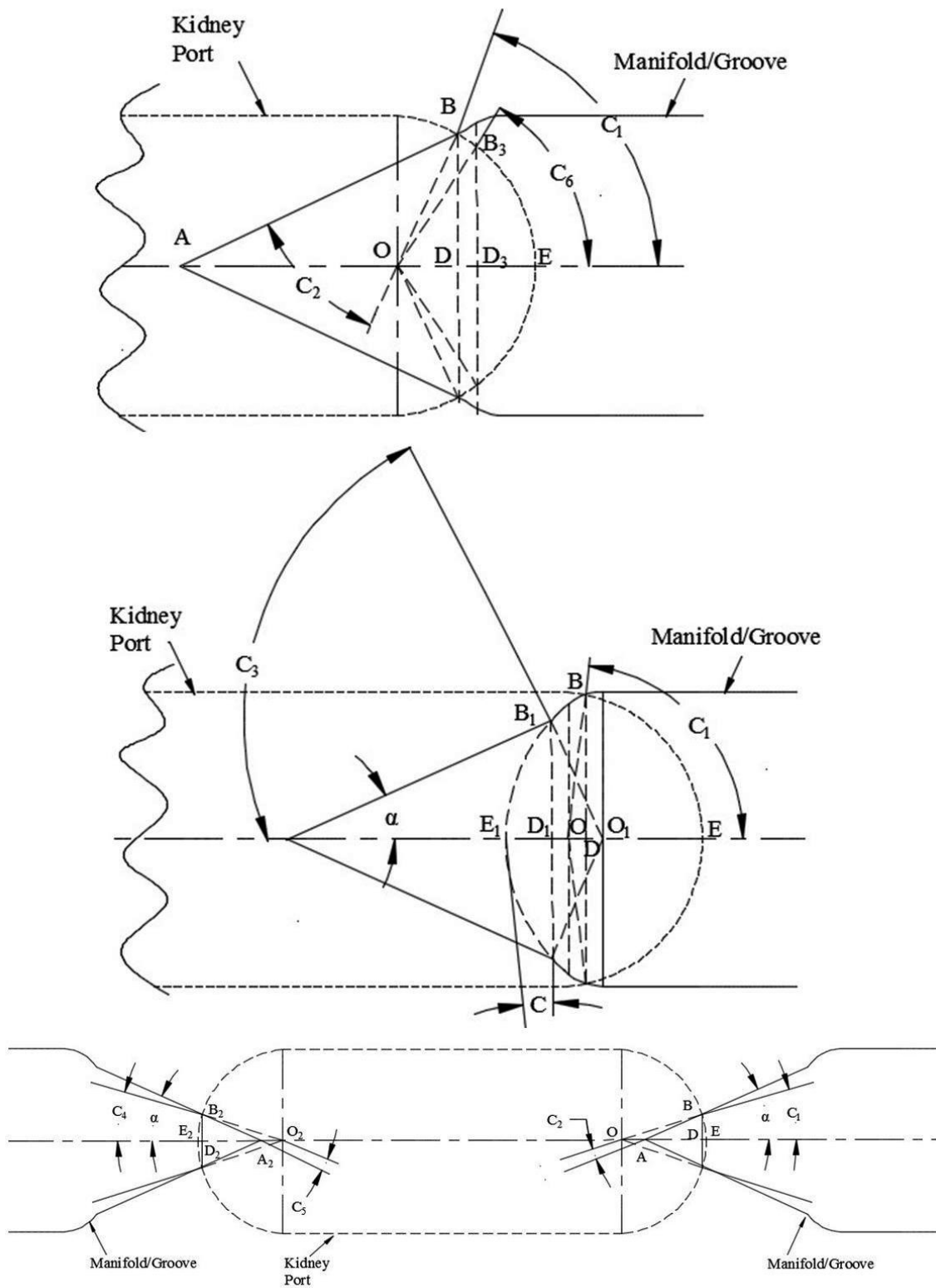
Figure A1.4: Geometric details of kidney port manifold/groove interaction for area formulation
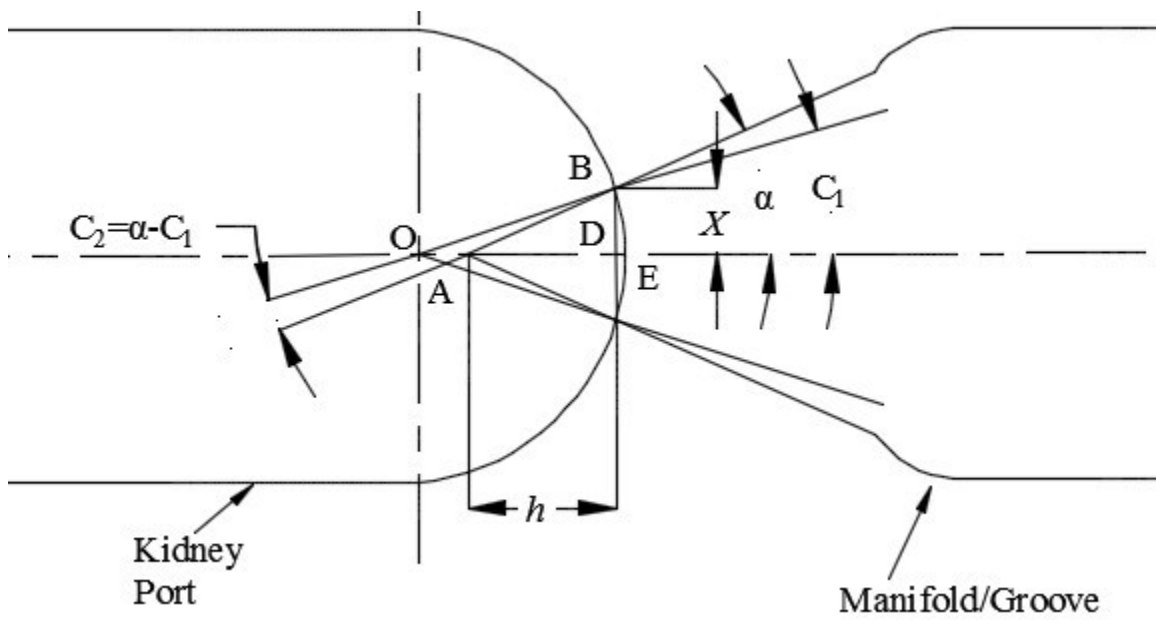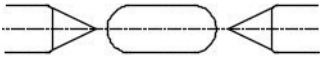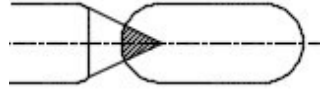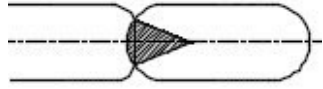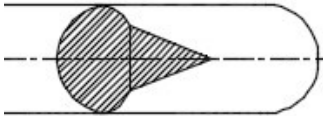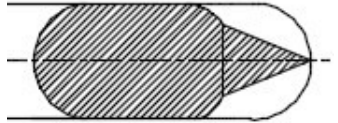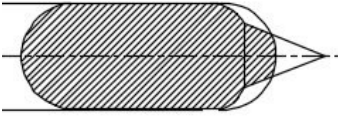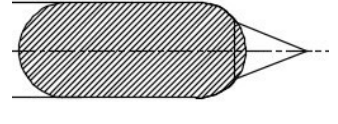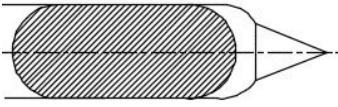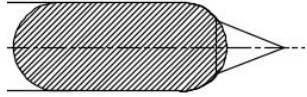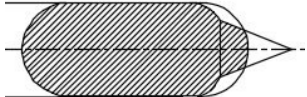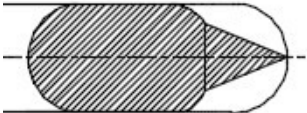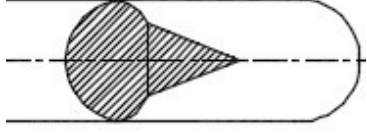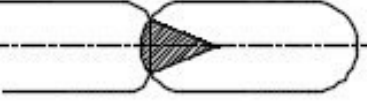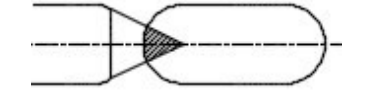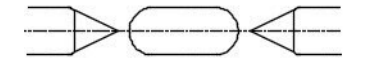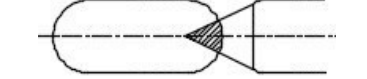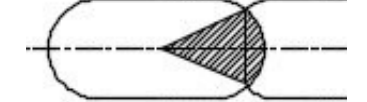
Figure A1.5: Enlarged view of kidney port-Manifold/Groove interaction for area formulation at a certain angle of interception
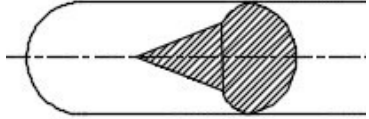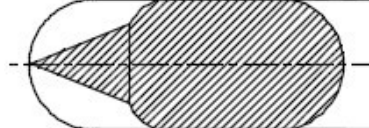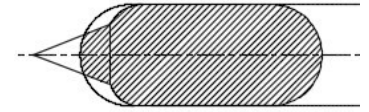
Table A1: Different area formulation for the delivery and suction ports
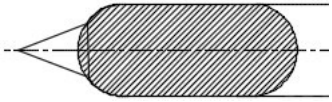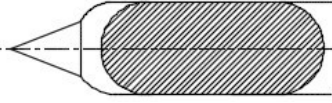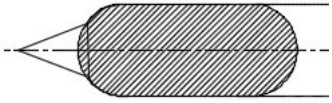
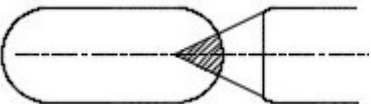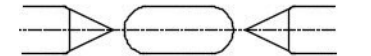| Sl no.	Condition	Area of the delivery manifold (A_d)	Linearized Figure
1.	$0 \leq \theta \leq \dfrac{\beta - \gamma}{2}$	0	
2.	$\dfrac{\beta - \gamma}{2} \leq \theta \leq \left\{ B + \dfrac{\beta - \gamma}{2} \right\}$	$BA^2 \sin \alpha \cos \alpha + \dfrac{\pi C_1 r_c^2}{180} + r_c BA \cos C_1 \sin \alpha$	
3.	$\left\{ B + \dfrac{\beta - \gamma}{2} \right\} \leq \theta \leq B + C + \dfrac{\beta - \gamma}{2}$	$\dfrac{\alpha}{180} \pi r_c^2$	
4.	$B + C + \dfrac{\beta - \gamma}{2} \leq \theta \leq \left\{ B + A + \left(\dfrac{\beta - \gamma}{2} \right) + A - C \right\}$	$2\left[\left\{ \dfrac{1}{180} \cos^{-1}\left(\dfrac{r_c - DE_2}{r_c} \right) \right\} \pi r_c^2 \right\} - $ $(r_c - DE_2) r \sin\left\{ \left[\cos^{-1}\left(\dfrac{r_c - DE_2}{r_c} \right) \right] \right\} \right] + \dfrac{Xh}{2}$ $DE_2 = \dfrac{\left[\theta + \left(\dfrac{\gamma - \beta}{2} \right) + B - C \right]}{360} \pi R_P$	
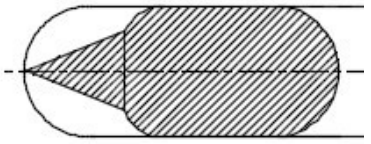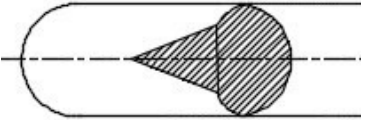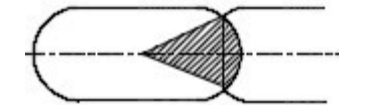
5.	$\left\{B + A + \left(\dfrac{\beta - \gamma}{2}\right) + A - C\right\} \le \theta \le \dfrac{\gamma + \beta}{2}$	$2C_2 - A_n + 2\pi R_P w_c\left(\theta + \dfrac{\gamma}{2} - A - \dfrac{\beta}{2} + B + A - C\right) + \dfrac{Xh}{2}$ Where, $C_2 = \dfrac{\pi w_c^2}{8}$, $DE_2 = \dfrac{\left[\theta + \left(\dfrac{\gamma - \beta}{2}\right) + B - C\right]}{360}\pi R_P$ and $A_n = \dfrac{\alpha_2}{180}\pi r_c^2 - (r_c - DE_2)r_c \sin\alpha$	
6.	$\dfrac{\gamma + \beta}{2} \le \theta \le \dfrac{\gamma + \beta}{2} + B - C$	$\dfrac{\pi w_c^2}{4} - A_n + 2\pi R_P w_c\left(\theta + \dfrac{\gamma}{2} - A - \dfrac{\beta}{2} + B + A - C\right) +$ $\dfrac{Xh}{2} - BA^2 \sin\alpha\cos\alpha + \dfrac{\pi C_1 r_c^2}{180} - r_c BA \cos C_1 \sin\alpha$	
7.	$\dfrac{\gamma + \beta}{2} + B - C \le \theta \le \left(\dfrac{\gamma + \beta}{2} + B\right)$	$\dfrac{\pi w_c^2}{4} + \dfrac{\pi R_P w_c(\gamma - 2A)}{180} - \dfrac{\alpha}{180}\pi r_c^2 + (r_c - DE_1)(r_c \sin\alpha)$ Where, $DE_1 = \dfrac{\pi R_P\left[\dfrac{\beta}{2} + B - \left(\theta - \dfrac{\gamma}{2}\right)\right]}{180}$	

No.	Range	Formula	Figure
8.	$\left(\dfrac{\gamma+\beta}{2}+B\right)\le\theta\le180-\left(\dfrac{\gamma+\beta}{2}+B\right)$	$\pi R_P w_c\left(\dfrac{\gamma-2A}{180}\right)+\dfrac{\pi w_c^2}{4}$	
9.	$180-\left(\dfrac{\gamma+\beta}{2}+B\right)\le\theta\le180-\left(\dfrac{\gamma+\beta}{2}+B-C\right)$	$A_s=\dfrac{\pi w_c^2}{4}+\dfrac{\alpha}{180}\pi r_c^2-(r_c-DE_1)(r_c\sin\alpha)+\pi R_P w_c\left(\dfrac{\gamma-2A}{180}\right)$ Where, $DE_1=\dfrac{\pi R_P\left[\dfrac{\beta}{2}+B-\left(\theta-\dfrac{\gamma}{2}\right)\right]}{180}$	
10.	$180-\left(\dfrac{\gamma+\beta}{2}+B-C\right)\le\theta\le180-\left(\dfrac{\gamma+\beta}{2}\right)$	$\dfrac{\pi w_c^2}{4}-A_n+\left(\dfrac{\pi R_P w_c}{180}\right)\left(180-\dfrac{\beta}{2}+B+A-C-\theta+\dfrac{\gamma}{2}-A\right)$ $+\dfrac{Xh}{2}-\left(BA^2\sin\alpha\cos\alpha\right)+\left(\dfrac{C_1}{180}\pi r_c^2\right)-r_c^2\cos C_1\sin\alpha$	
11.	$180-\left(\dfrac{\gamma+\beta}{2}\right)\le\theta\le180-B-A-\left(\dfrac{\gamma+\beta}{2}\right)-A+C$	$\dfrac{\pi w_c^2}{4}-A_n+\dfrac{\pi R_P w_c}{180}\left[\left(180-\dfrac{\beta}{2}+B+A-C\right)-\left(\theta-\dfrac{\gamma}{2}+A\right)\right]+\dfrac{Xh}{2}$	

	Condition	Area	Linearized Figure
12.	$180 - B - A - \left(\dfrac{\gamma + \beta}{2}\right) - A + C \le \theta \le 180 - \left(\dfrac{\beta - \gamma}{2} + B + C\right)$	$2\left[\dfrac{\alpha}{180}\pi r_c^2 - (r_c - DE_2)r_c \sin\alpha\right] + \dfrac{Xh}{2} - A_n$ Where, $DE_2 = \left[\left(180 - \dfrac{\beta}{2} + B - C\right) - \left(\theta - \dfrac{\gamma}{2}\right)\right]\dfrac{\pi r_p}{360}$	
13.	$180 - \left(\dfrac{\beta - \gamma}{2} + B + C\right) \le \theta \le 180 - \left(\dfrac{\beta - \gamma}{2} + B\right)$	$\dfrac{\alpha \pi r_c^2}{180}$	
14.	$180 - \left(\dfrac{\beta - \gamma}{2} + B\right) \le \theta \le 180 - \left(\dfrac{\beta - \gamma}{2}\right)$	$BA^2 \sin\alpha\cos\alpha + \dfrac{\pi C_1 r_c^2}{180} - r_c BA \cos C_1 \sin\alpha$	
15.	$180 - \left(\dfrac{\beta - \gamma}{2}\right) \le \theta \le 180$	0	
	Condition	**Area of the suction manifold (A_s)**	**Linearized Figure**
16.	$180 + \left(\dfrac{\beta - \gamma}{2}\right) \le \theta \le 180 + B + \left(\dfrac{\beta - \gamma}{2}\right)$	$BA^2 \sin\alpha\cos\alpha + \dfrac{\pi C_1 r_c^2}{180} - r_c BA \cos C_1 \sin\alpha$	
17.	$180 + B + \left(\dfrac{\beta - \gamma}{2}\right) \le \theta \le 180 + \left(\dfrac{\beta - \gamma}{2}\right) + B + C$	$\dfrac{\alpha \pi r_c^2}{180}$	

18.	$180 + \left(\dfrac{\beta - \gamma}{2}\right) + B + C \leq \theta \leq 180 + B + A + \left(\dfrac{\beta - \gamma}{2}\right) + A - C$	$2\left[\dfrac{\pi r_c^2}{180}\cos^{-1}\left(\dfrac{r_c - DE_2}{r_c}\right) - A_n - (r_c - DE_2)r_c \atop \sin\left\{\cos^{-1}\left(\dfrac{r_c - DE_2}{r_c}\right)\right\}\right] + \dfrac{Xh}{2}$ $DE_2 = \left[\left(180 - \dfrac{\beta}{2} + B - C\right) - \left(\theta - \dfrac{\gamma}{2}\right)\right]\dfrac{\pi r_p}{360}$	
19.	$180 + B + A + \left(\dfrac{\beta - \gamma}{2}\right) + A - C \leq \theta \leq 180 + \left(\dfrac{\beta + \gamma}{2}\right)$	$2C_2 - A_n + \dfrac{\pi R_P w_c}{180}\left(\theta + \dfrac{\gamma}{2} - A - \dfrac{\beta}{2} + B + A - C\right)$ $+ \dfrac{Xh}{2}$	
20.	$180 + \left(\dfrac{\beta + \gamma}{2}\right) \leq \theta \leq 180 + \left(\dfrac{\beta + \gamma}{2}\right) + B - C$	$2C_2 - A_n + \dfrac{\pi R_P w_c}{180}$ $\left(\theta + \dfrac{\gamma}{2} - A - \left(180 + \dfrac{\beta}{2}\right) + B + A - C\right)$ $+ \dfrac{Xh}{2} - (BA^2 \sin\alpha\cos\alpha) + \left(\dfrac{C_1}{180}\pi r_c^2\right)$ $- r_c^2 \cos C_1 \sin\alpha$	

No.	Condition	Formula	Figure
21.	$180 + \left(\dfrac{\beta+\gamma}{2}\right) + B - C + \dfrac{\gamma}{2} \leq \theta \leq$ $180 + \left(\dfrac{\beta+\gamma}{2}\right) + B$	$2C_2 + \dfrac{\alpha}{180}\pi r_c^2 + A_n - (r_c - DE_1)(r_c \sin\alpha) +$ $\pi R_P w_c \left(\dfrac{\gamma - 2A}{180}\right)$ Where, $DE_1 = \dfrac{\pi R_P \left[\dfrac{\beta}{2} + B - \left(\theta - \dfrac{\gamma}{2}\right)\right]}{180}$	
22.	$180 + \left(\dfrac{\beta+\gamma}{2}\right) + B \leq \theta \leq 360 - \left(\dfrac{\beta+\gamma}{2}\right) + B$	$\pi R_P w_c \left(\dfrac{\gamma - 2A}{180}\right) + \dfrac{\pi w_c^2}{4}$	
23.	$360 - \left(\dfrac{\beta+\gamma}{2}\right) + B \leq \theta \leq 360 - \left(\dfrac{\beta+\gamma}{2}\right) + B - C$	$2C_2 + \dfrac{\alpha}{180}\pi r_c^2 + A_n - (r_c - DE_1)(r_c \sin\alpha) +$ $\pi R_P w_c \left(\dfrac{\gamma - 2A}{180}\right)$ Where, $DE_1 = \dfrac{\pi R_P \left[\dfrac{\beta}{2} + B - \left(\theta - \dfrac{\gamma}{2}\right)\right]}{180}$	
24.	$360 - \left(\dfrac{\beta+\gamma}{2}\right) + B - C \leq \theta \leq 360 - \left(\dfrac{\beta+\gamma}{2}\right)$	$\dfrac{\pi w_c^2}{4} - A_n + \left(\dfrac{\pi R_P w_c}{180}\right)\left(360 - \dfrac{\beta}{2} + B + A - C - \theta + \dfrac{\gamma}{2} - A\right)$ $+ \dfrac{Xh}{2} - (BA^2 \sin\alpha \cos\alpha) + \left(\dfrac{C_1}{180}\pi r_c^2\right) - r_c^2 \cos C_1 \sin\alpha$	

No.			
25.	$360 - \left(\dfrac{\beta + \gamma}{2}\right) \le \theta \le 360 - \left(B + A + \dfrac{\beta + \gamma}{2} + A - C\right)$	$\dfrac{\pi w_c^2}{4} - A_n + \dfrac{\pi R_P w_c}{180}\left[\left(360 - \dfrac{\beta}{2} + B + A - C\right) - \left(\theta - \dfrac{\gamma}{2} + A\right)\right] + \dfrac{Xh}{2}$	
26.	$360 - \left(B + A + \dfrac{\beta + \gamma}{2} + A - C\right) \le \theta \le 360 - \left(\left(\dfrac{\beta - \gamma}{2}\right) + B + C\right)$	$2\left[\dfrac{\pi r_c^2}{180}\cos^{-1}\left(\dfrac{r_c - DE_2}{r_c}\right) - A_n - (r_c - DE_2)r_c \atop \sin\left\{\cos^{-1}\left(\dfrac{r_c - DE_2}{r_c}\right)\right\}\right] + \dfrac{Xh}{2}$ $DE_2 = \left[\left(180 - \dfrac{\beta}{2} + B - C\right) - \left(\theta - \dfrac{\gamma}{2}\right)\right]\dfrac{\pi r_p}{360}$	
27.	$360 - \left(\left(\dfrac{\beta - \gamma}{2}\right) + B + C\right) \le \theta \le 360 - \left(\left(\dfrac{\beta - \gamma}{2}\right) + B\right)$	$\dfrac{\alpha \pi r_c^2}{180}$	
28.	$360 - \left(\left(\dfrac{\beta - \gamma}{2}\right) + B\right) \le \theta \le 360 - \left(\dfrac{\beta - \gamma}{2}\right)$	$BA^2 \sin\alpha \cos\alpha + \dfrac{\pi C_1 r_c^2}{180} - r_c BA \cos C_1 \sin\alpha$	
29.	$360 - \left(\dfrac{\beta - \gamma}{2}\right) \le \theta \le 360$	0	

APPENDIX-II

DETAILS OF MATLAB/ SIMULINK MODELLING

MATLAB- Simulink Block Diagram of Swash Plate Pump

A complete Matlab/Simulink model of the axial piston pump with pressure compensator has been shown in the Fig.A2.1. Left side part is the pressure compensator part and right side part is the pump itself. The rectangular workspace block is used to store the programming data.
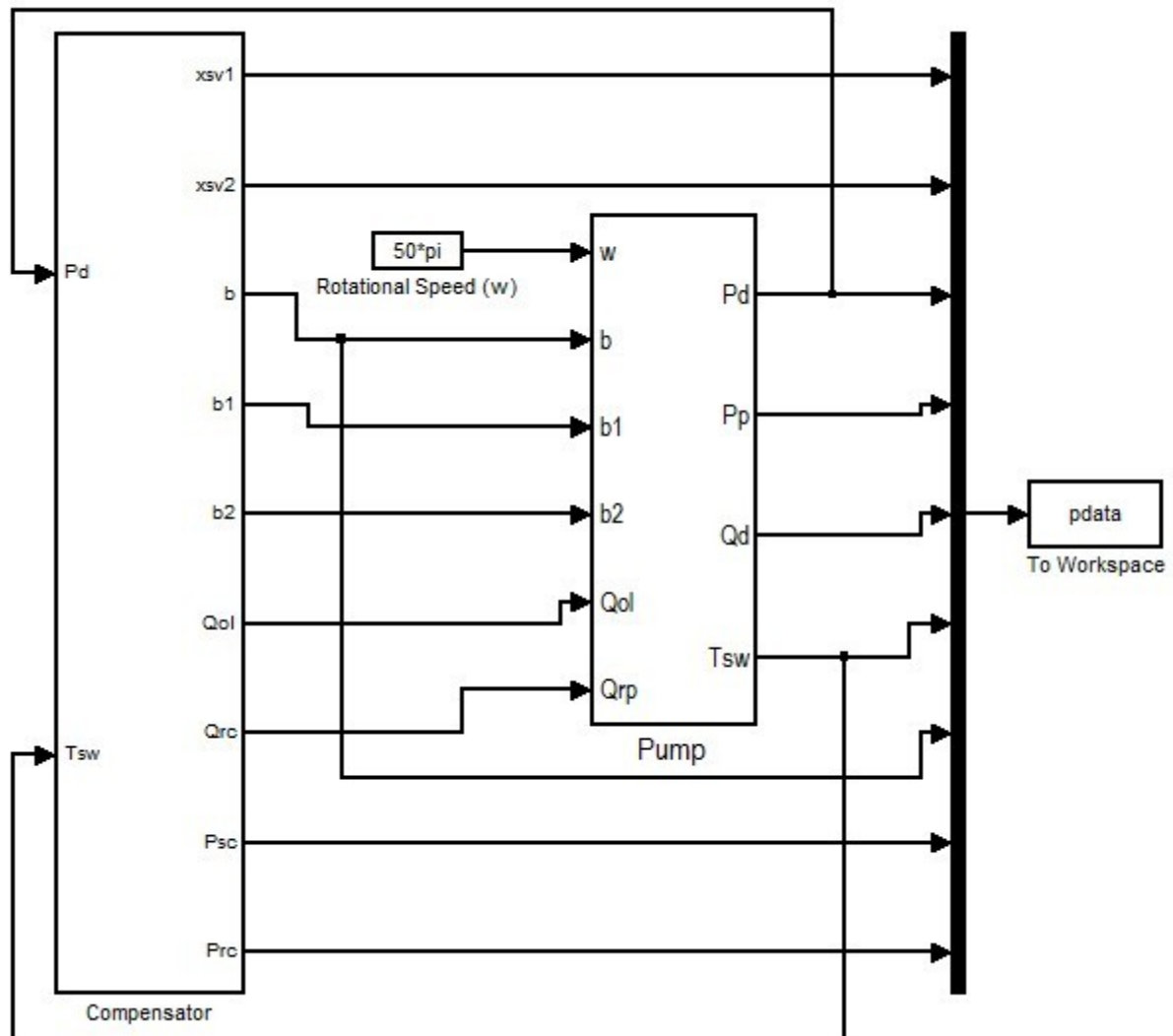
Figure A2.1: Model of pump with pressure compensator

Standard parameters for the programming have been put in two subsystems (mask) for pump body and for the compensator. As an example pump mask has been shown in Fig. A2.2a and the solver details have been shown in the Fig.A2.2b. Figure A2.2c indicates data import/export configuration of the simulink model.

111
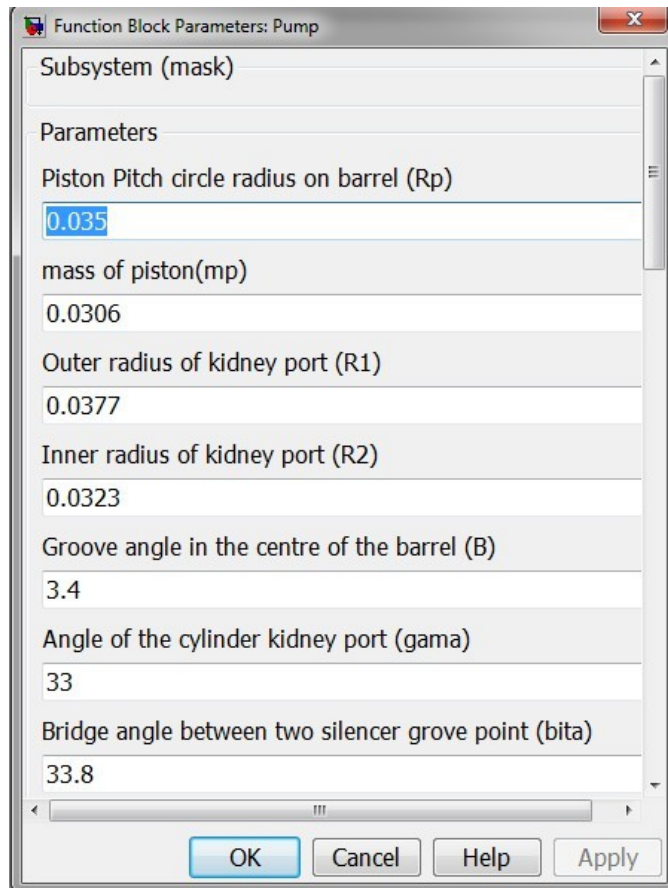
Figure A2.2a: Function block parameters
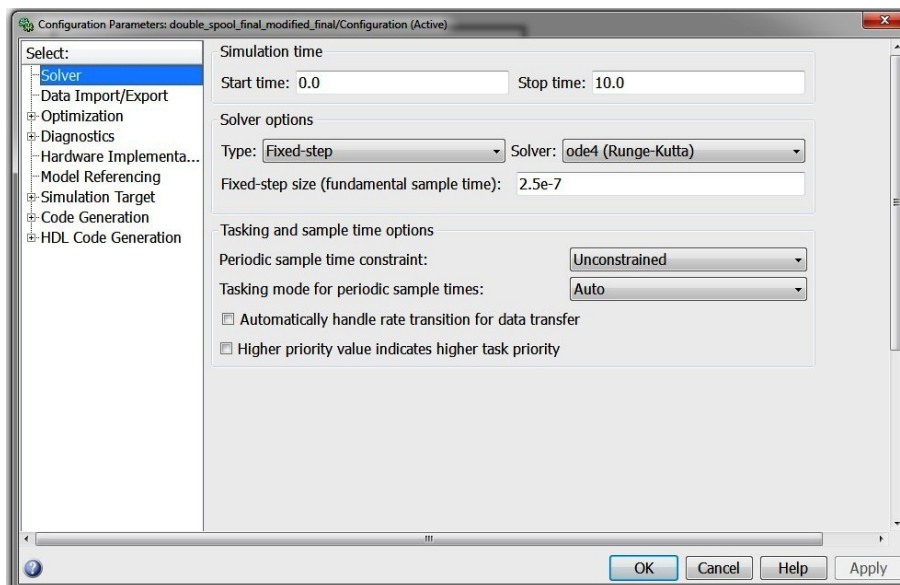
Figure A2.2b: Simulation configuration
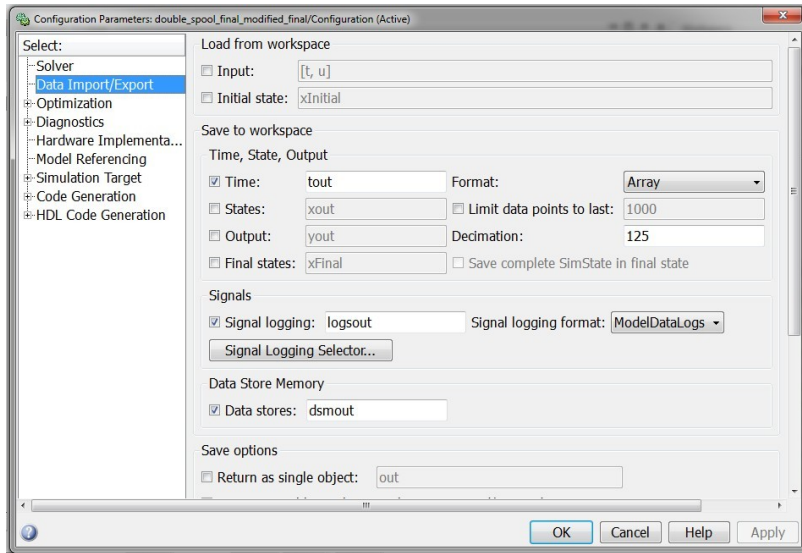
Figure A2.2c: Data import/export configuration
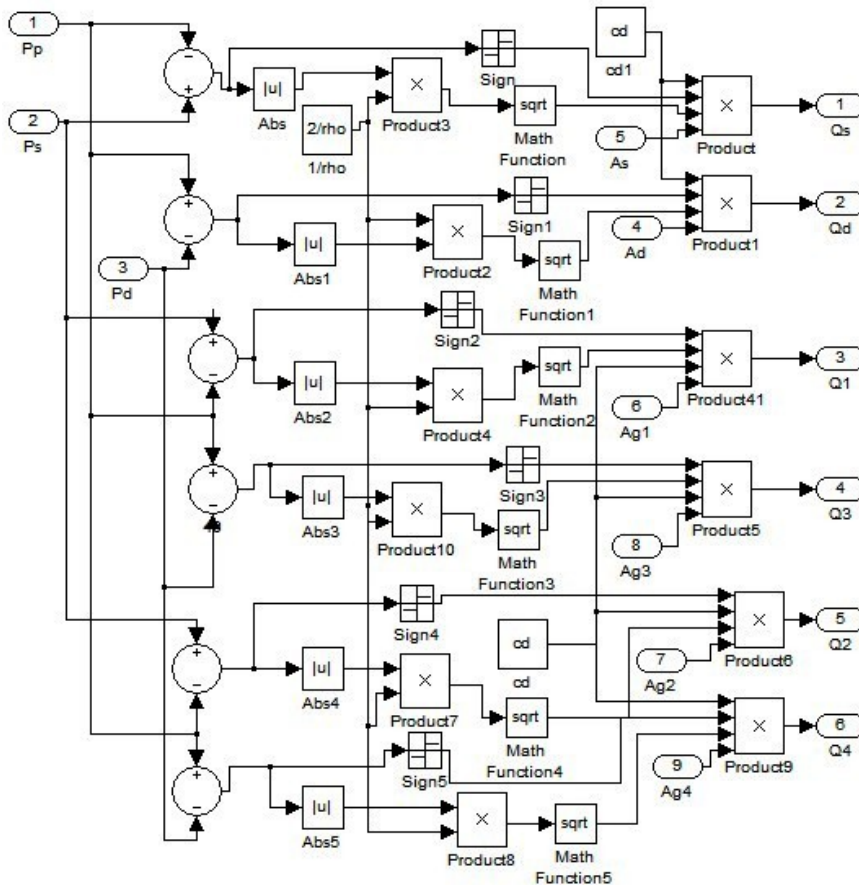
Figure A2.3: Flow dynamics for single piston for one rotation

Figure A2.3 shows the Flow over the manifold. Q_s and Q_d are indicate the flow over suction and delivery manifold. Q1 to Q4 indicates the flow through grooves. Figure A2.4 indicates the barrel piston pressure dynamics, where A_p, vk, v_{op} and Y indicates the cross sectional area of the barrel

piston, velocity, dead volume and stroke length of the piston and the term K indicates the bulk modulus of the working fluid. Figure A2.5 indicates the swivelling torque developed by a single barrel piston with respect to barrel axis from its instantaneous position. Torque pressure force, inertia force, viscous force all are related to this torque, where lr indicates the instantaneous position of the barrel piston on the manifold with respect to barrel axis.
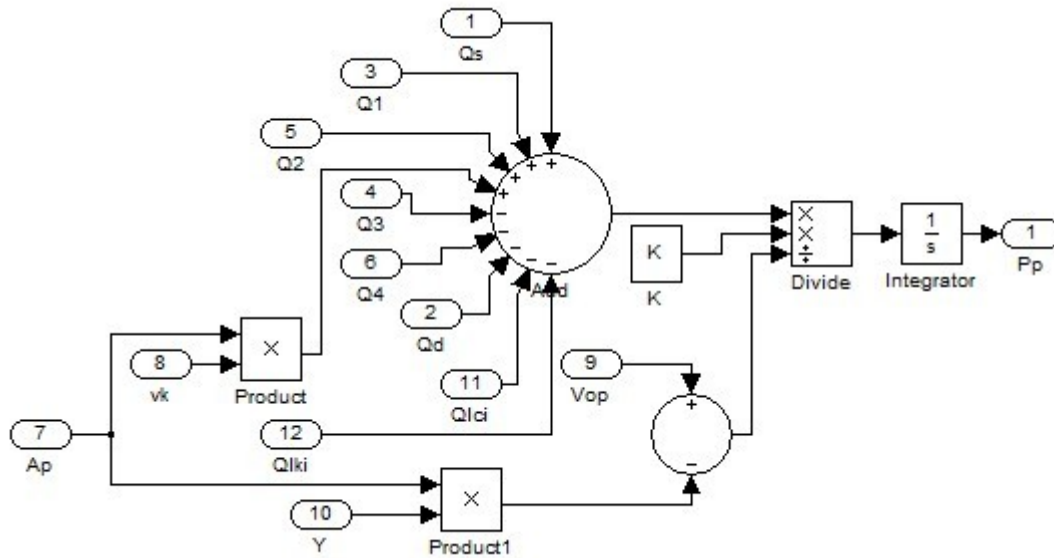
Figure A2.4: Barrel piston pressure dynamics
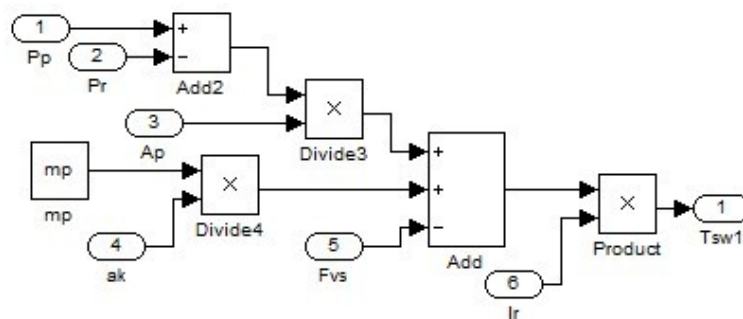
Figure A2.5: Torque developed by a single barrel piston

Figure A2.6 indicates the summary of a barrel piston dynamics. In the subsystem there are 24 outputs which are the inputs in the subsystem (mask) as shown in Fig. A2.2a. b, b1 and b2 are the instantaneous swash angle, angular velocity and acceleration for the corresponding swash position. 'Theta' is the barrel piston position on the manifold. Similarly, the dynamics of all barrel pistons are developed. The partial view of some pistons is shown in the Fig. A2.7. The details of the manifold dynamics has been shown the Fig. A2.8 and Fig. A2.9 indicates the leakage flow at the bridge portion of the valve plate.
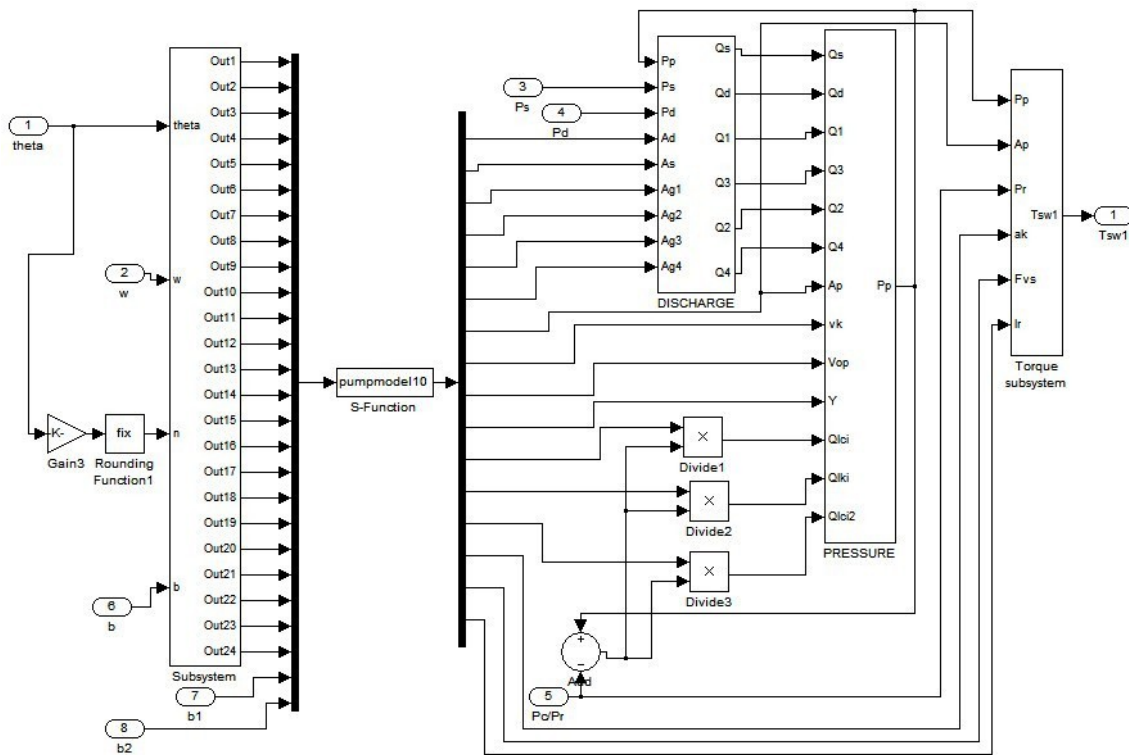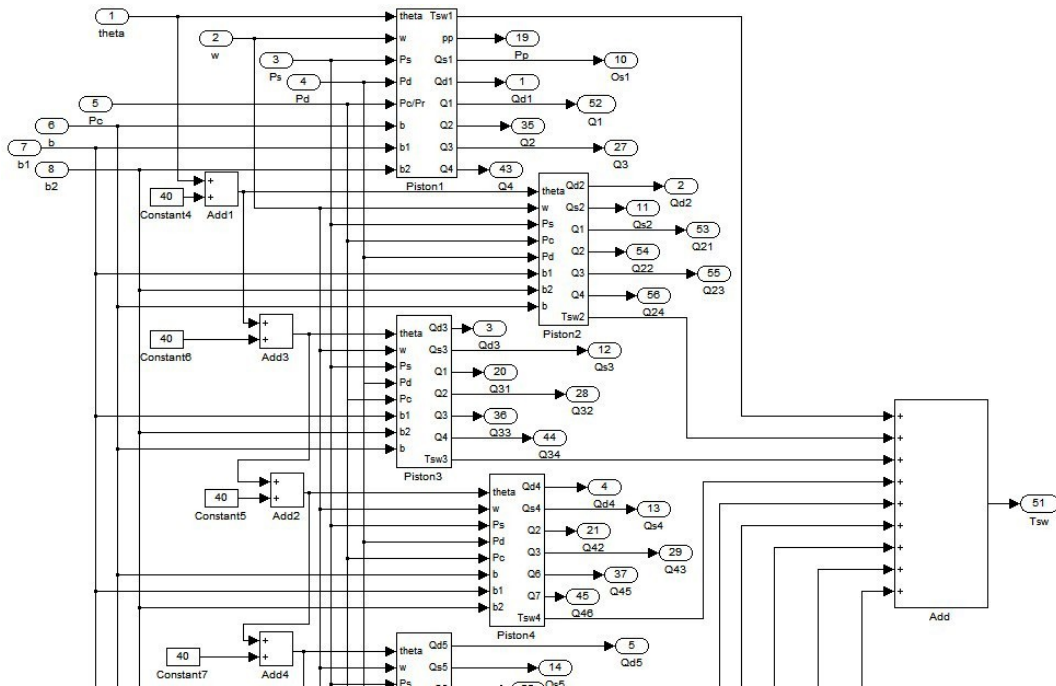
Figure A2.6: Complete view of a barrel piston

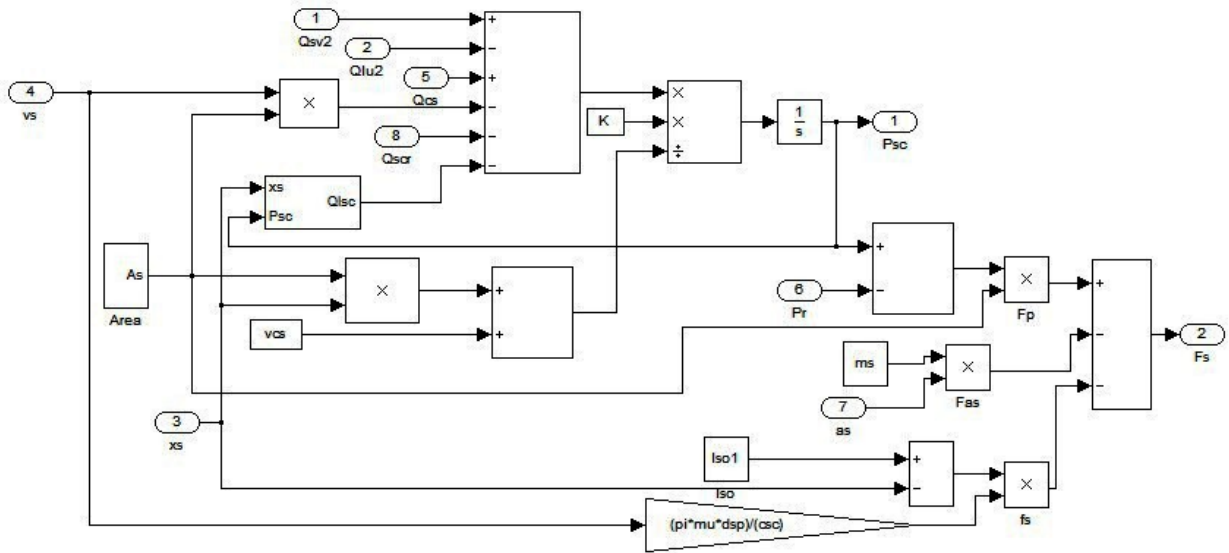**Figure A2.7: Part view of barrel pistons**

115

Figure A2.8: Details of manifold and load valve

Figure A2.9: Leakage at the bridge

Figure A2.10 indicates the stroking piston dynamics and Fig. A2.11 represents the pressure dynamics between the chamber top spool and bottom spool. Figure A2.12 shows the simulink model of the top spool of the control spool valve. Figure A2.13 to A2.16 represents elaborate view of the Fig. A2.12. Similarly the bottom spool also modelled.

Figure A2.10: Stroking cylinder dynamics
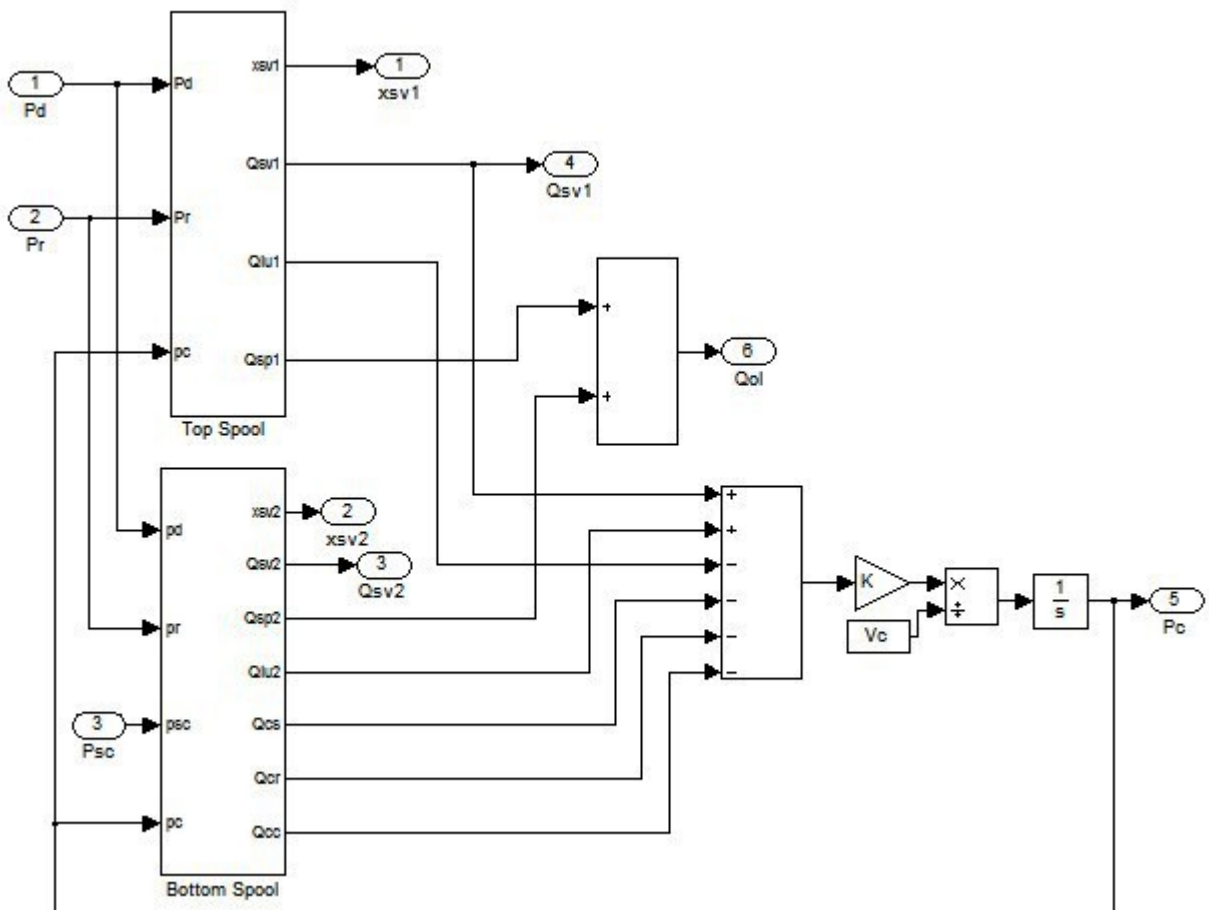
Figure A2.11: Pressure dynamics between top and bottom spool

117
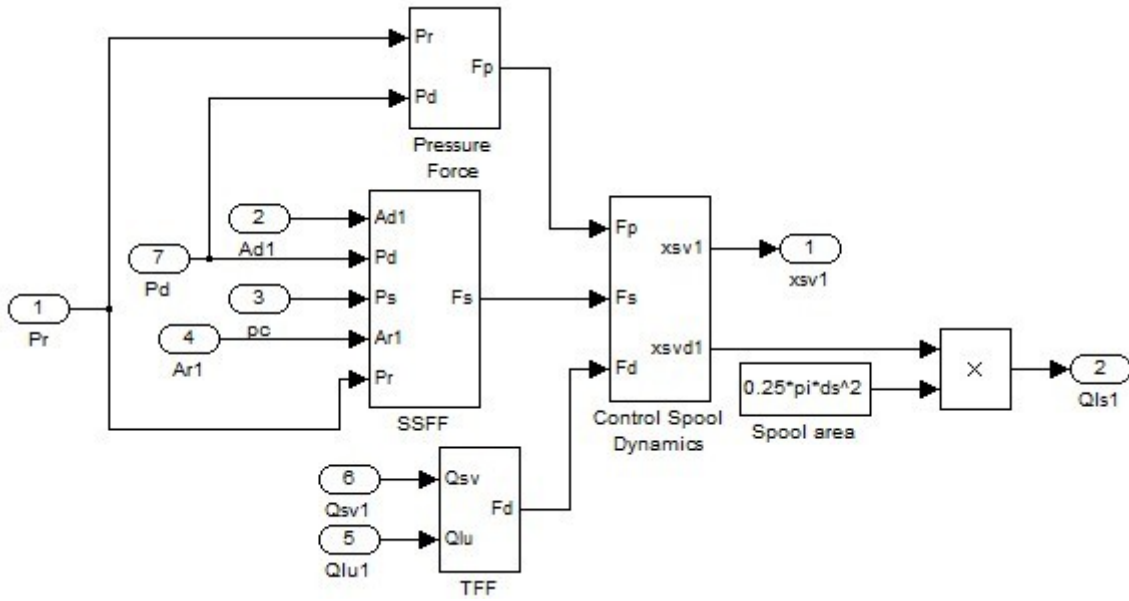
Figure A2.12: Simulink model of the spool valve
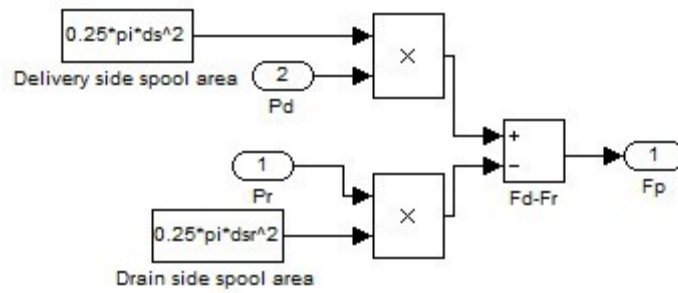
Figure A2.13: Model of the pressure force
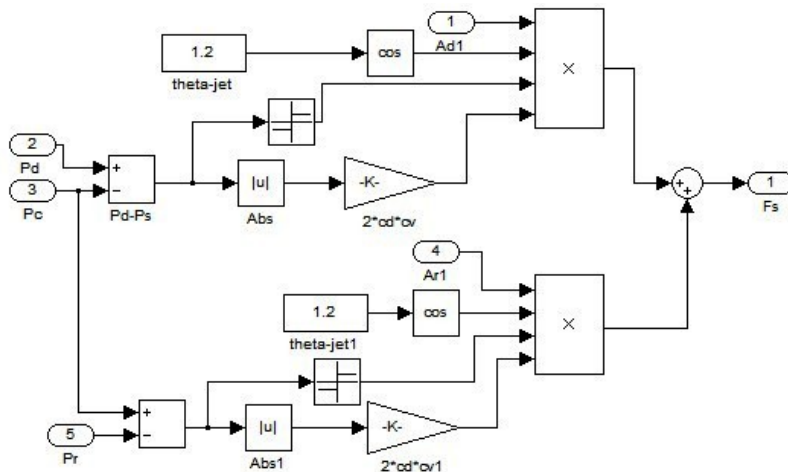
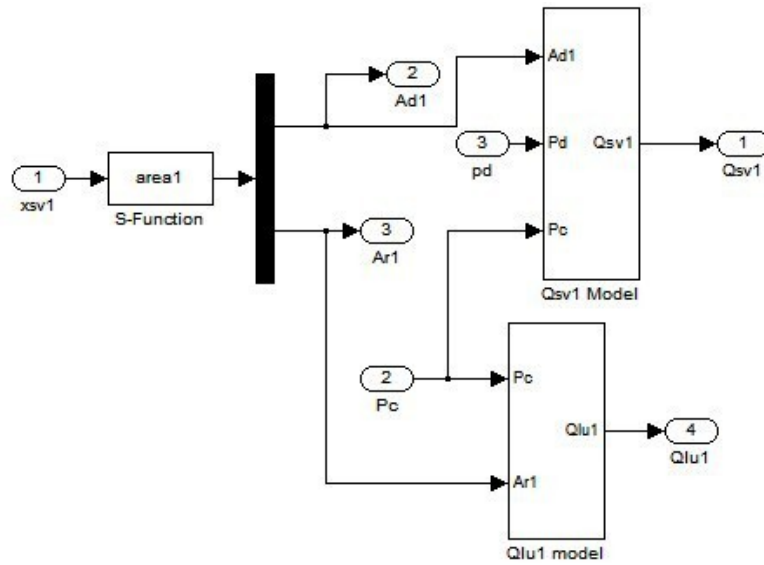**Figure A2.14: Model of the steady state flow force**
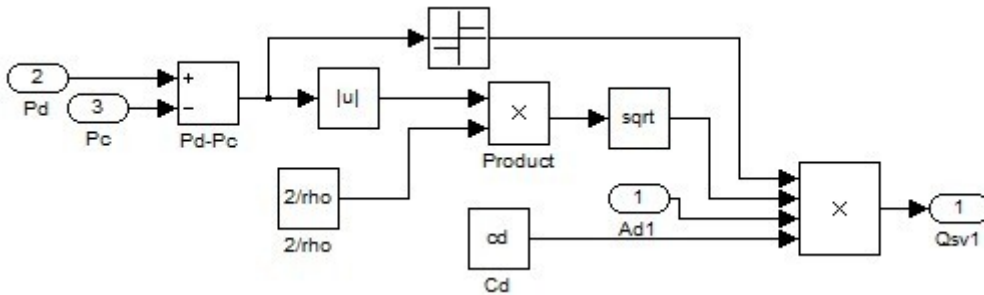
118

Figure A2.15: Flow model of the top spool port
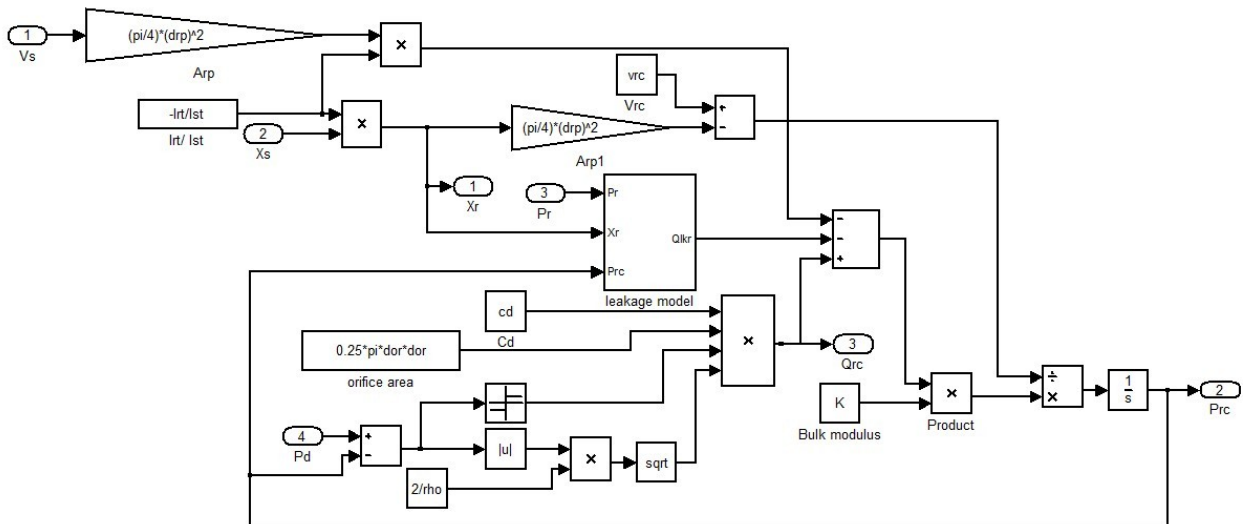

Figure A2.16: Flow model though metered orifice left side

Figure A2.17: Rate cylinder flow and pressure dynamics
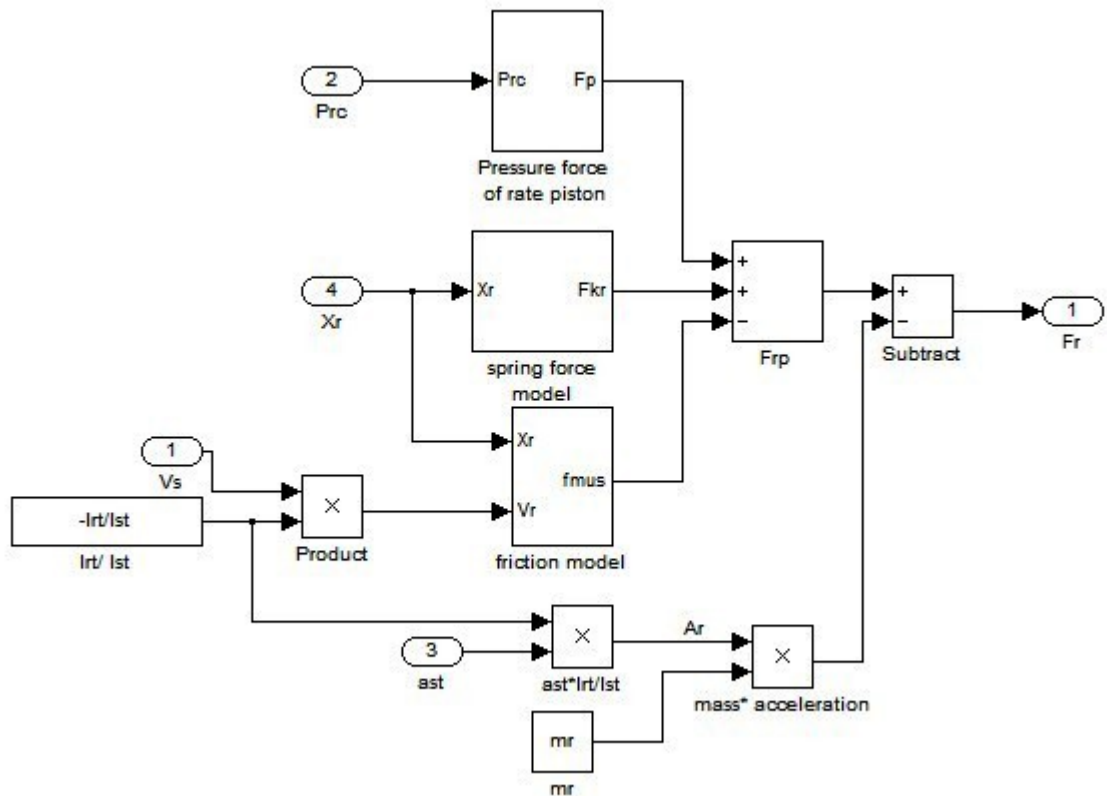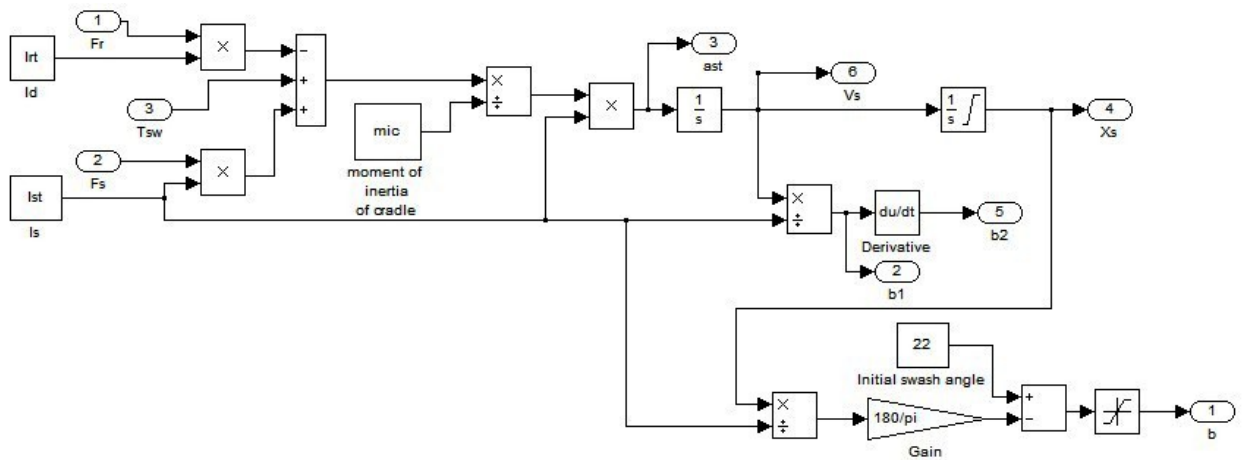
119

Figure A2.18: Rate cylinder force model

Figure A2.19: Swash plate dynamics model